Chapter 1
Introduction

1.1 History of the choice of organic technology

What is OLED? OLED is through finding a room for a series of organic membrane between two ticket collectors an electronic equipment made, made up of organic material of a kind of emissive. When the electric current is used, a light is sent out and can produce a fine deep dull and stereotyped display of color . This course is called as electrophosphorescence. Organic light emitting devices (OLED) with the layered system, these systems are very thin, usually less than 500 nm (0.5 thousandths of a millimeter) which make use of thin film materials that emit light when excited by electric current, are expected to become an increasingly popular form of flat panel display technology. When used to produce displays, OLED technology produces self-luminous displays that do not require backlighting. These properties result in thin, very compact displays. The displays also have a wide viewing angle, up to 160 degrees and require very little power only 2-10 volts. This is because OLEDs have a wide variety of potential applications (PDAs), computer displays, informational displays in vehicles. OLEDs can provide desirable advantages over today's liquid crystal displays (LCDs), as well as benefits to product designers and end users. The OLEDs feature including :

- High contrast
- Excellent grayscale
- Compatibility with Full-Motion Video
- Vibrant colors
- Wide viewing angles from all directions

- A Wide range of pixel sizes
- Low power requirements (Low operating voltages)
- Broader operating temperature range
- Long operating lifetime
- A thin and light-weight form factor
- The potential for low cost manufacturing processes
- Great durability
- Increased Brightness

Due to these features, OLEDs are seen as a future replacement technology for cathode ray tubes (CRTs) and liquid crystal displays (LCDs). Several factors make OLED superior to LCD or CRT technology. The most obvious difference is that OLED is so ultra-thin it can even be placed on plastic film! This makes it much lighter than older technology and a great advantage for hand-held devices, laptops and notebooks. It even opens the door to flexible displays. OLED is also brighter and has better contrast than LCD, but does not require back-lighting. It consumes about 20% less power than LCD, and has a response time every bit as fast as CRT displays. Add to this favorable list that OLED displays can be clearly viewed at nearly any angle -- a full 170 degrees. As if this wasn't enough, they boast exceptional clarity and refresh at a rate 3x faster than is necessary for standard video applications! As is typical in the development of many technologies, recent progress in organic devices has outstripped our fundamental understanding of the processes involved. Indeed, many aspects of device physics remain contentious and the subject of further study. For this reason we shall concentrate only on the major advances in organic devices together with advances in the supporting technologies of fabrication and patterning.

Organic materials are characterized by an immense variation in

structure and properties, and this flexibility is one of the principal reasons for studying their application to electrical engineering problems. For example, many molecules and polymers have pronounced optical qualities that can be adjusted by modifications of chemical structure. Electrical properties such as conductivity are also dependent on molecular design. But although the intramolecular conductivity of molecules and polymer chains may be enhanced by delocalized electrons from sp^2 hybridized carbon atoms, the intermolecular overlap of van der Waals bonded solids generally limits charge transport mobilities to $\mu < 10$ cm^2 /Vs at room temperature; [1-3] increasing to $\mu \sim 10^5$ cm^2/Vs at low temperature[2,4,5] shown in the Figure 1.1 and Figure 1.2.

The solid lines indicate a T^n power-law temperature dependence with exponents n as indicated in the Figure 1.1. These mobilities were obtained using the time of flight technique, which measures the transit time of a sheet of carriers moving through the semiconducting medium as a function of applied electric field. Both the electric field and the detected velocity were parallel to the crystallographic **a** direction. From Warta and Karl (1985).

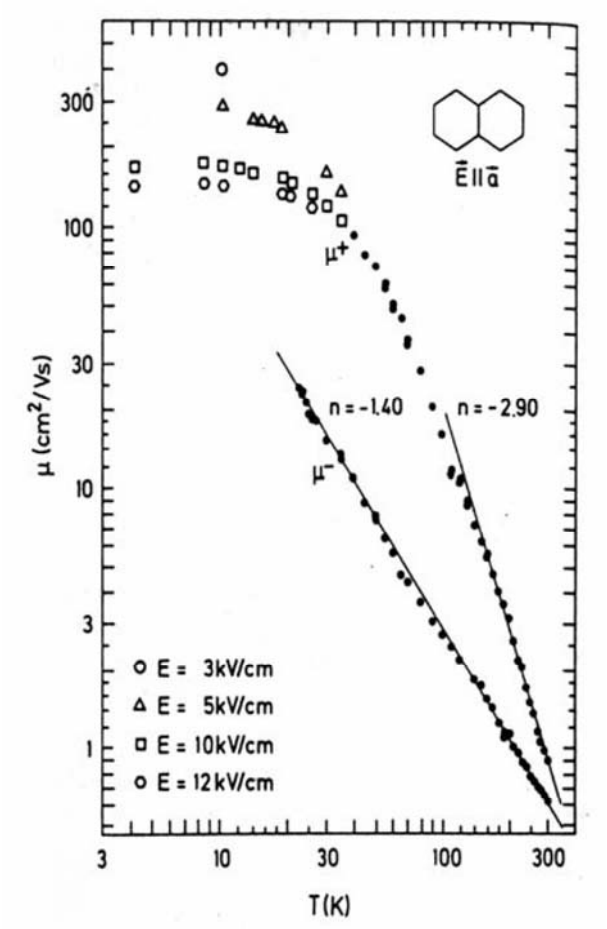

Figure 1.1 Electron and hole mobilities versus temperature in ultrapure naphthalene. At low temperatures the mobilities are electric field dependent.

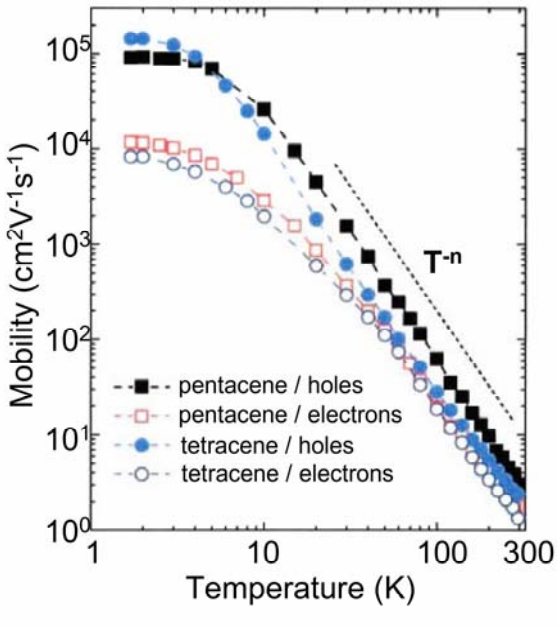

Figure 1.2 The temperature dependence of the field effect mobility of pentacene and tetracene molecular crystals. The organic materials are used as the semiconducting medium of a thin film transistor. Hence, the mobility measured is that of charges in a thin layer ~ 10Å on the surface of an organic crystal. The increase in mobility with decreasing temperature has been ascribed to electron-phonon interactions. At low temperatures, charged point defects are believed to limit the mobility. From Schön *et al*. (2000) Similar mobilities have been measured at low temperature in anthracene using cyclotron resonance; see Burland (1974,1977).

Thus, the transport characteristics of organic films are strongly dependent on molecular order. To avoid the need for very large voltages, organic devices should employ thin films of molecules designed for optimum molecular overlap. Most initial studies of the solid-state properties of these materials concentrated on molecular crystals because ordered crystals possess the best electronic transport properties. The first reported

observation of electroluminescence in organic crystals under steady-state bias was made by Helfrich and Schneider using anthracene;[6] see Figure 3. But because they used crystals several microns thick, the onset of electroluminescence required an applied potential of over 100 V, limiting the possible practical applications of this technology. Subsequently, light emitting devices were fabricated using thermal evaporation of polycrystalline anthracene thin films.[7] The ability to make much thinner devices using this technique significantly reduced the voltage required to generate light, however, in these early devices, electron-hole combination occurred very close to an injecting contact and the quantum efficiencies were limited to less than 0.1%.

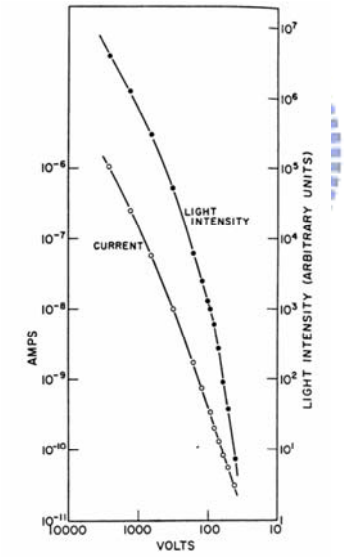

Figure 1.3. The transport and luminescence characteristics of the first organic electroluminescent device. From Helfrich and Schneider (1965).

1.2 The work of Tang and VanSlyke

A significant step forward in organic technology came with the publication by Tang and VanSlyke of solar cells[8] and light-emitting devices[9]

fabricated from thin amorphous and polycrystalline layers deposited by thermal evaporation in vacuum. Although disordered films possess inferior electron transport characteristics, they can satisfy the requirement for extremely thin, low voltage, organic devices: electrically continuous films with smooth interfaces and no pinholes. Indeed, thermal evaporation is capable of growing continuous, molecularly-smooth, films as thin as 100Å, allowing vertical device feature sizes approaching molecular scales. As with the anthracene thin-film devices,[7] the reduction in organic thickness to ~1000Å in the solar cells and light-emitting devices enabled a dramatic reduction in operating voltage. A significant step was to use amorphous films to fabricate the first organic heterostructure light emitting device,[9] increasing the quantum efficiency of luminescence by approximately two orders of magnitude to 1%, at an operating voltage of less than 10V; see Figure 1.4. As described in Figure 1.5, the heterostructure design was also used in a 1% power efficient solar cell.[8] With this work, organic materials first showed their potential as the basis for an efficient emissive technology applicable to all aspects of the display industry. An intense examination by chemists and electrical engineers followed.

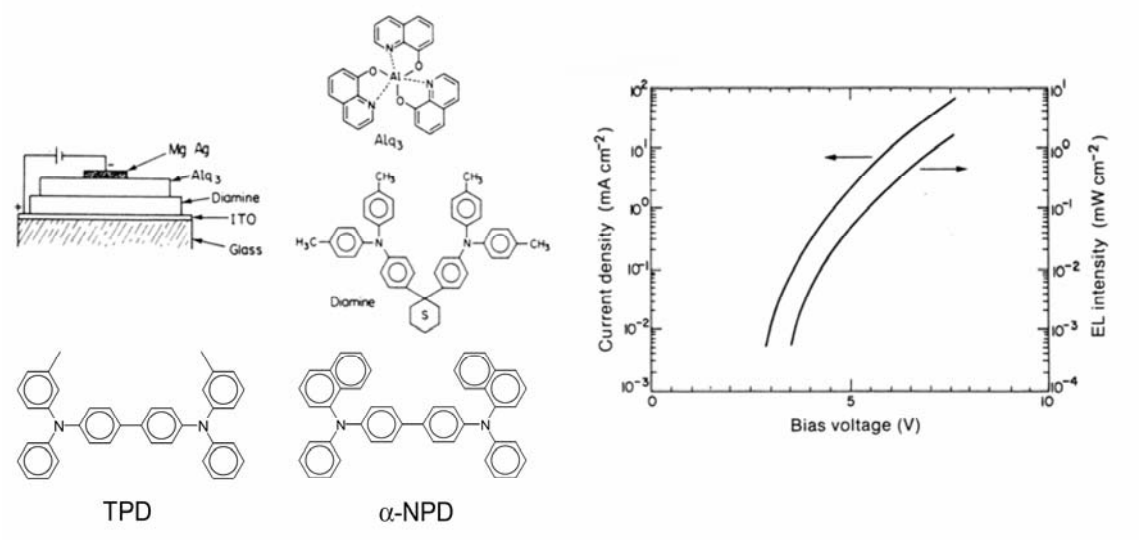

Figure 1.4 Tang and Van Slyke's organic light emitting device is built on a glass substrate coated with a transparent indium tin oxide layer acting as the anode.

A diamine was used as the hole transporting material since this class of materials was found to have stable conductivity properties in earlier work on photoconductors. Many variations on the basic diamine structure were later investigated; for example, both TPD and α-NPD were found to make successful hole transport layers. The electron transporting and luminescent material employed was Alq3. In these heterostructure devices electrons and holes combine at the diamine/Alq3 interface, but whereas there is minimal electron injection into the diamine layer, some holes penetrate into the first 100Å of Alq3. Thus, excitons are formed in the Alq3 and emission is observed from Alq3 fluorescence. Electrons are injected into the organic layers from a Mg:Ag alloy cathode with an additional layer of Ag to protect the Mg from oxidation. After Tang and Van Slyke (1987).

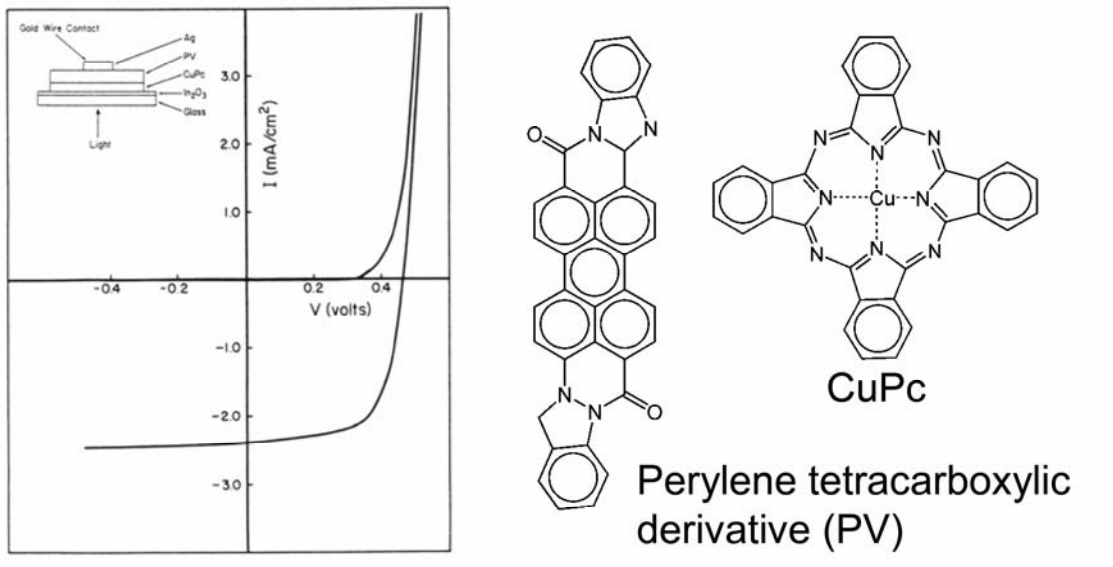

Figure 1.5 Tang's photovoltaic cell is built on a glass substrate coated with transparent indium tin oxide. Thermal evaporation in vacuum was used to deposit 250Å of copper phthalocyanine (CuPc) and then 450Å of a perylene tetracarboxylic derivative. A thin layer of Ag was used as the top contact. Light is absorbed in both the organic layers and the excitons diffuse to the organic/organic interface where they are dissociated. Holes are extracted from the CuPc and electrons from the perylene tetracarboxylic derivative. Relative to photovoltaic devices made using conventional semiconductors, the very high absorption of the organic layers allows the fabrication of an extremely thin photovoltaic cell. This minimizes losses from non-radiative exciton recombination and reduces the ohmic losses, maximizing the fill-factor. Tang's CuPc/perylene tetracarboxylic solar cell remained the benchmark in the organic solar cell community for over ten years. After Tang (1986).

The first molecular light-emitting device used tris(8-hydroxyquinoline) aluminum(III) (Alq3) as both an electron transport material and as an

efficient green luminescent dye. The need for emission at other colors was impeded by the difficulty of finding other materials with both suitable emissive and charge transporting properties. In 1989, Tang, Van Slyke and Chen[10] showed that it was possible to add small quantities of a highly luminescent dye to a charge transport material and achieve complete energy transfer in electroluminescence. The separation of charge transport and luminescence into two materials allowed individual chemical tailoring of both aspects of device performance. Indeed, red devices were demonstrated with quantum efficiencies as high as 2% shown in Figure 1.6.

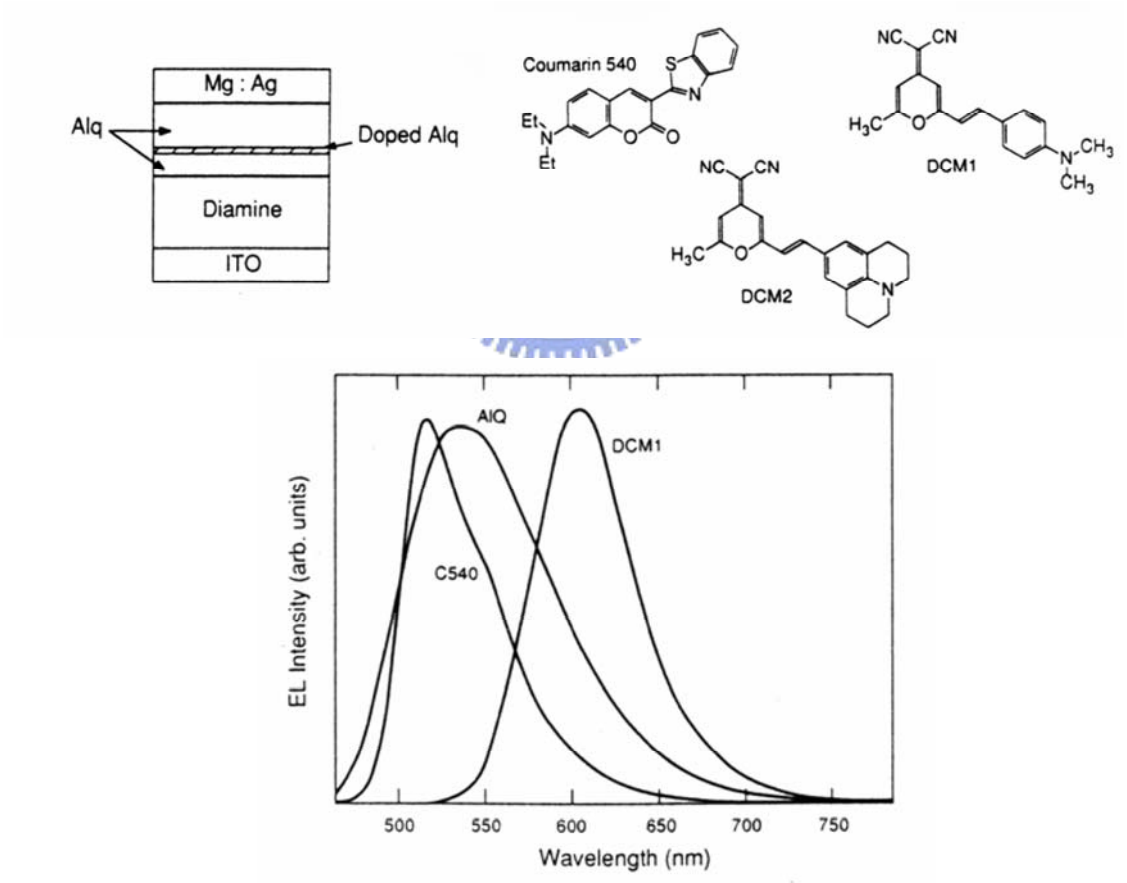

Figure 1.6 The electroluminescent device structure used to demonstrate emission from the organic dyes shown above. The spectra at left

demonstrate complete energy transfer from Alq3. After Tang, Van Slyke and Chen (1989).

1.3 Full color active matrix displays

Although the essential principles of organic electroluminescence were established in the initial papers by Tang *et al.*, the commercial development of this technology was retarded by reliability problems. The organic materials are sensitive to both oxygen and water, and maintaining the devices in an inert atmosphere is critical to their long-term stability. But with improvements in material purity and packaging technology, commercially acceptable lifetimes of ~ 10,000 hours were ultimately realized and several prototype full-color organic displays have now been demonstrated. One such display is shown below in Figure 1.7. On the left is a 5 inch active matrix display and the screen on the right has a 2.4 inch diagonal. They are both fabricated on a polysilicon thin film transistor backplane. Note that because the organic emissive devices are Lambertian emitters, the color is relatively independent of viewing angle; also note the very thin and flat display.

Figure 1.7 Organic active matrix displays, courtesy of Steven Van Slyke and Kodak.[13]

1.4 The Early Years of Development[14]

- 1996 - CDT gives world's first public demonstration of Light Emitting Polymer devices
- 1997 - UDC Demonstrates Flexible Flat Panel Display Technology
- 1997 - Universal Display Corporation Announces Transparent, Flexible Organic Display Breakthrough
- 1997 - Pioneer Electronic Produces EL Display with 260,000 Colors
- 1998 - Kodak and SANYO Electric Conclude Comprehensive Alliance Agreement for Organic EL Displays
- 1998 - Kodak, Sanyo Show Full-Color Active Matrix Organic Display; First Color OEL Display Increases Threat to LCD Display Dominance
- 1998- Green Organic LED Shows High Efficiency
- 2000 - Ritek plans to mass produce OLED
- 2000 - Toshiba Corp. plans to produce (organic EL) panels in 2001
- 2000 - Motorola Grants OLED Technology Rights To Universal Display And Takes Equity Position
- 2000 - UDC and PPG Industries Form Strategic Alliance for Development & Supply of Chemicals for OLED Manufacturers
- 2000 - Sanyo Electric to start mass production of color organic EL panels in 2001
- 2000 - NEC, Samsung To Develop Organic Wireless Displays
- 2000 - LG Electronics develops organic EL displays for mobile gadgets

2001

- January - Sanyo partnered with Kodak for color OLED display

screen

- February - Sony Develops World's Largest Full Color OLED (13 inches diagonally with a resolution of 800x600 pixels.)
- April - Universal Display Corporation and Sony Corporation Announce Joint Development Agreement Aimed at OLED Television Monitors
- April - Samsung Exhibits Color Organic EL LCD Panel for Mobile Phones at CeBIT (132 by 162 pixels)
- May - Toshiba Develops World's First 260,000-Color Polymer OLED
- June - RiTdisplay and Compaq sign CIM project agreement for OLED/polymer-OLED factory
- August - eMagin's OLED Microdisplay Selected by Air Force for F15E Aircraft
- October - Luxell's Black Layer OLED Patent Application Allowed
- October - Sony Demonstrates 13-Inch, Full-Color OLED Prototype
- October - Universal Display Reports New Red Phosphorescent OLED Materials, Significant Power Efficiency Advances
- October - Samsung SDI Develops World's Largest Organic Display Panel (15.1 inch)
- November - RiTdisplay opens new color OLED/PLED factory
- December - Kodak, SANYO Form Joint Venture to Manufacture OLED Displays

2002

- January - Universal Dispy Announces Advanced OLED Manufacturing Patent Issued for OVPD Technology
- February - Samsung SDI develops 2.2-inch AM OLED for mobile

phones

- April - Philips Announces Industry's First Volume Shipments of Polymer-Based OLED Modules
- May - Kodak Announces Availability of Evaluation Kit For Active-Matrix OLED Display
- May - RiTdisplay reportedly receives orders for over one million mobile phone OLEDs
- June - AU Optronics develops world's first OLED prototype combining a-Si TFT LCD technology
- June - Epson, CDT form polymer OLED production venture
- July - E-Ink, TOPPAN and Philips Demonstrate World's First High Resolution, Active-Matrix Color Display With Electronic Ink
- August - Universal Display Awarded Two U.S. Department Of Energy Contracts For OLEDs In General Lighting
- August - Daeyang and eMagin Announce $8 Million Purchase Agreement
- November - Pioneer Supplies OLED to LG Electronics for Cell Phones
- December - DuPont Displays and Universal Display Corporation Form Strategic Alliance to Develop Next Generation Displays Combining Aspects of Small Molecule and Polymer OLEDs
- December - RiTdisplay confirms receiving color OLED orders from Motorola

2003

- January - Philips invents EL material to generate both red and green ligh
- January - Kodak, Sanyo invest in active-matrix OLED production

- January - Universal Display Corporation Wins Army SBIR Contract To Focus On The Use Of Metal Foil For Flexible Displays
- January - Sanyo Unveils Mobile Phone with Organic EL Panel Designed for KDDI, announces plans to build full-color OLED production line
- February - RiTdisplay lands mobile phone OLED orders from Samsung and LGE
- February - Kodak Licenses Samsung NEC Mobile Display to Manufacture Passive-Matrix OLED Displays
- February - SNMD to Make Displays for Mobile Phones
- March - Kodak introduces the first digital camera with an OLED screen - the Kodak EasyShare LS633
- March - AIXTRON Delivers 1st Commercially Available OVPD R&D System to Princeton University
- March - Samsung shows Palm OS 5 smart phone; OLED sub-display
- March - IDTech develops 20-inch full-color OLED display
- March - Luxell receives U.S. patent for Black Layer OLED fabrication
- April - DuPont forges 'Olight' brand for emerging OLEDs
- April - Sony testing 24-inch OLED screen
- May - CDT Extends LEP Life to Over 11,000 Hours
- May - RiTdisplay selects AIXTRON's OVPD technology for OLED Display Production
- May - AUO and UDC develop 4-inch, a-Si TFT backplane-based, red phosphorescent AMOLED
- May - Samsung NEC develops 65,000-color PM OLED mobile

phone display

- May - Sony demonstrated a 24.2-in. OLED panel
- June - Hynix Announces Availability of 4,096 Color Organic EL Driver IC
- June - Sony to invest nine billion yen to build OLED production line
- September - AU Optronics has showcased its 1.93" AMOLED for Mobile Phone
- September - Princeton electrical engineers have invented a technique for making Organic Solar Cells that Could Lead To Widespread Use Of Solar Power
- October - Advances Using UDC's Phosphorescent OLED Technology can Provide Additional Power Efficiency Gains for White Lighting
- October - Sanyo Unveils Long-Lasting QVGA Organic EL Panel for Cell Phones
- October - Univision begins OLED production
- November - Tohoku Pioneer Corporation to Be First Manufacturer to use Universal Display Corporation's PHOLED Material in a Commercial OLED Display
- November - Univision showcases 65,000-color mobile phone OLED sub-display
- November - Epson Develops OLED Controller Chip for Car Audio
- November - Samsung SDI Develops Organic EL with Clearer Resolution
- December - eMagin Granted Key Patent for New Class of Higher Luminance, Higher Temperature OLED Device

- December - Univision reaches monthly capacity of 6,000 OLED substrates
- December - Casio Ventures into Organic EL Panels Driven by Amorphous Si TFT
- December - Samsung and 3M jointly developed a new color patterning method, laser induced thermal imaging (LITI), for fabricating full-color PLEDs

2004

- January - Opto Tech to invest NT$4.5 billion in four new OLED lines in 2004
- January - Kyocera Acquires International Display Technology, a subsidiary of Taiwanese LCD manufacturer, ChiMei Electronics.
- February - Lightronik licenses OLED technology from Kodak
- February - Philips 639 mobile phone applies PolyLED technology in unique 'Magic Mirror' display
- March - GE Global Research Breaks Two World Records For OLEDs As A Lighting Device. Demo Lighting Panel is Biggest and Most Efficient Ever Created
- March - NEC drops its OLED business
- March - Chi Mei Optoelectronics Corp. (CMO) has announced a fully functional prototype of a 20-inch full-color OLED display - the largest Amorpheous Si TFT
- March - First-Generation Electronic Paper Display from Philips,Sony and E Ink to Be Used in New Electronic Reading Device
- March - TI Introduces New Power Management ICS To Enhance OLED Color Displays, White LED Backlighting

- April - Teco Optronics to invest NT$300 million to build new PM OLED plant
- April - Fuji Photo Film, Vitex System to Join Development of Encapsulating Organic EL Panel
- April - RiT Display ships mobile phone OLED sub-displays to Samsung, says paper
- April - Seiko Epson Reveals 12.5-Inch Organic EL Panel for Large TVs
- April - RiT Display shipping OLED panels to Motorola
- April - TI has released an OLED display power conversion integrated circuit
- May - Philips Demonstrates Feasibility of PLED for TV Applications
- May - Seiko Epson unveils first 40" colour OLED display
- May - Universal Display Corporation Announces Record-Breaking Power Efficiencies for its Phosphorescent White OLED Technology
- May - Taiwan's AU Begins Mass Production of Organic EL Panels
- May - Universal Display Corporation Unveils Ground breaking Flexible OLED Prototype on Metallic Substrate
- May - Luxell signs OLED License agreement with Hyundai LCD Inc
- June - DigiTimes: Fuji Electric Holdings to produce OLED panels in 2005
- June - Samsung SDI Unveils 17-inch, 2.2-inch Organic EL Display with High Picture Quality

- June - SEL, Others Develop Organic EL Panel for Displaying Pictures on Both Sides
- June - Toppan to volume produce large-size OLED panels
- July - CDT files for an IPO, estimated 40m$
- August - Samsung SDI to volume produce OLED panels in August
- September - Sony Starts Mass Production of Organic EL Displays, and released first a new clie PDA with a 3.8in 480 x 320 OLED screen
- October - AU Optronics Successfully Develops World's First Double Sided Active Matrix OLED
- October - LG.Philips develops 20-inch OLED display
- October - Japan OLED makers aggressively expanding AM OLED capacity
- November - Competition heats up as more players enter the OLED display market
- November - OLED displays with 50,000h operating lifespan from URT
- November - Seiko Epson will commercialize OLED TVs by 2007
- December - CDT IPOs, lists on NASDAQ.

2005

- January - Samsung Electronics develops 21-inch OLED for TVs, claims world's largest
- January - Samsung SDI To double the OLED output
- January - OLED Technology Poised to Become Core Business for Daewoo Electronics
- February - MP3-player demand boosts sales of Taiwan OLED

makers

- February - LG.Philips LCD launches AM OLED Business
- March - Sony introduces Flash based MP3 players with OLED display
- March - Canon says to start making OLED displays next year.
- April - Samsung Licenses OLED Patents from Universal Display
- May - Kodak Licenses OLED Technology to Fuji Electric Holdings
- May - CDT Achieves 100,000 Hour Blue Polymer Lifetime
- May - Samsung Electronics Develops World's First 40-inch a-Si-based OLED
- June - Toppoly develops a 7" AMOLED display
- June - UDC announces fundamental breakthrough in blue PHOLEDs - New sky blue achieves over 15,000 hours of lifetime
- July - Samsung SDI to invest over 850M$ in AMOLED production
- August - LG Electronics Launches Full-Scale OLED Operations
- October - Samsung SDI's Organic LED Display Shipments Top 30 Million units
- November - CDT Prints a 14" P-OLED display
- November - China's first OLED production line set up
- November - Samsung SDI, LG Philips to build AMOLED production lines
- December - Pioneer withdraws from AM-OLED market

2006

- January - BenQ announces camera, phone with large (2.0") OLED screen
- January - Kodak Broadens its Participation in OLED Technology, ends OLED joint venture with Sanyo

- March - Univision to invest $40M in OLED line expansion
- March - World's first print head using an OLED light source

1.5 Summary

This brief overview of organic technology is not intended to be comprehensive. Rather, it is intended to justify the current enthusiasm for organic materials by giving examples of some of the exciting developments in patterning and fabrication technology, as well as describing the range of organic devices currently under investigation: organic light emitting devices, transistors, phosphors materials, photodetectors and lasers. We will return to this subject in the conclusion, where the future of organic devices will be considered.

1.6 References

1. Warta, W. & Karl, N. Hot holes in naphthalene: High, electric-field-dependent mobilites. *Physical Review B* 32 (1985) 1172-1182.

2. Schön, J. H., Kloc, C. & Batlogg, B. Fractional Quantum Hall Effect in Organic Molecular Semiconductors. *Science* 288 (2000) 2338-2340.

3. Karl, N., Kraft, K.-H., Marktanner, J., Muench, M., Schatz, F., Stehle, R. & Uhde, H.-M. Fast electronic transport in organic molecular solids. *Journal of Vacuum Science and Technology A* 17 (1999) 2318-2328.

4. Burland, D. M. Cyclotron Resonance in a Molecular Crystal - Anthracene. *Physical Review Letters* 33 (1974) 833-835.

5. Burland, D. M. & Konzelmann, U. Cyclotron resonance and carrier scattering processes in anthracene crystals. *Journal of Chemical Physics* 67 (1977) 319-331.

6. Helfrich, W. & Schneider, W. G. Recombination radiation in anthracene

crystals. *Physical Review Letters* 14 (1965) 229-231.

7. Vincett, P. S., Barlow, W. A., Hann, R. A. & Roberts, G. G. *Thin Solid Films* 94 (1982) 171.

8. Tang, C. W. Two-layer organic photovoltaic cell. *Applied Physics Letters* 48 (1985) 183-185.

9. Tang, C. W. & VanSlyke, S. A. Organic electroluminescent diodes. *Applied Physics Letters* 11 (1987) 913-915.

10. Tang, C. W., VanSlyke, S. A. & Chen, C. H. Electroluminescence of doped organic thin films. *Journal of Applied Physics* 65 (1989) 3610-3616.

11. Burroughes, J. H., Bradley, D. D. C., Brown, A. R., Marks, R. N., MacKay, K., Friend, R. H., Burn, P. L. & Holmes, A. B. Light emitting diodes based on conjugated polymers. *Nature* 347 (1990) 539-541.

12. Brown, A. R., Bradley, D. D. C., Burroughes, J. H., Friend, R. H., Greenham, N. C., Burn, P. L., Holmes, A. B. & Kraft, A. Poly(p-phenylenevinylene) light-emitting diodes: Enhanced electroluminescent efficiency through charge carrier confinement. *Applied Physics Letters* 61 (1992) 2793-2795.

13. Matrix size, combined with the active display area, specifies the display device's nominal pixel **...** 32.1, pp. 115–118, 1997. Tang CW, Van Slyke SA. (1987).

14. http://www.oled-info.com/history

Chapter 2

Principles

2.1 How Does It Work?

In this chapter, we will derive the essential theory used in the remainder of this work. As this schematic shows, an OLED is a monolithic, solid-state device that typically consists of a series of organic thin films sandwiched between two thin-film conductive electrodes. The choice of organic materials and the layer structure determine the device's performance features: emitted color, operating lifetime and power efficiency.

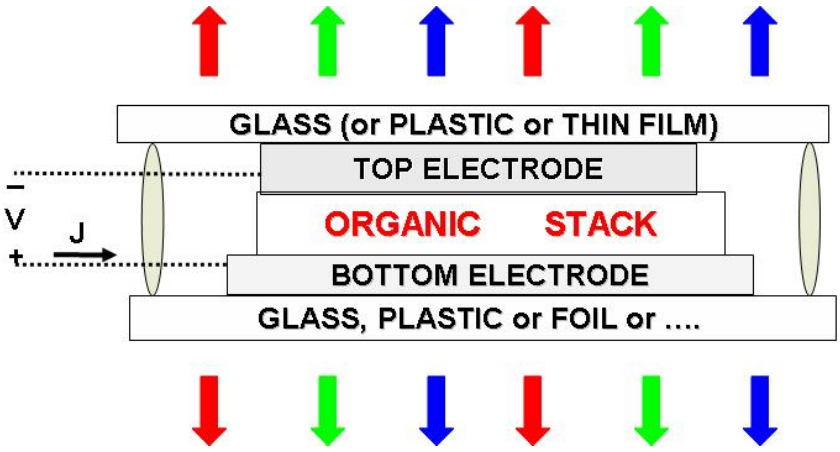

When electricity is applied to an OLED, charge carriers (holes and electrons) are injected from the electrodes into the organic thin films. They migrate through the device under the influence of an electrical field. The charge carriers then recombine, forming excitons. In the past, conventional wisdom suggested that only about 25% of these excitons could generate light, with the remaining 75% lost as heat. This was known as fluorescent emission. Through a breakthrough by our academic partners at Princeton University and the University of Southern California, however, 100% of the excitons can be converted into light using a process known as

electrophosphorescence, now commonly referred to as phosphorescence. Thus, the efficiency of a phosphorescent OLED is up to four times higher than that of a conventional fluorescent OLED. Universal Display Corporation is the founder and recognized leader in developing the high-efficiency PHOLED™ phosphorescent OLED technology and materials to exploit this discovery.[1]

2.2 The Born-Oppenheimer approximation

Even the simplest molecules are too complex for analytic analysis. Much molecular physics therefore relies on the Born-Oppenheimer approximation. This states that electrons respond approximately instantaneously to the movement of nuclei because of their large mass difference. Thus, when determining the energy levels of a molecule, we may hold the nuclear positions fixed and solve for the electron energies in a static potential. Then by choosing different nuclear arrangements, and repeating the calculation of electron energy, the equilibrium structure of a molecule may be determined. The set of solutions obtained allows us to construct a molecular potential energy curve as a function of configuration coordinates. [2] The analog of this approximation in optical transitions is the Franck-Condon principle. It states that electronic transitions occur within a stationary nuclear framework. As a result, the nuclear configuration of a molecule is unchanged during the process of absorption or emission of a photon, a process that occurs in approximately 10-15 s. But after the electronic transition, the molecule will relax in approximately 10 -13 s and obtain its equilibrium nuclear configuration. The process of absorption is shown in Figure 2.1. The transition occurs from the ground vibrational state of the lower electronic manifold to the vibrational state that it most

resembles in the upper electronic manifold. In that way, the vibrational wavefunction undergoes the least change, which corresponds to the preservation of the nuclear coordinates as required by the Franck-Condon principle. Transitions that alter the electronic configuration but preserve the nuclear coordinates are known as vertical. [2]

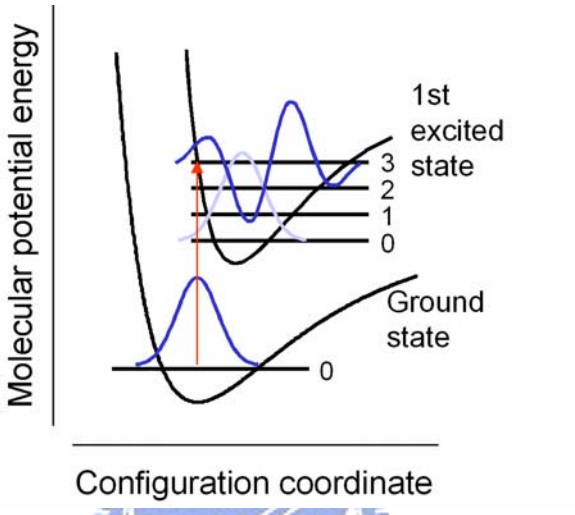

Figure 2.1 The molecule makes a transition from the ground vibrational state to the state with a vibrational wavefunction with the highest overlap with the initial vibrational wavefunction. Adapted from Atkins and Friedman (1997).

2.3 Basic model of exciton formation

It is instructive to discuss, how the process of electron-hole recombination and the formation of a neutral exciton and finally the population of an excited state of the emitter molecule can be visualized. Here, it is focused on processes that occur within the emitter layer of an OLED. This layer of a thickness of about 100 nm consists of an organic matrix which is doped with emitter molecules (dopants). In the subsequent model it is assumed that the recombination of electrons and holes occurs at the dopants. The importance of this process can be deduced from a

comparison of photo-luminescence and electro-luminescence properties.[3] These results show that one of the charge carriers, either hole or electron, can indeed be trapped first at the dopant.

Figure 2.2 displays a simplified and schematic model to describe the process of exciton formation.[4] The first step is characterized by trapping of a charge carrier. In our model it is assumed that the hole is trapped first at the emitter molecule. This has been proposed, for example, for $Ir(F\text{-}ppy)_3$ (= *fac*-tris[2-(4',5'-difluorophenyl)pyridine]Ir(III)) in a PVK matrix.[5] The described process induces (for a short time interval) the formation of an oxidized $Ir(F\text{-}ppy)_3$ complex. Trapping of an electron as first step would result in an equivalent model and might be of relevance for other emitter molecules. The process of charge carrier trapping can induce a reorganization at the emitter molecule. However, this effect is not depicted in the model of Figure 2.2. Under an applied external potential, the electron will migrate along the matrix material towards the anode. Usually, this process of electron hopping (more exactly: polaron hopping) requires a thermal activation energy due to inhomogeneities from spatial and energy disorder and due to matrix reorganization effects. The related energy shifts should be less or of the order of the thermal energy k_BT with k_B being the Boltzmann constant and T the absolute temperature. For clearness, the diagram is simplified and does not show the inhomogeneous distribution of the energy levels of matrix molecules and their energy shifts induced by the external potential.[6]

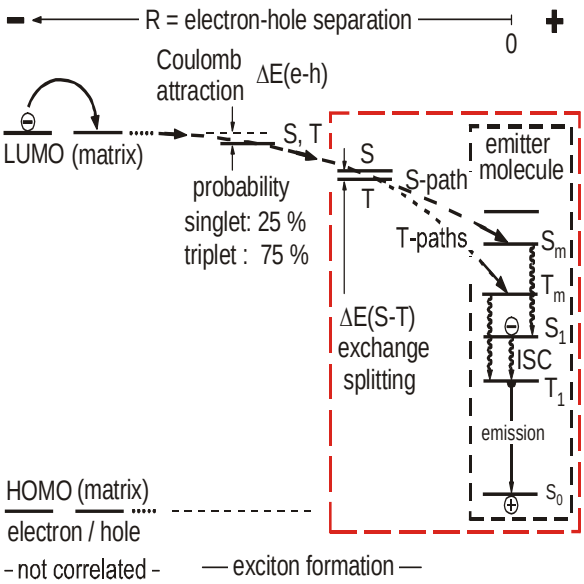

Figure 2.2 Dynamics of exciton formation. It is assumed that at first the hole (+) is trapped on the doped emitter molecule. The exciton formation starts due to Coulomb interaction between the trapped hole and the electron (–) on a matrix molecule. In the beginning of the exciton formation the spins of hole and electron are already correlated to one singlet and three triplet substates. This corresponds in a statistical limit to a ratio of 25 % to 75 %. The S-path and T-paths populate the excited states of the emitter molecule. ISC: intersystem crossing, △E(e-h): electron (e) – hole (h) binding energy; △E(S-T): singlet – triplet splitting.

When the electron is still far from the trapped hole, it will migrate independently from this hole towards the anode. Thus, hole and electron are not bound or correlated. This situation corresponds to the exciton continuum in solid-state semiconductors. However, when the electron migrates into a region given by a specific electron-hole separation R, the positively charged hole will attract the electron. This separation is reached, when the energy of the Coulomb attraction is of similar size as the larger one of the two values,

the mean inhomogeneous distribution of the energy levels of the matrix material or the thermal energy k_BT. Due to the Coulomb attraction, an electron (e) - hole (h) binding results. The binding energy $\Delta E(e\text{-}h)$ is proportional to $1/(\varepsilon \cdot R)$ and thus depends on the separation R and on the dielectric constant ε of the matrix material. Induced by this attraction, the exciton is formed. The Coulomb attraction represents a long-range interaction as compared to nearest neighbor separations.

For the further processes, it is very important to take also the spins of both electron and hole into account. The spin of the hole is given by the spin of the residual electron at the emitter molecule. In a quantum mechanical treatment, the two spins can be coupled to four new combined states: One singlet state and one triplet state. The triplet consists of three triplet substates. These substates differ from each other mainly by their relative spin orientations. An energy splitting between the resulting singlet and triplet states may be disregarded at large electron-hole separations. Therefore, the corresponding exciton state is shown in Figure 2.2 just by one energy level. In a statistical limit, all four substates of this exciton state will be formed (populated) with an equal probability. Consequently, one obtains a population ratio of one to three for singlet and triplet substates, respectively.

Driven by electron-hole attraction, the electron will further move on matrix molecules towards the trapped hole. At least, when the electron reaches nearest neighbor matrix molecules of the emitter, an overlap of electron and hole wavefunctions has to be taken into account. The resulting (short-range) exchange interaction leads to an energy splitting of singlet (S) and triplet (T) states by $\Delta E(S\text{-}T)$. This energy is approximately

proportional to exp(-a·R), wherein a is a constant which depends on the respective matrix and the emitter material.

In a final step, the electron jumps in a very fast process directly to the emitter molecule and it results an excited emitter. This process may occur as singlet or triplet path (S-path, T-paths) depending on the initial spin orientation of the electron-hole pair. The corresponding time constants are of the order of one picosecond (see next section). The population of S_m and T_m states, as shown in Fig. 2.2, is only depicted as an example. Subsequently, the system will exhibit the usual behavior of an optically excited emitter molecule with typical relaxation processes to the lowest excited states and typical emission properties. For detailed discussions of photophysical properties of organometallic triplet emitters it is referred to the Refs.[7,8,9] The electronic states of the emitter compound are characterized by the small frame in the diagram of Figure 2.2**.**

2.4 Charge transfer states and relaxation paths

The final steps of the mechanisms described above can also be discussed in a slightly different way, to illustrate the occurrence of specific singlet and triplet paths. The situation of a lacking electron in the ground state of the doped emitter molecule (dopant D) and of additional electron charge density on nearest neighbor matrix molecules M can be characterized by dopant-to-matrix charge transfer (DMCT) states, specifically by singlet (^{1}DMCT) and triplet (^{3}DMCT) states.

It may be visualized that these states belong to a large molecular unit that consists of the doped emitter itself and of the first nearest neighbors of matrix molecules. The energy level diagram of this emitter-matrix-cage unit is

schematically displayed in Figure 2.3. It corresponds to the large frame depicted in Figure 2.2. In particular, the states S and T shown in the frame represent the ^{1}DMCT and ^{3}DMCT states of the large molecular unit. The lower excited states S_0, T_1, S_1 to S_m are largely confined to the doped molecule itself, while the higher lying charge transfer states are spatially more extended to the first matrix coordination sphere. For these latter states, the exchange interaction between the two electrons involved is relatively small. Thus, the energy separation between the ^{1}DMCT state and the ^{3}DMCT state is expected to be much smaller than singlet-triplet separations of the spatially more confined states of the original dopant itself.

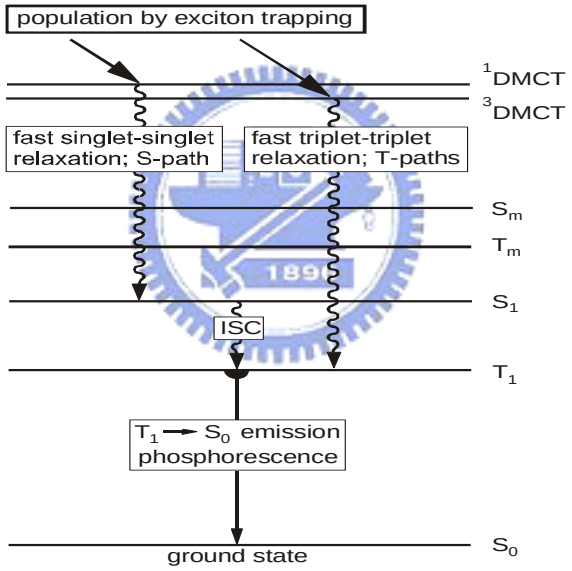

Figure 2.3 Energy level diagram of an emissive molecule with its first coordination sphere of matrix molecules. The states ^{1}DMCT and ^{3}DMCT represent dopant-to-matrix charge transfer states. The lower lying states are largely those of the isolated emitter molecule itself. The relaxations from the ^{1}DMCT and ^{3}DMCT states, respectively, represent the S-path and T-paths of exciton formation as depicted in Figure 2.2.

On the basis of the energy level diagram of Figure 2.3, one also obtains

an information about the relaxation paths from the excited charge transfer states. In particular, the relaxation from the ^{1}DMCT to lower states will be faster within the system of singlet states than making a spin-flip first. This is due to the fact that spin-orbit coupling in the organic matrix material will be relatively small and thus, intersystem crossing (ISC) is not favored. Consequently, one obtains the fast singlet path that finally populates the S_1 state. Subsequently, the population of the S_1 state will be followed by an ISC to the T_1 state, though usually with a smaller rate. An initial population of the ^{3}DMCT state is similarly followed by a very fast relaxation within the system of triplet states down to the lowest triplet state T_1. (Figure 2.3) The beginning of this relaxation process corresponds to the triplet paths in the exciton formation model shown in Figure 2.2. The relaxation times within the singlet and triplet system, respectively, are of the order of one picosecond or faster, while the ISC processes can be significantly

2.5 Triplet harvesting

Spin-orbit coupling induced by the central metal ion of the emitter complex will not strongly alter the mechanism of exciton formation in an organic matrix material, but it will have drastic effects on the efficiency of electro-luminescence in an OLED device. To illustrate this property, we will compare the efficiency which is obtainable with a purely organic molecule to the efficiency achievable with a transition metal complex, if both molecules exhibit equal photo-luminescence quantum yields. If one assumes that the initial process of exciton formation occurs statistically with respect to the spin orientations, one obtains 25 % of excitons with singlet character and 75 % with triplet character. At least for small molecules,

this view is largely accepted. [3-5,10-16]

After exciton formation and relaxations according to the specific singlet and triplet paths, as discussed in the preceeding section, the lowest excited singlet and triplet states are populated. This is valid for organic as well as for organo-transition-metal emitter materials. The corresponding processes are schematically displayed in the middle of Figure 2.4. The organic molecule can exhibit an efficient emission as $S_1 \rightarrow S_0$ fluorescence, since usually the $S_1 \rightarrow T_1$ intersystem crossing rate is small. On the other hand, since the radiative $T_1 \rightarrow S_0$ rate is also small, the deactivation of the T_1 state occurs normally non-radiatively at ambient temperature. Therefore, 75% of the excitons, the triplet excitons, are lost. Their energy is transferred into heat. (Figure 2.4, left hand side.) The conditions are more favorable for transition metal complexes, in which the central metal ion carries significant spin-orbit coupling. (Figure 2.4, right hand side.) This is particularly valid for transition metal ions of the third row of the periodic table. For these complexes, ISC to the lowest T_1 state is usually very efficient and thus a singlet S_1 emission is not observable. Moreover, the radiative $T_1 \rightarrow S_0$ rate can become sufficiently high so that efficient phosphorescence can occur, even at ambient temperature. (For a more detailed discussion see Ref. 4.) Consequently, all four possible spin orientations of the excitons can be harvested to populate the lowest T_1 state. In conclusion, by this process of triplet harvesting one can in principle obtain a four times larger electro-luminescence efficiency for triplet emitters than for singlet emitters.

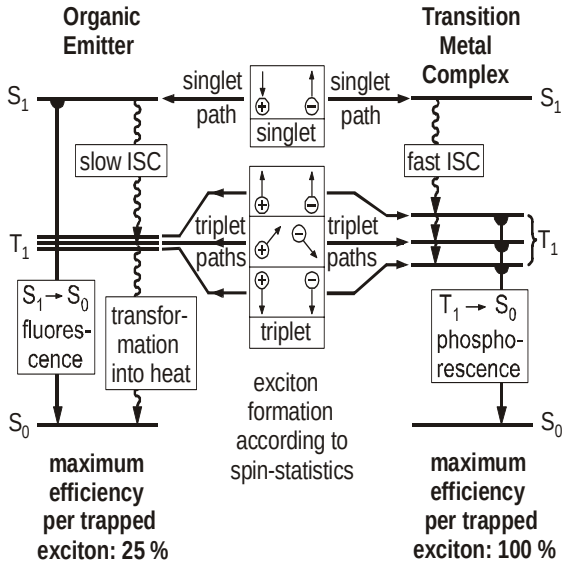

Figure 2.4 The diagram explains the effect of triplet harvesting. Due to spin-statistics, electron-hole recombination leads to 25% singlet and 75% triplet state population. This is a consequence of the occurrence of only one singlet state, but of three triplet substates. In an organic molecule, only the singlet emits light (fluorescence), while the triplet state excitation energy is transferred into heat (left hand side). On the other hand, organometallic compounds with transition metal centers do not exhibit fluorescence, but show a fast intersystem crossing (ISC) to the lowest triplet state. Thus, singlet and triplet excitation energy is harvested in the triplet state and from there can efficiently be converted into light. In principle, a triplet emitter can reach a four times higher light emission efficiency than a singlet emitter.

2.6 Exciton formation at matrix molecules versus charge carrier trapping at emitter compounds[6]

Exciton formation and trapping can also occur at matrix sites. Both the lowest singlet and triplet states of matrix molecules will be populated. From

there, triplet and singlet exciton diffusion as Frenkel excitons can occur, however, with different transport probabilities. This will alter the spatial distribution of matrix molecules that are excited in singlet and triplet states, respectively, as compared to the situation immediately after excitation. For an efficient OLED, it is mostly requested to harvest the excitation energy completely in an efficiently phosphorescent triplet state of an organometallic dopant. This requires the realization of two distinctly different processes of energy transfer. For example, the singlet excitation energy is transferred by a long-range Förster transfer mechanism from a matrix molecule to the acceptor (dopant). Independently, the triplet excitation energy is also transferred to the acceptor, though by a different process of energy transfer, in particular by the short-range Dexter transfer mechanism. Both transfer mechanisms should be highly efficient and therefore should fulfill the resonance conditions. This can be expressed by non-vanishing spectral overlap integrals of donor emissions and acceptor absorptions.

2.7 Fluorescence and Phosphorescence

In most stable molecules, the highest occupied molecular orbital (HOMO) is completely filled in the ground state. Consequently, the ground state wavefunctions of these molecules are spatially symmetric under electron exchange. There are important exceptions such as molecular oxygen, which has two unpaired electrons in different orbitals; but in general, molecules in the ground state have filled orbitals and this determines that they are singlets. Thus, the decay of excited singlet states is allowed, but the decay of triplet states to the ground state is disallowed. Singlet decay is rapid (with rate $k \sim 10^9 s^{-1}$) and if a photon is emitted, the process is known as

fluorescence; see Figure 2.5. Although triplet-to-singlet transitions are forbidden under the processes described above, certain second order effects may mix singlet and triplet states, making the decay of a triplet weakly allowed. Under these circumstances, triplet decay is slow ($k < 10^6 s^{-1}$) and if a photon is emitted, the process is known as phosphorescence.

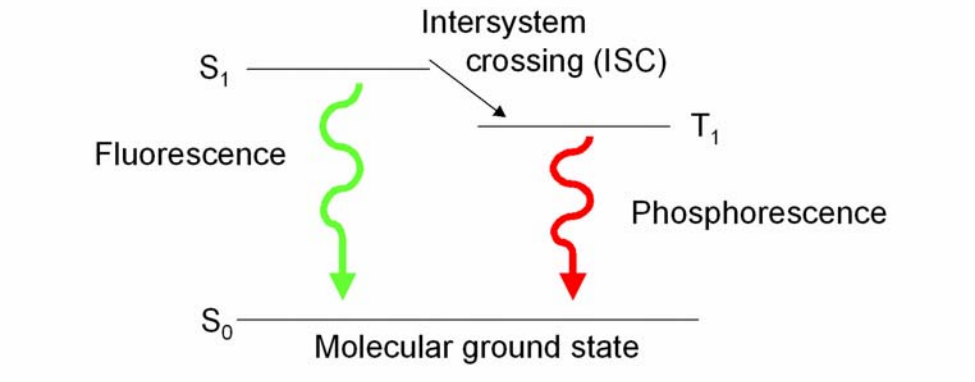

Figure 2.5 The relative positions of the first excited singlet and triplet levels in a typical molecule, showing the origins of fluorescence and phosphorescence.

Singlet-triplet mixing also encourages singlet-to-triplet energy transfer within a molecule, known as intersystem crossing (ISC). The energetic impetus for ISC are electron-electron interactions that break the degeneracy between singlet and triplet levels; for example, if we take a and b to be the individual electron wavefunctions that comprise the wavefunction of the excited state, the Coulomb integral J is defined by

$$J = \frac{e^2}{4\pi\varepsilon_0}\left\langle a(1)b(2)\left|\frac{1}{r_{12}}\right|a(1)b(2)\right\rangle,$$

and the exchange integral K is defined by:

$$K = \frac{e^2}{4\pi\varepsilon_0}\left\langle a(1)b(2)\left|\frac{1}{r_{12}}\right|a(2)b(1)\right\rangle.$$

Considering electron-electron repulsion for wavefunctions that are spatially symmetric and antisymmetric under electron exchange, we get:

$$
\begin{aligned}
E_+ &= \frac{e^2}{4\pi\varepsilon_0}\langle\psi_+|\frac{1}{r_{12}}|\psi_+\rangle \\
&= \frac{e^2}{4\pi\varepsilon_0}\left\langle \tfrac{1}{\sqrt{2}}\{a(1)b(2)+b(1)a(2)\}\middle|\frac{1}{r_{12}}\middle|\tfrac{1}{\sqrt{2}}\{a(1)b(2)+b(1)a(2)\}\right\rangle \\
&= J+K
\end{aligned}
$$

$$
\begin{aligned}
E_- &= \frac{e^2}{4\pi\varepsilon_0}\langle\psi_-|\frac{1}{r_{12}}|\psi_-\rangle \\
&= \frac{e^2}{4\pi\varepsilon_0}\left\langle \tfrac{1}{\sqrt{2}}\{a(1)b(2)-b(1)a(2)\}\middle|\frac{1}{r_{12}}\middle|\tfrac{1}{\sqrt{2}}\{a(1)b(2)-b(1)a(2)\}\right\rangle \\
&= J-K
\end{aligned}
$$

The spatial wavefunction that is antisymmetric under exchange of electrons has a lower energy. Consequently, the triplet state has a lower energy and as shown in Figure 2.5, intersystem crossing of species in their first excited state converts singlets to triplets. The difference between the levels is the exchange energy. Possibly the most important interaction mixing singlet and triplet states is spin- orbit coupling. This refers to the interaction between an electron's spin and the magnetic moment created by the electron oscillating in a closed orbit. We expect that the energy of interaction between the field generated by the electron, **B** , and a magnetic dipole, **m** , should be **-m** • **B** . The magnetic field, **B** , can be related to the angular momentum, **l** , of the electron and consequently, the spin-orbit interaction is proportional to **l** • **s** . It is possible to show that: [17]

$$
H_{so} = -\frac{e}{2m_e^{\,2}c^2 r}\frac{d\phi}{dr}\mathbf{l}\cdot\mathbf{s}, \qquad (2.1)
$$

where m_e is the mass of an electron and $\varphi(r)$ is an isotropic potential. For an electron in

hydrogenic atom, the potential arising from a nucleus of charge Z_e is $\varphi = Z_e/4\pi\varepsilon_0 r$. Substituting this into (2.1) gives:

$$H_{so} = -\frac{Ze^2}{8\pi\varepsilon_0 m_e^2 c^2 r^3}\mathbf{l}\cdot\mathbf{s}$$

The expectation value of r^{-3} for hydrogenic orbitals is proportional to Z^3 . Thus the overall interaction is proportional to Z^4 and spin-orbit coupling is much stronger in heavy atoms than in light atoms. To understand how spin-orbit coupling mixes triplet and singlet states, we re-express the interaction for two electrons as follows:

$$\begin{aligned} H_{so} &= \xi_1\mathbf{l}_1\cdot\mathbf{s}_1 + \xi_2\mathbf{l}_2\cdot\mathbf{s}_2 \\ &= \tfrac{1}{2}(\xi_1\mathbf{l}_1 + \xi_2\mathbf{l}_2)\cdot(\mathbf{s}_1 + \mathbf{s}_2) + \tfrac{1}{2}(\xi_1\mathbf{l}_1 - \xi_2\mathbf{l}_2)\cdot(\mathbf{s}_1 - \mathbf{s}_2) \end{aligned}$$

The operator $s_1 + s_2$ commutes with S^2, the total spin operator, and so it cannot mix states of different multiplicity. However, the operator $s_1 - s_2$ does not commute with S^2, and so this component of the operator is responsible for singlet-triplet mixing.

2.8 Förster energy transfer

Marcus transfer and polaron theories are important examples of electron and exciton transport mediated by the exchange interaction. But dipole-dipole interactions may also facilitate energy transfer. As first recognized by Förster, [18] if the emission of the 'donor' molecule overlaps with the absorption of the 'acceptor' molecule then rapid, long range (< 100Å) energy transfer may occur without the emission of a photon. Where sufficient overlap occurs, this process will dominate and it is essential to the

operation of many biological machines such as photosynthetic units. [19] In this section, we summarize the derivation of the Förster transfer integral. We follow Dexter's derivation, [20] which may be extended to include exchange effects. [§] From Fermi's golden rule we may express the energy transfer rate in terms of a Hamiltonian *H* and the density of states ρ.

$$P_{da} = (2\pi/\hbar)\left|\left\langle \Psi_I^* \middle| H \middle| \Psi_F \right\rangle\right|^2 \rho(E), \quad (2.27)$$

where Ψ_I^* is the initial state with excited donor and ground state acceptor, and Ψ_F is final state with ground state donor and excited acceptor. Now, the dipole-dipole interaction is:

$$H(\mathbf{R}) = \frac{1}{4\pi\varepsilon_r\varepsilon_0 R^3}\left(\boldsymbol{\mu}_d \cdot \boldsymbol{\mu}_a - 3\left(\boldsymbol{\mu}_d \cdot \hat{\mathbf{R}}\right)\left(\boldsymbol{\mu}_a \cdot \hat{\mathbf{R}}\right)\right), \quad (2.28)$$

where ε_r is the relative dielectric constant, and ε_0 is the permittivity of free space; μ_d and μ_a are the respective electric dipole moment operators on the donor and acceptor molecules; and $\hat{R}$ is the unit vector between the donor and acceptor molecules. Substituting this into the expression the transition probability:

$$P_{da} = \frac{1}{12\pi\hbar\varepsilon_r^2\varepsilon_0^2 R^6}\int dE \int \rho_a(\omega_a)\left|\left\langle \psi_a^* \middle| \boldsymbol{\mu}_a \middle| \psi_a \right\rangle\right|^2 d\omega_a \int \rho_d(\omega_d)\left|\left\langle \psi_d \middle| \boldsymbol{\mu}_d \middle| \psi_d^* \right\rangle\right|^2 d\omega_d \quad (2.29)$$

where $E=h\nu$ is the energy of the transition on both the donor and acceptor molecules, and where we have averaged Eq. (2.28) over all possible orientations of R , i.e.

$$\left\langle \left| \langle \boldsymbol{\mu}_d \rangle \cdot \langle \boldsymbol{\mu}_a \rangle - (3/R^2)(\langle \boldsymbol{\mu}_d \rangle \cdot \mathbf{R})(\langle \boldsymbol{\mu}_a \rangle \cdot \mathbf{R}) \right|^2 \right\rangle = (2/3)\left|\langle \boldsymbol{\mu}_d \rangle\right|^2 \left|\langle \boldsymbol{\mu}_a \rangle\right|^2.$$

[§] Although Dexter highlighted the importance of exchange interactions in the transfer of excitons, he did not consider molecular distortions and phonons. Thus, as a quantitative description, Marcus or polaron theory is preferred.

We may express Eq. (2.29) in terms of the emission and absorption spectra of the donor and acceptor molecules. For example:

$$A(E)=\frac{E^3}{3\pi\varepsilon_0\hbar^4c^3}\int\rho_d(\omega_d)\left|\langle\psi_d|\mu_d|\psi_d^*\rangle\right|^2 d\omega_d\,, \tag{2.30}$$

$$\alpha(E)=\frac{n(E)E\pi}{3\varepsilon_0\hbar c}\int\rho_a(\omega_a)\left|\langle\psi_a^*|\mu_a|\psi_a\rangle\right|^2 d\omega_a\,, \tag{2.31}$$

where $A(E)$ is the coefficient of spontaneous emission of the donor, $\alpha(E)$ is the absorption coefficient of the acceptor, and $n(v)$ is the number density of acceptor molecules able to absorb light in the energy range E , $E + dE$. Substituting Eqs. (2.30) and (2.31) into Eq. (2.29) we get:

$$P_{da}=\frac{3\hbar^4c^4}{4\pi\varepsilon_r^{\,2}R^6}\int\frac{\alpha(E)A(E)}{E^4n(E)}dE\,. \tag{2.32}$$

In terms of the normalized donor emission spectrum $f_d(E)$ and the normalized acceptor absorption spectrum $F_d(E)$:

$$P_{da}=\frac{3\hbar^4c^4}{4\pi\varepsilon_r^{\,2}R^6}\frac{\alpha_a}{N_a}\frac{1}{\tau_d}\int\frac{f_d(E)F_a(E)}{E^4}dE\,. \tag{2.33}$$

Here a $\alpha_a=\int\alpha\,dE$ is the total absorption coefficient of the acceptor ($J\cdot m^{-1}$), N_a a is the number density of acceptor molecules (m^{-3}), and $\tau_d=1/A$ is the actual mean lifetime of the donor. Equation (2.33) can be expressed conveniently as:

$$P_{da}=\left(\frac{R_0}{R}\right)^6\frac{1}{\tau_d}, \tag{2.34}$$

where

$$R_0^6=\frac{3\hbar^4c^4}{4\pi\varepsilon_r^{\,2}}\frac{\alpha_a}{N_a}\int\frac{f_d(E)F_a(E)}{E^4}dE\,. \tag{2.35}$$

In typical cases, R_0 ranges from 50Å to 100Å. Many organic electroluminescent devices employ an amorphous emissive layer comprising a charge transport material together with a highly luminescent guest molecule. Providing that there is sufficient overlap between the absorption of the luminescent guest molecules and the emission of the charge transport host materials, then an R_0 value of 50-100Å corresponds to a required minimum guest molecule concentration of between 0.01% and 0.1%. Note that from Eq. (2.34) the efficiency of energy transfer is:

$$\eta_{ET} = \frac{1}{1+(R/R_0)^6}. \qquad (2.36)$$

Thus, we have almost complete energy transfer for $R < R_0$.

2.9 Dexter energy transfer (electron exchange excitation transfer)

The field from a charge carrier in an amorphous organic material distorts the local lattice. Excitation transfer occurring as a result of an electron exchange mechanism. It requires an overlap of the wavefunctions of the energy donor and the energy acceptor. It is the dominant mechanism in triplet-triplet energy transfer. The transfer rate constant, k_{ET}, is given by:

$$k_{ET} \propto [h/(2\pi)]P^2 J \exp[-2r/L]$$

where r is the distance between donor (D) and acceptor (A), L and P are constants not easily related to experimentally determinable quantities, and J is the spectral overlap integral. For this mechanism the spin conservation rules are obeyed. If the electron clouds of D* and A overlap, electron exchange (simply a noting of the indistinguishability of electrons) may occur in the overlap region. The closer the donor acceptor distance RDA, the better the overlap. This is essentially energy transfer via collisions

(interpenetrating electron cloud density).

The rate of dexter energy transfer:

k_{ET}(exchange) = KJ exp(-2RDA/L) , K = specific orbital interactions

$$J = \int_0^\infty a(\tilde{\nu}) f(\tilde{\nu}) d\tilde{\nu}$$

spectral overlap for normalized εA of acceptor (this means it does not depend on the absolute magnitude of εA but on the relative values)

Fluorescence Same as Forster

$$f(\tilde{\nu}) = \frac{F_D(\tilde{\nu})}{\int_0^\infty F_D(\tilde{\nu}) d\tilde{\nu}} \quad thus \quad \int_0^\infty f\ (\tilde{\nu}) d\tilde{\nu} = 1$$

Absorption is normalized, thus may use A (absorbance instead of εA)

$$a(\tilde{\nu}) = \frac{A_A(\tilde{\nu})}{\int_0^\infty A_A(\tilde{\nu}) d\tilde{\nu}} \quad thus \quad \int_0^\infty a_A(\tilde{\nu}) d\tilde{\nu} = 1$$

Thus J has units of (energy)$^{-1}$ or cm. **L** = van der Waals radii of D&A.

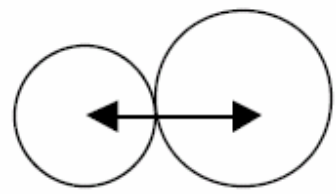

Note: Both Forster and Dexter theory depend on spectral overlap integral, J.

Visualization of energy transfer via electron exchange – essentially this occurs by exchanging a high energy electron of D* (LUMO of D) with low energy electron (HOMO) of A resulting in D A*

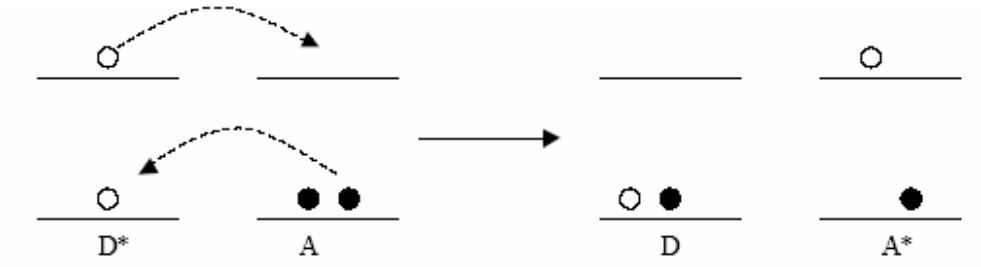

This exchange may occur via (1) a concerted process (2) stepwise via radical ion pair or (3) chemical or covalent bonding exchange of electrons via intermediate diradical or zwitterion formation.

2.10 Summary

Organo-transition-metal triplet emitters have a great potential to be applied in OLEDs. Thus, an understanding of the processes, which lead to electron-hole recombination (exciton formation) and to the population of the emissive triplet states is presented. In particular, it is shown that the dynamical process of exciton formation and trapping on an emitter molecule involves charge transfer states which result from excitations of the dopant to its nearest neighbor matrix environment. Individual singlet and triplet relaxation paths lead to the population of the lowest excited singlet and triplet states of the dopant. In typical organic molecules with weak spin-orbit coupling and highly forbidden triplet-singlet transitions, triplet state population is transferred into heat (at ambient temperature). Only the singlet state can emit radiatively (fluorescence). On the other hand, in organo-transition-metal compounds, fast intersystem crossing induced by spin-orbit coupling (SOC) effectively depopulates the excited singlet into the lowest triplet state. Again due to SOC, the triplet can decay radiatively as phosphorescence even with high emission quantum yield at ambient temperature. In case of validity of spin statistics only 25% of the excitons

can be exploited by organic emitters, while for triplet emitters additional 75% of the excitons are harvested. Thus, the efficiency of light emission in an electro-luminescent device with triplet emitters can be by a factor of four higher than with singlet emitters.[6] Successful utilization of phosphorescence holds enormous promise for organic electroluminescent devices. An advantage of phosphorescence is that all excitons (formed by the recombination of holes and electrons in an EL), which are formed either as a singlet or triplet excited state, may participate in luminescence. This is because the lowest singlet excited state of an organic molecule is typically at a slightly higher energy than the lowest triplet excited state. This means that, for typical phosphorescent organometallic compounds, the lowest singlet excited state may rapidly decay to the lowest triplet excited state from which the phosphorescence is produced. In contrast, only a 25% of excitons in fluorescent devices are believed to be capable of producing the fluorescent luminescence that is obtained from a singlet excited state. In the lowest triplet excited state of an organic molecule are typically not capable of being converted into the energetically unfavorable higher singlet excited states from which the fluorescence is produced. This energy, thus, becomes lost to radiationless decay processes that only tend to heat-up the device.

2.11 References

1. http://www.universaldisplay.com/pholed.htm

2. Atkins, P. W. & Friedman, R. S. Molecular Quantum Mechanics (Oxford University Press, New York, 1997).

3. Su, Y.-J.; Huang, H.-L.; Chien-Le, L.; Chien, C.-H.; Tao, Y.-T.; Chou, P.-T.; Datta, S.; Liu, R.-S.: *Adv. Mater*. 15 (2003) 884

4. Yersin, H.: *Top. Curr. Chem*. 241 (2004) 1

5. Lamansky, S.; Kwong, R.C.; Nugent, M.; Djurovich, P.I.; Thompson, M.E.: *Organic Electronics* 2 (2001) 53

6. http://www.uni- regensburg.de/Fakultaeten/ nat_Fak_IV/ Physikalische_Chemie/ Yersin/ OLEDvde.htm

7. Yersin, H.; Donges, D.: Top. *Curr. Chem*. 214 (2001) 81

8. Finkenzeller, W.; Yersin, H.: *Chem. Phys. Lett.* 377 (2003) 299

9. Finkenzeller, W.; Stoessel, P.;Yersin, H.: *Chem. Phys. Lett*. 397 (2004) 289

10. Lin, Y.-Y.; Chan, S.-C.; Chan, M.C.W.; Hou, Y.-J.; Zhu, N.; Che, C.-M.; Liu Y.; Wang Y.: *Chem. Eur. J*. 9 (2003) 1263

11. Lamansky, S.; Djurovich, P.I.; Murphy, D.; Abdel-Razzaq, F.; Kwong, R.; Tsyba, I.; Bortz, M.; Mui, B.; Bau, R.; Thompson, M.E.: *Inorg. Chem*. 40 (2001) 1704

12. Brooks, J.; Babayan, Y.; Lamansky, S.; Djurovich, P.I.; Tsyba, I.; Bau, R.; Thompson, M.E.: *Inorg. Chem*. 41 (2002) 3055

13. Grushin, V.V.; Herron, N.; LeCloux, D.D.; Marshall, W.J.; Petrov, V.A.; Wang, Y.: *Chem. Commun*. 41 (2001) 1494

14. Lo, S.-C.; Male, N.A.H.; Markham, J.P.J.; Magennis, S.W.; Burn, P.L.; Salata, O.V.; Samuel, I.D.W.: *Adv. Mater.* 14 (2002) 975

15. Tsuzuki, T.; Shirasawa, N.; Suzuki, T.; Tokito, S.: *Adv. Mater*. 15 (2003) 1455

16. Gong, X.; Robinson, M.R.; Ostrowski, J.C.; Moses, D.; Bazan, G.C.; Heeger, A.J.: *Adv. Mater*. 14 (2002) 581

17. Atkins, P. W. & Friedman, R. S. Molecular Quantum Mechanics (Oxford University Press, New York, 1997).

18. Förster, T. Transfer mechanisms of electronic excitation. Discussions of the Faraday Society 27 , 7-17 (1959).

19. Renger, T., May, V. & Kuhn, O. Ultrafast excitation energy transfer dynamics in photosynthetic pigment-protein complexes. *Physics Reports* 343 (2001) 137-254.

20. Dexter, D. L. A theory of sensitized luminescence in solids. *Journal of Chemical Physics* 21 (1953) 836-850.

Chapter 3

Effect of Substituents in the photoluminescent and electroluminescent properties of substituted cyclometalated iridim(III) complexes

Abstract

The photophysics of octahedral $4d^6$ and $5d^6$ complexes has been studied extensively. The d^6 iridium(III) complexes show intense phosphorescence at room temperature. Our goal of this research is to study the synthesis, characterization and applications of the light emitting dopants based on iridium(III) complexes. We have prepared and characterized a series of substituted (4-CF_3, 4-Me, 4-OMe, 4-F, 3-F) 2-phenylbenzoxazole ligand. The intermediate di-irrido and the six-coordinated mononuclear iridium (III) dopants of the above ligands have been synthesized and characterized. These complexes are thermally stable between 280-320°C depending upon the substituents and sublimable. They emit bright yellow to green light. The peak emission wavelengths of the dopants can be finely tuned depending upon the electronic properties of the substituents as well as their positions in the ring. The emission spectral diagrams show that the emissive states of the complexes have major contribution of MLCT state. In the absorption spectra, the ^{1}MLCT and ^{3}MLCT transitions have been resolved in the range, 385-500 nm.. The physical parameters of the electroluminescent devices for the substituted and the unsubstituted complexes has been compared and discussed.

3.1 Introduction

A significant research effort has been focused on the synthesis and

photophysical characterization of octahedral $4d^6$ and $5d^6$ metal complexes. Luminescent d^6 metal complexes of Re(I), Ru(II), Os(II) and Ir(III) have attracted considerable attention due to their intriguing photophysical, photochemical and excited state redox properties[1] and potential applications in photonic and photoelectronic devices.[2] Strong spin-orbit coupling of the 4d or 5d ion leads to efficient intersystem crossing of the singlet excited states to the triplet manifold. More recently, a number of groups have investigated the Rh^{3+} and Ir^{3+} metal complexes and there also have been growing interests in electroluminescent devices (EL) with phosphor complex dopants of the above metals as emitting layers.[3-6] The research group lead by Mark Thompson *et al* has synthesized and reported a series of neutral emissive cyclometalated complexes of iridium(III)[7] and platinum(II)[8] and used them in the fabrication of organic light emitting diode (OLEDs) as a phosphorescent dopant successively. Researchers from Dupont de Nemours and Co. have also synthesized and characterized a series of iridium(III) complexes with fluorinated 2-arylpyridines and showed that the emissive colors of the materials can be finely tuned by systematic control of the nature and position of the substituents of the ligands.[9] These research activities inspired us to initiate a systematic study to investigate the color tuning of the iridium(III) complexes by choosing a particular cyclometalated ligand with substituents exhibiting different electronic properties. Of the above phosphor emitters that have been reported for (OLED) devices, iridium(III)- based materials have displayed the most promising due to their high stability, high photoluminescence (PL) efficiency and relatively short excited state lifetime. So, we choose 2-phenylbenzoxazole (bo) as the cyclometalated ligand with substituents (i.e., $-CF_3$, -F, -Me, -OMe) showing different electronic properties to synthesize mononuclear emissive complex

with iridium(III). We present the syntheses and photo physical studies of $(x/ybo)_2Ir(acac)$ (x = 4-CF_3, 4-F, 4-Me, 4-OMe; y = 3-F; acac = acetylacetonate) and their applications in OLEDs.

3.2 Experimental Section

3.2.1 Materials.

All of the preparative work involving iridium(III) trichloride hydrate ($IrCl_3 \cdot 3H_2O$, Alfa Aesar Company Ltd.), 2-ethoxyethanol ($H_5C_2OC_2H_4OH$, Fluka) and all other reagents (Tokyo Chemical Industry, Japan) were carried out in inert atmosphere and used without further purification.

3.2.2 Optical Measurements and Compositions Analysis.

The ultraviolet-visible (UV-VIS) spectra of the phosphorescent Ir(III) complexes were measured on an UV-VIS spectrophotometer (Agilent model 8453) and corrected for background due to solvent absorption. Photoluminescence (PL) spectra were carried out with a spectrophotometer (Jobin-Yvon Spex, model Fluorolog-3). Solution photoluminescence quantum efficiency were measured by a relative method [22] using $Ir(ppy)_3$[21] as standard in dichloromethane. NMR spectra were recorded on Varian 300 MHz and MS spectra (both EI and FAB) were taken on an Micromass TRIO-2000. Cyclic voltammetry (CV) analyses were performed by using CHI 2.05, the TG-DTA analysis was carried out by using a thermal analyzer (SEIKO 1TG/DTA 200).

(a) Synthesis of x/y(bo) (x = 4-CF_3, 4-F, 4-Me, 4-OMe and y = 3F ; bo = 2-phenylbenzoxazole) and complexes with unsubstituted ligands .

Synthesis of x/y(bo) (x = 4-CF_3, 4-F, 4-Me, 4-OMe and y = 3-F; bo = (2-phenyl) benzoxazole): These were prepared by a general method [10] where

10 mmol o-aminophenol was dissolved into 20 ml of 1-methyl-pyrrolidinone under inert atmosphere; then the stoichiometric amount of the corresponding acid chloride was added slowly at room temperature. The mixture was heated at 100°C for one hour. After cooling, the solution was poured into cold water and the mixture was adjusted to pH 8-9 with 7N aqueous ammonia. A white colored solid compound was separated out. The crude material was filtered, washed with water for several times and then purified by column chromatography.

bo：2-phenylbenzoxazole. ^{1}H NMR (300 MHz, $CDCl_3$): 7.86 (m, 3H), 7.64 (d, 8.1, 1H), 7.25 (m, 4H), 7.13 (m, 1H), EIMS : m/z 195, Calc. 195.

(4-MeO)bo : (4-methoxy)2-phenylbenzoxazole. ^{1}H NMR (300 MHz, $CDCl_3$) : 8.22 (d, 2H, J 1.5 Hz), 7.74 (m, 1H), 7.56 (m, 1H), 7.31 (m, 2H), 3.90 (s, 3H), EIMS : m/z 225, Calc. 225.

(4-CF_3)bo : (4-trifluoromethyl)2-phenylbenzoxazole. ^{1}HNMR (300 MHz, $CDCl_3$) : δ, ppm 8.38 (d, 2H, J 8.1 Hz), 8.11 (d, 3H, J 3.3 Hz), 7.61 (m, 1H), 7.44 (m, 2H), EIMS: m/z: 263, Calc. 263.

(4-Me)bo : (4-methyl)2-phenylbenzoxazole. ^{1}HNMR (300 MHz, $CDCl_3$) : δ, ppm 8.05 (d, 1H, J 8.4 Hz), 7.98 (d, 2H, J 8.4 Hz), 7.88 (dd, 1H, J 0.6, 8.1 Hz), 7.47 (t, 1H, J 7.5 Hz), 7.36 (t, 1H, J 7.2 Hz), 7.27 (d, 2H, J 7.8 Hz). EIMS: m/z: 209, Calc. 209.

(4-F)bo : (4-fluoro)2-phenylbenzoxazole. ^{1}HNMR (300 MHz, $CDCl_3$) : δ, ppm 8.35 (s, 1H), 7.93 (m, 1H), 7.90 (m, 2H), 7.14 (m, 2H),

7.05 (d, 1H, J 8.1 Hz), 6.91 (t, 1H, J 6.6, 6.9 Hz). EIMS: m/z: 213, Calc. 213.

(3-F)bo : (3-fluoro)2-phenylbenzoxazole. ^{1}HNMR (300 MHz, $CDCl_3$) : δ, ppm 8.21 (s, 1H), 7.66 (m, 2H), 7.52 (m, 2H), 7.17 (d, 1H. J 8.7), 7.07 (d, 1H, J 8.1 Hz), 6.95 (t, 1H, J 6.3, 6.9 Hz). EIMS: m/z: 213, Calc. 213.

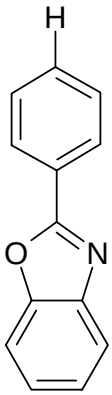

bo

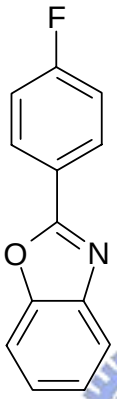

(4-F)bo

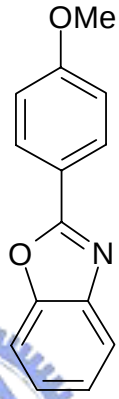

(4-MeO)bo

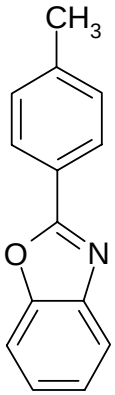

(4-Me)bo

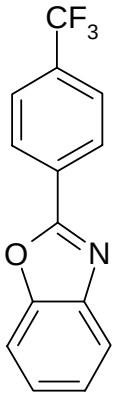

(4-CF_3)bo

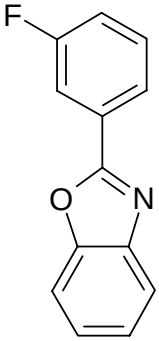

(3-F)bo

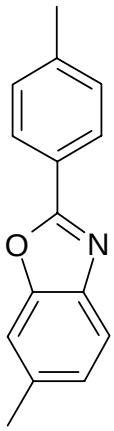

(4-MeO)-2-phenyl-3-methoxy-benzoxazole

(b) Synthesis of dinuclear iridium(III) complexes, x/y(bo)$_2$Ir(μ-Cl)$_2$x/y(bo)$_2$

Synthesis of the dichoro-bridged iridium (III) complexes, x/ybo$_2$Ir(μ-Cl)$_2$x/ybo$_2$: These were prepared by refluxing the mixture of $IrCl_3$ (1 mmol) and the ligands (x/ybo) (2.4 mmol) in 2-ethoxyethanol for 24~25hr. The orange-yellow mixture was cooled to room temperature and 20 ml 1 M HCl was added to precipitate the product. The mixture was filtered and washed with 100 ml 1M HCl followed by 50 ml methanol solution for several times then dried.

[Ir(bo)$_2$Cl$_2$]$_2$: ^{1}HNMR (300 MHz, $CDCl_3$) :δ, ppm 8.23 (d, 4H, J 7.8 Hz), 7.56 (d, 4H, J 7.5 Hz), 7.16 (d, 4H, J 7.2 Hz), 6.96 (d, 4H, J 7.5 Hz), 6.72 (d, 4H, J 7.2 Hz), 6.05 (s, 4H), 1.98 (s, 12 H). FABMS : m/z 1232, Calc. 1232.

[Ir(4-MeObo)$_2$Cl$_2$]$_2$: ^{1}HNMR (300 MHz, $CDCl_3$) : δ, ppm 8.14 (d, 4H, J 7.8 Hz), 7.55 (d, 4H, J 8.4, 2.4 Hz), 7.25 (d, 4H, J 9.0 Hz), 7.00 (t, 4H, J 7.5, 8.4 Hz), 6.86 (t, 4H, J 8.1, 7.2 Hz), 6.44 (d, 4H, J 8.7 Hz), 5.71 (s, 4H), 3.25 (s, 12 H). FABMS: m/z 1351, Calc. 1351.

[Ir(4-CF$_3$bo)$_2$Cl$_2$]$_2$: ^{1}HNMR (300 MHz, $CDCl_3$) : δ, ppm 8.12 (d, 4H, J 7.2 Hz), 7.76 (d, 4H, J 8.1 Hz), 7.41 (d, 4H, J 8.4 Hz), 7.29 (d, 4H, J, 0.06 Hz), 7.16 (d, 4H, J, 7.8 Hz), 7.01 (t, 4H, J, 8.4, 8.1 Hz), 6.38 (s, 4H). FABMS: m/z 1504, Calc. 1504.

[Ir(4-Mebo)$_2$Cl$_2$]$_2$: ^{1}HNMR (300 MHz, $CDCl_3$) : ^{1}HNMR (300 MHz, $CDCl_3$) : δ, ppm 8.23 (d, 4H, J 7.8 Hz), 7.56 (d, 4H, J 7.5 Hz), 7.16 (d, 4H, J 7.2 Hz), 6.96 (d, 4H, J 7.5 Hz), 6.72 (d, 4H, J 7.2 Hz), 6.05 (s, 4H), 1.98 (s, 12 H).

FABMS : m/z 1287, Calc. 1287.

$[Ir(4\text{-}Fbo)_2Cl_2]_2$: ^{1}HNMR (300 MHz, $CDCl_3$) :δ, ppm 8.16 (d, 4H, J 8.1 Hz), 7.69 (dd, 4H, J 5.7, 7.8 Hz), 7.35 (d, 4H, J 8.1 Hz), 7.17 (t, 4H, 8.4, 7.8 Hz), 6.96 (t, 4H, 8.1, 7.5 Hz), 6.67 (t, 4H, J 8.7, 8.6 Hz), 5.82 (dd, 4H, 9.9, 1.2 Hz). FABMS: m/z 1303, Calc. 1303.

$[Ir(3\text{-}Fbo)_2Cl_2]_2$: ^{1}HNMR (300 MHz, $CDCl_3$) :δ, ppm 8.33 (d, 4H, J 8.1 Hz), 7.63 (d, 4H, J 6.6 Hz), 7.20 (m, 8H), 7.02 (m, 8H), 6.37 (s, 4H). FABMS: m/z 1303, Calc. 1303.

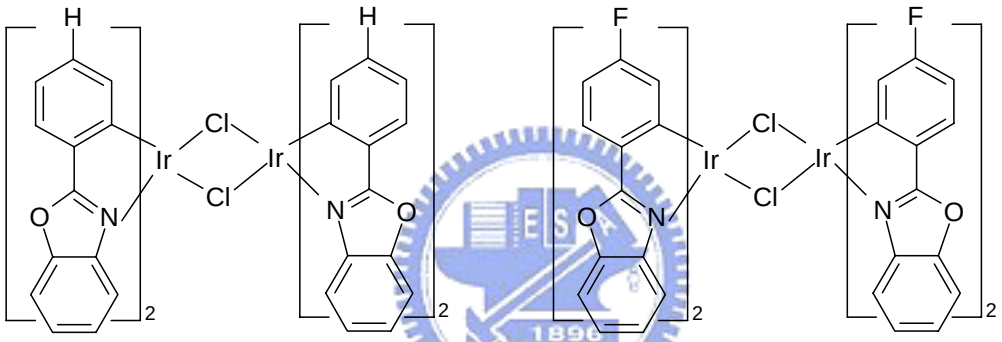

$[Ir(bo)_2Cl_2]_2$ $[Ir(4\text{-}Fbo)_2Cl_2]_2$

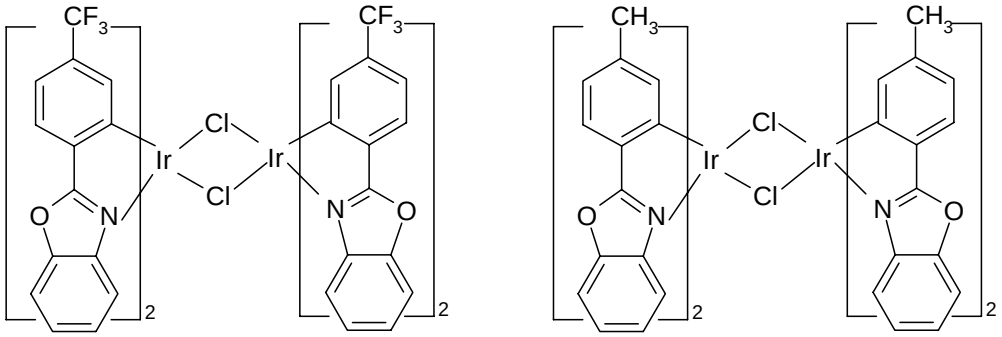

$[Ir(4\text{-}CF_3bo)_2Cl_2]_2$ $[Ir(4\text{-}Mebo)_2Cl_2]_2$

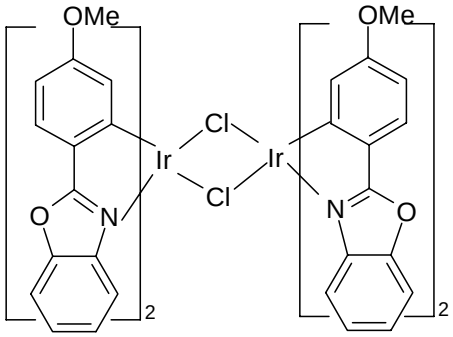

$[Ir(4\text{-}MeObo)_2Cl_2]_2$

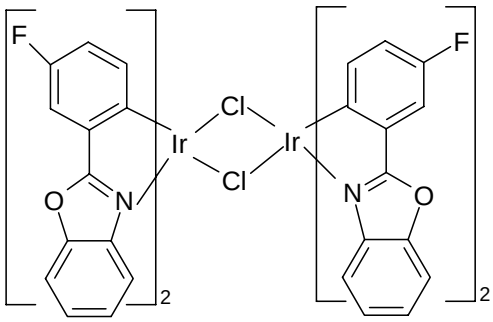

$[Ir(3\text{-}Fbo)_2Cl_2]_2$

(c) Syntheses of mononuclear iridium(III) complex dopants $(x/ybo)_2Ir(acac)$

The chloride bridged dinuclear iridium(III) complex $(x/ybo)_2Ir(\mu\text{-}Cl)_2Ir(x/ybo)_2$ (0.1 mmol), acetylacetone (0.3 *m*mol) and sodium carbonate (1 *m*mol) were mixed in 10 ml of 2-ethoxyethanol (30 ml). The mixture was refluxed under nitrogen for 11 - 12 hr. The reaction mixture was then cooled and the resulted precipitate was collected through filtration. The product was purified by recrystallization from a solution of the mixture of dichloromethane and methanol (2 : 1).

$Ir(bo)_2(acac)$: ^{1}HNMR (300 MHz, $CDCl_3$) : δ, ppm 8.25 (d, 2H), 7.93 (m, 2H), 7.74 (dd, 2H, J 8.1, 1.9 Hz), 7.56 (m, 4H), 6.86 (td, 2H, J 7.8, 1.1 Hz), 6.59 (td, 2H, J 7.5, 1.0 Hz), 6.2 (d, 2H, 7.5 Hz), 5.12 (s, 1H), 1.71 (s, 6H). FABMS : m/z 680, Calc. 680.

$Ir(4\text{-}MeObo)_2(acac)$: ^{1}HNMR (300 MHz, $CDCl_3$) : δ, ppm 7.59 (d, 4H, J 8.4 Hz), 7.47 (m, 2H), 7.34 (m, 4H), 6.45 (dd, 2H, J 8.4, 2.4 Hz), 5.98 (s, 2H), 5.22 (s, 2H), 3.47 (s, 6H), 1.82 (s, 6H). FABMS : m/z 741, Calc. 741

$Ir(4\text{-}CF_3bo)_2(acac)$: ^{1}HNMR (300 MHz, $CDCl_3$) : δ, ppm 7.74 (t, 4H, J 8.1,

7.8 Hz), 7.51 (t, 4H, J 6.9, 7.2 Hz), 7.43 (d, 2H, J 8.1 Hz), 7.13 (d, 2H, J 8.7 Hz), 6.64 (s, 2H), 5.24 (s, 1H), 1.83 (s, 6H). FABMS : m/z 816, Calc. 816.

$Ir(4\text{-}Mebo)_2(acac)$: ^{1}HNMR (300 MHz, $CDCl_3$) : ^{1}HNMR (300 MHz, $CDCl_3$) : δ, ppm 7.64 (d, 2H, J 6.9 Hz), 7.51 (m, 4H), 7.36 (m, 4H), 6.67 (d, 2H, J 7.2 Hz), 6.29 (s, 2H), 1.95 (s, 6H), 1.81 (s, 6H). FABMS : m/z 708, Calc. 708.

$Ir(4\text{-}Fbo)_2(acac)$: ^{1}HNMR (300 MHz, $CDCl_3$) : δ, ppm 7.65 (t, 4H, J 8.7, 5.7 Hz), 7.43 (m, 6H), 6.60 (m, 2H), 6.09 (d, 2H, J 9.9 Hz), 5.26 (s, 1H), 1.83 (s, 6H). FABMS : m/z 716, Calc. 716.

$Ir(3\text{-}Fbo)_2(acac)$: ^{1}HNMR (300 MHz, $CDCl_3$) : δ, ppm 7.65 (d, 2H, J 7.8 Hz), 7.54 (m, 4H), 7.41 (m, 4H), 6.91 (m, 2H), 6.39 (t, 2H, J 8.4, 8.4 Hz), 5.30 (s, 2H), 1.86 (s, 6H). FABMS : m/z 716, Calc. 716.

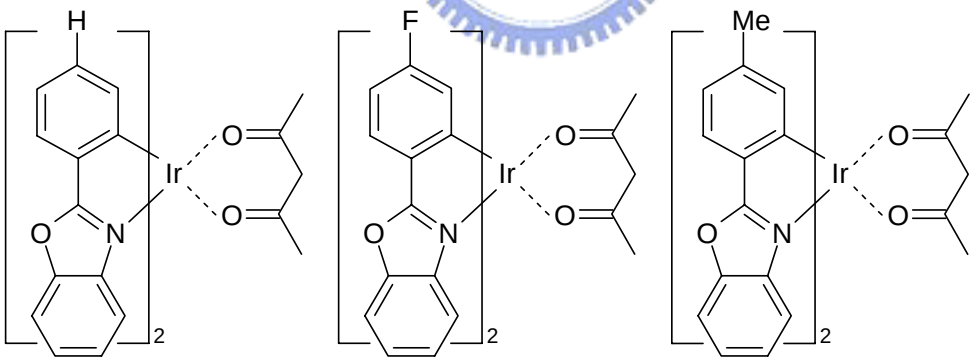

$Ir(bo)_2(acac)$ $Ir(4\text{-}Fbo)_2(acac)$ $Ir(4\text{-}Mebo)_2(acac)$

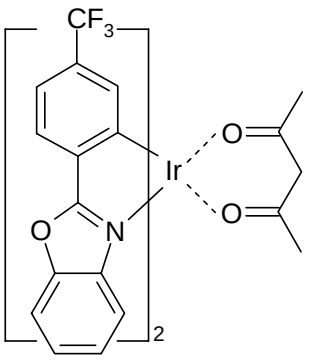

Ir(4-CF_3bo)$_2$(acac)

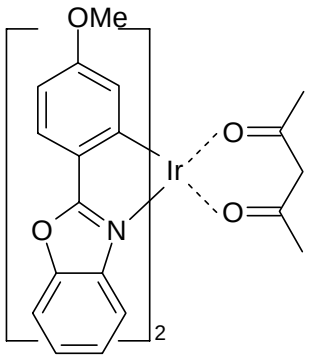

Ir(4-OMebo)$_2$(acac)

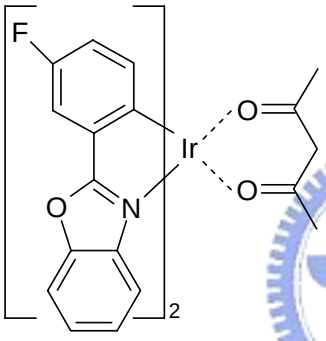

Ir(3-Fbo)$_2$(acac)

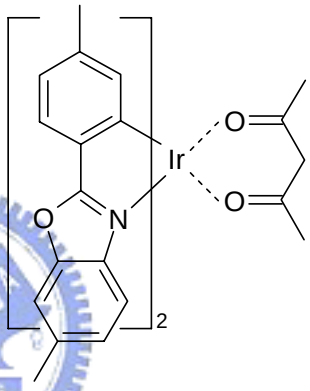

Ir(4-Me-2-phenyl-3-methoxy-bo)$_2$(acac)

3.2.3 Crystallography

Diffraction data for (CF_3bo)$_2$Ir(acac) single crystals were collected on a Bruker CCD diffractometer with Mo Kα (λ= 0.71073 Å). Data collection in the 2θ scan mode, cell refinement and data reduction were carried out using program Bruker SHELXTL. The structure was solved by direct methods using the SHELXS-97 package of computer programs. The structure was refined by full-matrix least-squares methods based on F^2 using SHELXL-97. The non-hydrogen atom positions were refined anisotropically whereas the hydrogen positions were not refined.

3.2.4 OLED Fabrication and Testing

Organic layers were fabricated by high-vacuum thermal evaporation onto a glass substrate precoated with an indium-tin-oxide (ITO) layer with a sheet resistance of 20 Ω. Prior to use, the ITO surface was ultrasonicated in a detergent solution followed by rinsing with deionized (DI) water, dipped into acetone, trichloroethylene, and 2-propanol, and then degreased with a vapor of 2-propanol. After degreasing, the substrate was oxidized and cleaned in a UV-ozone chamber before it was loaded into an evaporator. In a vacuum chamber at pressure of 10^{-6} torr, 500 Å of NPB as the hole transporting layer; 200 Å the complex doped (7%) CBP as the emitting layer; 100 Å of 2, 9-dimethyl-4,7-diphenyl-1, 10-phenanthroline (BCP) as a hole and exciton blocking layer (HBL); 650 Å of Alq_3 as electron transport layer; and a cathode composed of 10 Å lithium fluoride and 2000 Å aluminum were sequentially deposited onto the substrate to give the device structure. The current-voltage (I-V) profiles and light intensity characteristics for the above-fabricated devices were measured in a vacuum chamber of 10^{-6} Torr at ambient temperature using a Keithley 2400 Source Meter/2000 Multimeter coupled to a PR 650 Optical Meter.

3.3 Results and Discussion

3.3.1 Synthesis and Characterization of $(x/ybo)_2Ir(acac)$ complexes.

Iridium complexes were prepared according to the procedure reported previously [11]. The synthesis of the ligands and iridium complexes is depicted in equation (3.1). Complexes of $(x/ybo)_2Ir(acac)$ have been prepared[7] with all the substituents in the cyclometalated ligand bo. The synthetic method used to prepare these complexes involves two steps. In the first step, $IrCl_3 \cdot 3H_2O$ is allowed to react with an excess of the cyclometalated ligand

(2.5 times) to give a chloro-bridged dinuclear complex, i.e., $(x/ybo)_2Ir_2(\mu\text{-}Cl)_2(x/ybo)_2$.

$$2(IrCl_3 \cdot 3H_2O) + 4\,(x/ybo) \rightarrow (x/ybo)_2Ir(\mu\text{-}Cl)_2Ir(x/ybo)_2 + 4\,HCl + 3H_2O \quad (3.1)$$

$$(x/ybo)_2Ir(\mu\text{-}Cl)_2\,Ir_{(}x/ybo)_2 + 2\,L\text{^}XH \rightarrow 2\,(x/ybo)_2Ir(L\text{^}X) + 2\,HCl \quad (3.2)$$

The chloro-bridged dinuclear complexes can be readily converted to emissive, mononuclear complexes $(x/ybo)_2Ir(acac)$ by replacing the two bridging chlorides with bidentate acetylacetonate. Thus, the iridium(III) ion is octahedrally coordinated by the three chelating ligands. The coordination geometry of the "$(x/ybo)_2Ir$" fragment in the mononuclear complex is the same as that for the dinuclear complexes. All the mononuclear complex dopants with different substitutions are thermally stable up to 280-320℃. The mononuclear Ir(III) complexes can be sublimed easily at reduced pressure.

As indicated by the reported NMR data, the resonance spectra of ligands show poorly resolved multiplets, whereas the well-resolved multiplets are observed for the complexes. The maximum high-field chemical shift is observed for the proton to the ortho-metalated carbon atom that experiences the largest shielding of any of the ligand protons. Again the chemical shift of this particular proton varies with the electronic properties of the substituents present in the ligand. The complex containing $-CF_3$ substituted ligand shows the lowest field chemical shift for the proton to the ortho-metalated carbon atom due to the less shielding power arising from the strong electron withdrawing property of the substituent, whereas the strongest electron-releasing substituent (i.e., $-OCH_3$ group) shows the highest field chemical shift for the same proton. The $(x/ybo)_2Ir(acac)$ complexes are stable in air and can be sublimed in a vacuum without decomposition during device fabrication.

3.3.2 UV-Vis Absorption spectra

Figure 3.1 shows the UV-visible absorption spectra for six different ligand substituted $(x/ybo)_2Ir(acac)$ complexes in CH_2Cl_2 solution at room temperature. The strong absorption bands observed at 250-300 nm are assigned to ligand centered $^1\pi$-π^* transitions, whilst the broad absorption bands at lower energy (λ_{max} > 350 nm) are typical metal to ligand charge-transfer (MLCT) transitions.[12,13] In other cyclometalated complexes these bands have been assigned to singlet and triplet MLCT transitions, and the same assignment is likely here[23, 24]. The long tail toward lower energy is assigned to ^{3}MLCT transitions that gains intensity by mixing with the higher lying ^{1}MLCT transition through the spin-orbit coupling of iridium(III). This mixing is strong enough in these complexes that the formally spin forbidden ^{3}MLCT has an extinction coefficient that is almost equal to the spin-allowed ^{1}MLCT transition. The presence of another transition observed at around 385 nm for the complexes is also well pronounced, which corresponds to an admixture of MLCT and ligand π-π^* states.

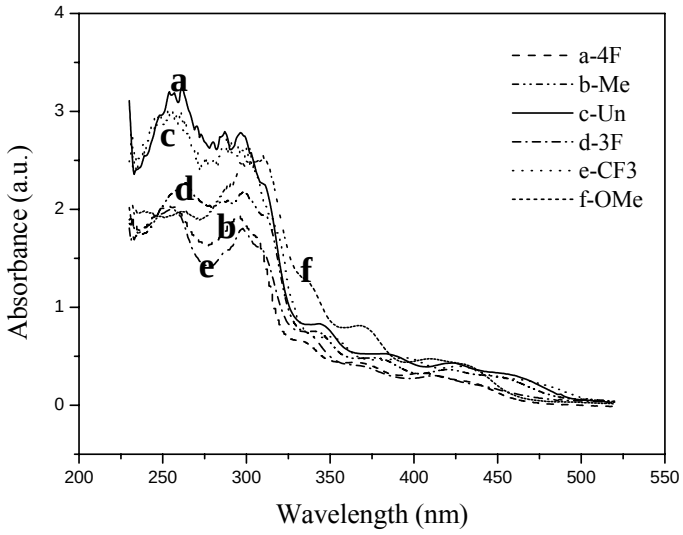

Figure 3.1. Comparison of the UV-Vis absorption spectra of five cyclometalled iridium complexes in CH_2Cl_2.

3.3.3. Photoluminescence (PL) spectra

Figure 3.2 shows the PL emission spectra for $(x/y/bo)_2Ir(acac)$ complexes in CH_2Cl_2 solution at room temperature. All of these complexes show strong luminescence from the triplet states in dichloromethane solution. The emission spectra shows that all of these complexes emit in the range of 500-600 nm, which corresponds to green-yellow light. It is known that the emission bands from MLCT states are generally broad and featureless, while $^3(\pi\text{-}\pi^*)$ states typically give highly structured emission. It is observed that on changing the substituents in $(x/y/bo)_2Ir(acac)$ typically have effect on the maximum emission wavelength in the spectrum. Amongst all of the substituents, trifluoromethyl is the strongest electron-withdrawing group showing the emission wavelength red shift than the corresponding unsubstituted complex, $(bo)_2Ir(acac)$, and the other groups (F/OMe/Me) has

electron-donating effects, so exhibiting the emission wavelength blue shift than the corresponding unsubstituted complex, $(bo)_2Ir(acac)$. When the position of the substitution (4F $\rightarrow$ 3F) is changed, the maximum emission wavelength (λ_{max}) of the complex shows an apparent red shifted emission.[15]

The HOMO/LUMO energies have also been calculated for all the complexes and reported in Table 3.1 based on the experimental redox potentials and the absorption wavelengths. It is observed that the energy gap (HOMO-LUMO) for the trifluoromethyl substituted complex is the least, whereas 4-OMe and 3-F substituted complexes show the maximum energy gap and the rest exhibit intermediate values among all the investigated and these energy gap data can well be correlated with the corresponding maximum emission wavelengths of the respective complexes.

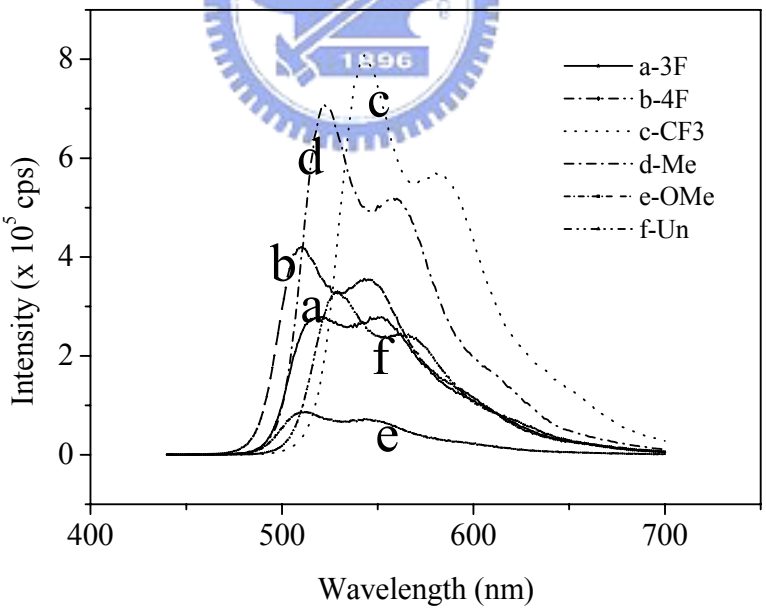

Figure 3.2 Comparison of solution PL spectra for six triplet Ir (III)-based complexes in CH_2Cl_2.

Table 3.1. Spectroscopic, redox and photophysical properties for all Ir-complexes synthesized in this research

Complex (x-Subs)	Absorbance λ (nm)	Emission λ_{max} (nm) in CH_2Cl_2	Ox. Potential vs Ferrocene (volt)	HOMO (eV) [a]	LUMO (eV)	Energy Gap (eV) [b]	Absolute PL efficiency [C]
(Unsubstituted)	386；400	529, 562	1.036	5.317	2.837	2.48	0.4
(-4CF_3)	361；437	543, 578	1.263	5.544	3.297	2.25	0.6
(-4F)	370；408	511, 543	1.209	5.490	2.920	2.57	1.6
(-4Me)	377；430	522, 558	0.995	5.276	2.726	2.55	0.8
(-4OMe)	362；410	510, 543	1.013	5.294	2.754	2.54	0.1
(-3F)	374；418	520, 552	1.208	5.489	2.989	2.50	0.4

a. Electrochemical properties were obtained by cyclic voltammetry using CHI 604A.
b. The energy gap can be calculated from the edge of UV-Vis absorption peak.
c The standard material is $Ir(ppy)_3$ in CH_2Cl_2 ($\phi = 0.4$) [21].

3.3.4 Redox Chemistry

Analytical results from cyclic voltammetry indicate that all of the $(x/ybo)_2Ir(acac)$ complexes undergo a reversible one-electron oxidation; however, no reduction processes were observed in dichloromethane. The increasing order of oxidation potential of the complexes is as followings: $-CF_3$ > -F > -Me >$-OCH_3$ and the results are summaried shown in Table 3.1, which show the order of the strength of electron-withdrawing nature of the substituents in the complexes and, conversely, it is the increasing order of oxidation potentials.

3.3.5 Structure of $(CF_3bo)_2Ir(acac)$ Complex

The ORTEP drawing of the $(CF_3bo)_2Ir(acac)$ complex is shown in Figure 3.3. Selected bond lengths (Å) are presented in Table 3.2 and relevant crystallographic data are given in Table 3.3,. These complexes have an octahedral coordination geometry around Ir and has *cis*-C,C *trans*-N,N chelate disposition. The Ir-C bonds of these complexes ($Ir\text{-}C_{av}$= 2.007 Å) are shorter than the Ir-N bonds ($Ir\text{-}N_{av}$ = 2.039 Å). But the Ir-C bond length is similar to the analogues complexes reported[16]. The Ir-N bond lengths also fall within the range of values for the similar type of reported complexes. The Ir-O bond lengths of 2.110(10) and 2.124(9) Å are longer than the mean Ir-O value of 2.088 Å reported in the Cambridge Crystallographic Database[17] and reflect the large *trans* influence of the phenyl groups. All other bond lengths within the chelate ligands are analogues to the similar type of complexes reported[18-20].

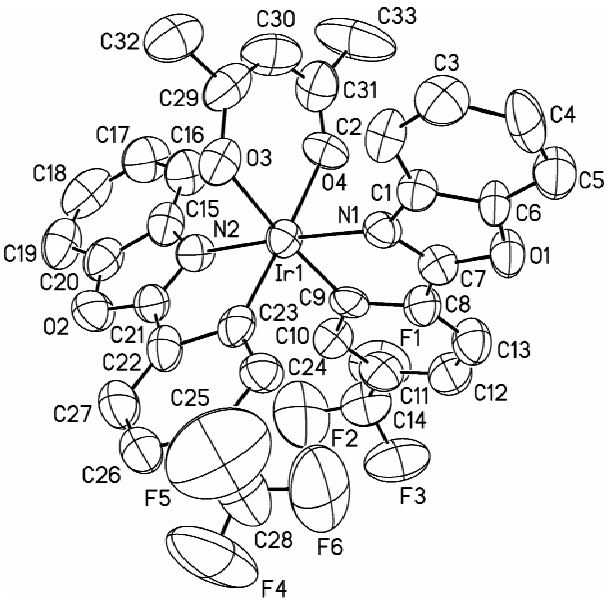

Figure 3.3 ORTEP drawing of $(CF_3\text{-bo})_2Ir(acac)$: the thermal ellipsoids represent 50% probability limit.

Table 3.2. Selected Bond lengths [Å] for $(CF_3\text{-bo})_2Ir(acac)$

atom(1)-atom(2)	distance (Å)
Ir(1)-C(23)	2.003(15)
Ir(1)-C(9)	2.012(14)
Ir(1)-N(2)	2.029(10)
Ir(1)-N(1)	2.049(10)
Ir(1)-O(3)	2.110(10)
Ir(1)-O(4)	2.124(9)

Table 3.3 Crystal data and structure refinement for $(CF_3bo)_2Ir(acac)$

Identification code	ot40m	
Empirical formula	$C_{33}\ H_{27}\ F_6\ Ir\ N_2\ O_7$	
Formula weight	869.77	
Temperature	294(2) K	
Wavelength	0.71073 Å	
Crystal system	Monoclinic	
Space group	P2(1)/c	
Unit cell dimensions	a = 12.211(2) Å	= 90°.
	b = 20.967(4) Å	= 112.872(4)°.
	c = 14.774(3) Å	= 90°.
Volume	3485.1(11) $Å^3$	
Z	4	
Density (calculated)	1.658 Mg/m^3	
Absorption coefficient	3.911 mm^{-1}	
F(000)	1704	
Crystal size	0.20 x 0.08 x 0.05 mm^3	
Theta range for data collection	1.78 to 24.73°.	
Index ranges	$-14 \le h \le 12$, $-24 \le k \le 24$, $-17 \le l \le 17$	
Reflections collected	19584	
Independent reflections	5958 [R(int) = 0.1328]	
Completeness to theta = 24.73°	99.8 %	
Absorption correction	Empirical	
Max. and min. transmission	0.82563 and 0.45062	
Refinement method	Full-matrix least-squares on F^2	
Data / restraints / parameters	5958 / 0 / 442	
Goodness-of-fit on F^2	0.982	
Final R indices [I>2sigma(I)]	R1 = 0.0587, wR2 = 0.1604	
R indices (all data)	R1 = 0.1178, wR2 = 0.1768	
Largest diff. peak and hole	1.604 and -1.132 $e.Å^{-3}$	

3.3.6 Description of OLED devices fabricated with $(CF_3bo)_2Ir(acac)$, $(CH_3bo)_2Ir(acac)$ and $(bo)_2Ir(acac)$ dopants in the emissive layer.

We have also fabricated three electroluminescent (EL) devices using three different iridium(III) complexes [$(CF_3bo)_2Ir(acac)$, $(CH_3bo)_2Ir(acac)$ and $(bo)_2Ir(acac)$] as dopants in the emitting layers. In order to compare the relative EL properties, we have selected two ligand substituted complex dopants [$-CF_3$ (device a) and –Me (device b)] with opposite electronic properties and the other is the unsubstituted bo complex (device c). These complexes were doped into the emissive layer of the OLED devices at a concentration of mole 7 %. The device structure and their thickness of the layers (i.e., ITO/NPB (500 Å)/ CBP + 7 % dopant (200 Å) / BCP (100 Å)/Alq_3 (650 Å)/LiF (10 Å)/Al (2000 Å)) have been kept constant (Figure 3.4).

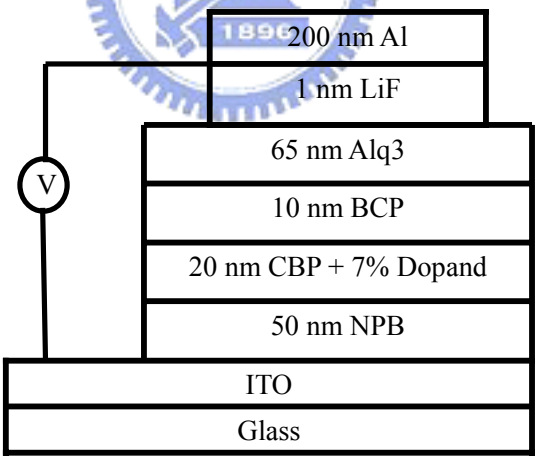

Figure 3.4 EL device structures with (a) CF_3-, (b) Me- substituted, and (c) parent complexes as a dopant.

The comparative variation of quantum efficiency as a function of current density for these devices is shown in the Figure 4. Furthermore, Table 3.4 also summarizes and compares the EL performances of devices **a**, **b** and **c**. It has been observed that the quantum efficiency of the devices **a, b** and **c** was found to increase with increasing current density and it shows a maximum at 9.95, 10.5 and 8.94 cd/A at 20 $mAcm^{-2}$, respectively. The turn-on voltage was found to be 5.33, 4.64 and 4.62 for the devices, **a, b** and **c,** respectively. The luminance efficiency was found to decrease with increasing current density for all the devices as indicated in Figure 3.5 which may be attributed due to the triplet-triplet annihilation. The power efficiencies were found to be 4.53, 6.20 and 4.03 lm/W for the devices, **a, b** and **c**, respectively. At a current density 100 cdm^{-2}, the brightness of the EL device **a** is 9189 cdm^{-2}, whereas that for the device **b** and **c** are 8018 cdm^{-2} and 7546 cdm^{-2}, respectively. The C.I.E. was measured to be (0.44, 0.54), (0.37, 0.58) and (0.38, 0.56) for the devices, **a, b** and **c** respectively.

The lower efficiency of the $(bo)_2Ir(acac)$ based OLED relative to that of the $(CF_3bo)_2Ir(acac)$ - based device may be attributed to a lower phosphorescence efficiency of the former as compared to the latter. On comparison of these devices with the corresponding devices **a, b** and **c,** power efficiency is always higher throughout the current densities and voltages applied, as indicated in Table 4, whereas the luminance and the quantum yield (described in Figure 5) are also found to increase at lower current densities. Furthermore, no emission from CBP or Alq_3 was observed, indicating a complete energy transfer from the host exciton to the Ir-dopant. Meanwhile, there is no exciton decay in the Alq_3 layer due to the hole blocking action of the BCP layer. As shown in the insets of Figures 5(a)-5(c), the device **a** having trifluoromethyl-substituted dopant shows the

expected red-shift and stronger intensity in the EL spectra as compared to that observed in the device **c** with unsubstituted dopant. Similarly, the device **b** having methyl-substituted dopant shows the expected blue-shift and stronger intensity in the EL spectra as compared to that observed in the device **c** with unsubstituted dopant. The EL spectra of a, b and c devices are similar to the PL spectra of same phosphors in a dilute solution. Thus, the EL emission is confirmed to originate from the triplet excited states of the phosphors. It is expected that the devices with the rest of the dopants synthesized and investigated in our work will exhibit more or less similar EL properties with those of devices **a**, **b** and **c**.

Table 3.4 Comparative study of the electroluminescent performance of three EL devices based on $(bo)_2Ir(acac)$, $(bo\text{-}Me)_2Ir(acac)$ an$(bo\text{-}CF_3)_2Ir(acac)$ as a dopant.

	$(bo)_2Ir(acac)$	$(Me\text{-}bo)_2Ir(acac)$	$(CF_3\text{-}bo)_2Ir(acac)$
Turn-on voltage (V) at 0.5 mA/cm^2	4.62	4.64	5.33
EL Color	green	green	yellow
Peak wavelength (nm)	532	528	544
Luminance (cd/m^2) at 100 mA/cm^2	7546	8100	9200
Yield (cd/A) at 20 mA/cm^2	8.94	10.5	9.95
C.I.E.coordinate (x,y)	(0.38, 0.56)	(0.37, 0.58)	(0.44, 0.54)
Power efficiency (lm/W)	4.03 (at 4.62V)	6.20 (at 4.64V)	4.53 (at 5.33V)

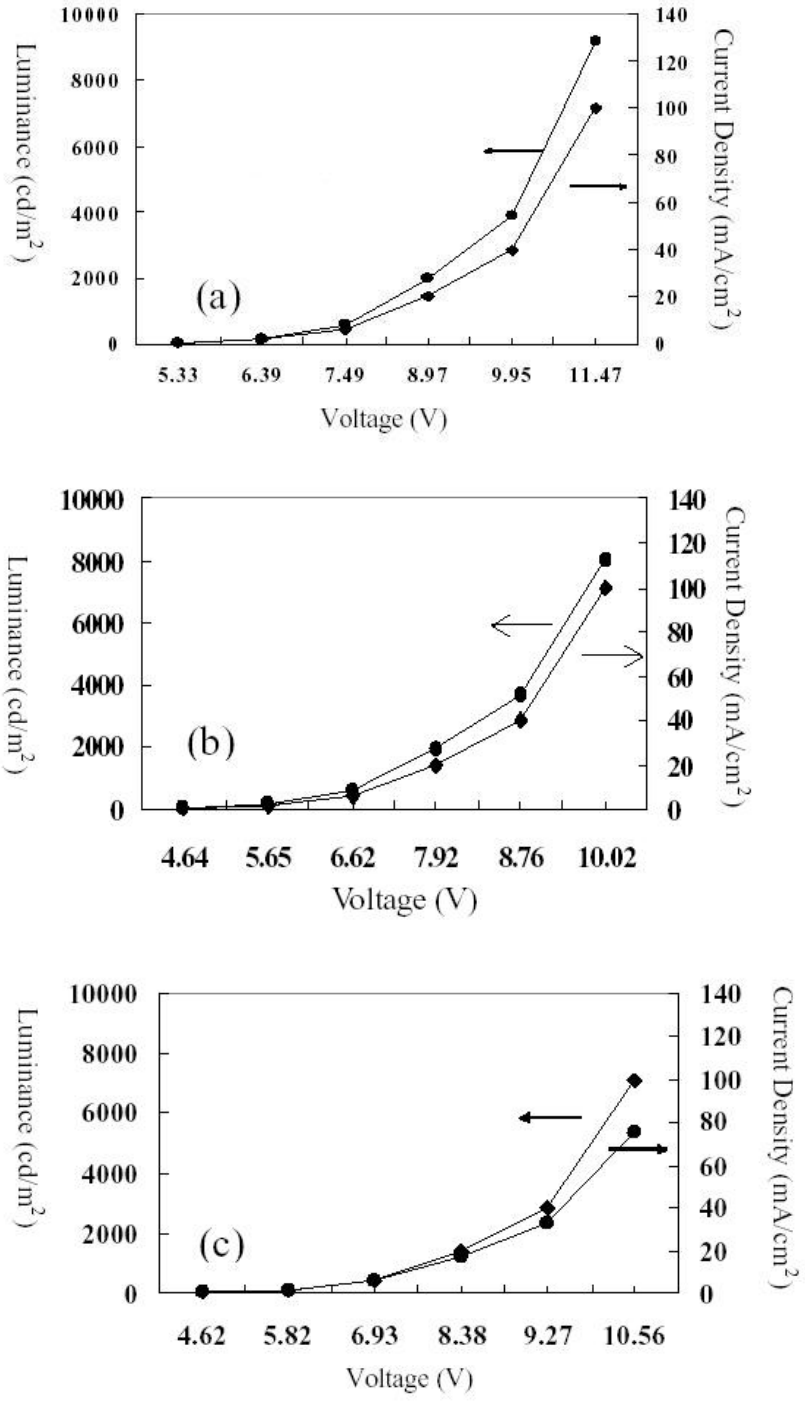

Figure 3.5 EL performance of three (x/y-bo)$_2$Ir(acac) doped EL devices with x = (a) CF_3-, (b) Me-, and (c) parent (bo)$_2$Ir(acac).

3.4 **Conclusions**

Four new cyclometallated iridium complex dopants using various types of substituted (2-phenyl)benzoxazole ligands have been synthesized and shown to exhibit high phosphorescence efficiency which made them ideal for OLED applications. These complexes show different quantum efficiencies in solution depending upon the nature of the substituents. All the complexes show one-electron oxidation in solution. The wavelength can be tuned by *ca.* 25 nm depending upon the electronic properties of the substituents present in the ligand. We have fabricated and investigated three EL devices and observed that the device dopants with substituted ligands show the higher luminance yield compared to the dopant with unsubstituted ligands .

3.5 References

1. (a) Balzani, V.; Credi, A.; Scandola, F. *In Transition Metals in Supramolecular Chemistry*; Fabbrizzi, L., Poggi, A., Eds.; Kluwer: Dordrecht, The Netherlands, 1994; p1. (b) Lehn, J.-M. Supramolecular Chemistry — Concepts and Properties; VCH: Weinheim, Germany, (1995). (c) Bignozzi, C. A.; Schoonover, J. R.; Scandola, F. Prog. *Inorg. Chem.* 44 (1997**)** 1.
2. (a) Tan-Sien-Hee, L.; Mesmaeker, A. K-D. *J. Chem. Soc., Dalton Trans.* 24 (1994) 3651. (b) Chin, K-F; Cheung, K.-K.; Yip, H.-K.; Mak, T. C. W.; Che, C. M. *J. Chem. Soc., Dalton Trans.* 4 (1995) 657. (c) Kalyanasundaram, K.; Gratzel, M. Coord. *Chem. Rev.* 177 (1998) 347.
3. (a) Lee, J. K.; Yoo, D.; Rubner, M. F. *Chem. Mater.* 9 (1997) 1710. (b) Gao, F. G.; Bard, A. *J. Am. Chem. Soc.* 122 (2000) 7426.
4. (a) Li, Y.; Liu, Y.; Guo, J.; Wu, F.; Tian, W.; Li, B.; Wang, Y. *Synth. Met.*

118 (2001) 175. (b) Wang, K.; Huang, L.; Gao, L.; Jin, L.; Huang, C. *Inorg. Chem.* 41 (2002) 3353.

5. Gao, F. G.; Bard, A. *J. Chem. Mater.* 14 (2002) 3465.
6. (a) Lee, C-L.; Lee, K. B.; Kim, *J-J. Appl. Phys. Lett*. 77 (2000) 2280. (b) Das, R. R.; Lee C-L; Kim *J-J. Mat. Res. Soc. Symp. Proc.* 708 (2002) BB3.39.1. (c) Markham, J. P. J.; Lo S.-C.; Magennis S. W.; Burn P. L.; Samuel I. D. W. *Appl. Phys. Lett*. 80 (2002) 2645.
7. (a) Lamansky, S; Djurovich, P.; Murphy, D.; Abdel-Razzaq, F.; Lee, H-F.; Adachi, C.; Burrows, P. E.; Forrest, S. R.; Thompson, M. E. *J. Am. Chem. Soc.* 123 (2001) 4304. (b) Thompson, M. E.; Lamansky, S; Djurovich, P.; Murphy, D.; Abdel-Razzaq, F.; Kwong, R.; Forrest, S. R.; Baldo, M. A.; Burrows, P. E. patent US 20020034656A1.
8. Brooks, J.; Babayan, Y.; Lamansky, S.; Djurovich, P. I.; Tsyba, I.; Bau, R.; Thompson, M. E. *Inorg. Chem.*, 41 (2002) 3055.
9. Grushin V. V.; Herron, N.; LeCloux, D. D.; Marshall, W. J.; Petrov, V. A.; Wang, Y. *Chem. Commun.* (2001) 1494.
10. Brembilla, A.; Roizard, D.; Lochon, P. *Syn. Commun*. 20 (1990) 3379.
11. Zhang, Y.; Baer,C. D.; Neto,C. C.; O'Brien P. and Sweigart**,**D. A.; *Inorg. Chem*. 30 (1991) 1685
12. Maestri, M.; Sandrini, D.; Blazani, V.; Maeder, U. and VonZelewsky, A;. *Inorg. Chem.*, 26 (1987) 1323.
13. Colombo, M. G.; Hauser, A. and H. U. Gu¨ del, *Inorg. Chem*., 32 (1993) 3088.
14. Lamansky, S; Djurovich, P.; Murphy, D.; Abdel-Razzaq, F.; Kwong, R.; Tsyba, I.; Bortz, M.; Mui, B.; Bau, R.; Thompson, M. E. *Inorg. Chem.* 40 (2001) 1704.
15. Inamur R. L.; Teng-Ming Chen; *Chem. Mater*. (2004) in press.

16. Vicente J.; Arcas, A.; Bautista, D.; Arellano, M. C. R. de *J. Organomet. Chem.* 663 (2002) 164.
17. Allen, F. H.; Davies, J. E.; Galloy, J. J.; Johnson, O.; Kennard, O.; Macrae, C. F.; Mitchell, E. M.; Mitchell, G. F.; Smith, J. M.; Watson, D. G.; *J. Chem. Inf. Comput. Sci.* 31 (1991) 187.
18. Garces, F. O.; Dedian, K.; Keder, N. L.; Watts, R. *J. Acta Crystallogr.* C49 (1993) 1117
19. Urban, R; Krämer, R.; Mihan, S.; Polborn, K.; Wagner, B.; Beck, W. *J. Organomet. Chem.* (2000) 1039.
20. Neve, F.; Crispini, A. Eur. *J. Inorg. Chem.* (2000) 1039.
21. King, K. A.; Spellane P.J.and Watts R.J. *J.Am.Chem.Soc*. (1985) 1431.
22. Demas, J.N.;Crosby, G.A., *J. Phys. Chem*. (1971) 99

Chapter 4

Synthesis and Electroluminescence studies of the New Iridium(III) Complexes Posseessing the 2-Phenyl-1-pyrroline Ligands

Abstract

Organic triplet-state light-emitting materials (organic phosphorescent) have been one of the most important recent developments in the field of organic light-emitting diodes (OLEDs). Cyclopentane-containing cyclometalated iridium(III) complexes are rarely found in literature that inspired us to focus on these complexes. This work involves a systematic study to observe the color tuning of the iridium(III) complexes by choosing a particular cyclometalated ligand with substituents exhibiting different electronic properties. Tuning of maximum emission wavelengths depending upon the extent of conjugation and/or ring size and also the effect of hetero atom will also be discussed.

4.1 Introduction

The photophysical properties of bis- and tri-cyclometalated complexes of Ir(III) make them very useful for several photonic applications.[1] Strong spin-orbit coupling of the 4d or 5d ion leads to efficient intersystem crossing of the singlet excited states to the triplet manifold. The research group lead by Mark Thompson *et al* has synthesized and reported a series of neutral emissive cyclometalated complexes of iridium(III)[2] and platinum(II)[3] and used them in the fabrication of OLEDs successively. The photophysical properties of bis- and tri-cyclometalated complexes of Ir(III) make them very useful for several photonic applications. A recent application for these compounds is in the field of organic light-emitting devices (OLEDs) where they have been used as phosphorescent dopants in the emitting layer. The singlet and triplet excited states that are created during charge recombination are trapped at the phosphor, where the effective intersystem crossing leads to efficient electrophosphorescence at room temperature.

A significant research effort has focused on the synthesis and photophysical characterizations of octahedral $4d^6$ and $5d^6$ metal complexes.[4,5] Of the above phosphor emitters that have been reported for OLED devices, iridium(III) based materials have displayed the most promising due to their high stability, high photoluminescence (PL) efficiency and relatively short excited state lifetime.

Our attempt is mainly focused on the syntheses of new emitting iridium(III) based cyclometalated complexes. We choose the pyrroline ligands and decreasing the conjugation and ring size of the ligands has also been investigated. In this paper, we compare the phototluminescence (PL) of iridium(III) complexes in solution. In the neat films, these complexes are characterized by PL quantum efficiency photo-physical measurements.

4.2 Experimental Section

4.2.1 Materials

All of the preparative work involving iridium(III) trichloride hydrate ($IrCl_3 \cdot 3H_2O$, Alfa Aesar Company Ltd.), 2-ethoxyethanol ($H_5C_2OC_2H_4OH$, Fluka) and all other reagents (Tokyo Chemical Industry, Japan) were carried out in an inert atmosphere and used without further purification.[6,7]

4.2.2 Optical Measurements and Compositions Analysis.

The ultraviolet-visible (UV-VIS) spectra of the phosphorescent Ir(III) complexes were measured on an UV-VIS spectrophotometer (Agilent model 8453) and corrected for background due to solvent absorption. Photoluminescence (PL) spectra were carried out with a spectrophotometer (Jobin-Yvon Spex, model Fluorolog-3). Comparative quantum efficiencies have been measured using a ARC sense analysis, v 1.08 software. NMR spectra were recorded on Varian 300 MHz and MS spectra (both EI and FAB) were taken on an Micromass TRIO-2000. Cyclic voltammetry (CV) analyses were performed by using CH INSTRUMENT CHI 604A, and the TG-DTA analysis was carried out by using a thermal analyzer (SEIKO 1TG/DTA 200).

4.2.3 Syntheses of mononuclear iridium(III) complex dopants

All of the preparative work involving iridium(III) trichloride hydrate ($IrCl_3 \cdot 3H_2O$, Alfa Aesar Company Ltd.), 2-ethoxyethanol ($H_5C_2OC_2H_4OH$, Fluka) and all other reagents (Tokyo Chemical Industry, Japan) were carried out in an inert atmosphere and used without further purification. The ligands, 2-phenyl-1-pyrroline, 2-(4-methoxyphenyl)-1-pyrroline and 2-(4-fluorophenyl)-1-pyrroline have been prepared by following the method described in the literature.[16,17] These were prepared by refluxing the mixture

of $IrCl_3 \cdot 3H_2O$ (1 mmol) and the ligands (2.4 mmol) in 2-ethoxyethanol for 24~25hr. The orange-yellow mixture was cooled to room temperature and 20 ml 1 M HCl was added to precipitate the product. The mixture was filtered and washed with 100 ml 1M HCl followed by 50 ml methanol solution for several times then dried. The chloride bridged dinuclear iridium(III) complex (0.1 mmol), acetylacetone(acac) (0.3 *m*mol) and sodium carbonate (1 *m*mol) were mixed in 10 ml of 2-ethoxyethanol (30 ml). The mixture was refluxed under nitrogen for 11 - 12 hours. The reaction mixture was then cooled and the resulted precipitate was collected through filtration. The product was purified by recrystallization from a solution of the mixture of dichloromethane and methanol (2 : 1).

Ir monomer complex $(ppl)_2Ir(acac)$ 4a：

Yeild：60%（crude mixture）^{1}H NMR($CDCl_3$) δ, ppm 7.16 (m, 2H, Ph); 6.70 (m, 4H, Ph); 6.40 (m, 2H, Ph); 5.25 (s, 1H, acac); 4.63 (m, 2H, CH_2N), 4.41 (m, 2H, CH_2N), 3.50 (s, 6H, acac); 2.61 (m, 4H, CCH_2); 2.41 (m, 4H, CCH_2C). EIMS: m/z: 580, Calc. 580.

Ir monomer complex $(4OMeppl)_2Ir(acac)$ 4b：

^{1}HNMR (300 MHz, $CDCl_3$) : δ, ppm 7.16 (d, 2H, Ph); 6.33 (m, 2H, Ph); 6.15 (d, 2H, Ph); 5.15 (s, 1H, acac); 4.15 (dd, 2H, CH_2N), 3.89 (dd, 2H, CH_2N), 3.55 (s, 6H, acac); 3.35 (m, 4H, CCH_2); 2.40 (m, 4H, CCH_2C); 1.99 (s, 6H, OMe). EIMS: m/z: 640, Calc. 640.

Ir monomer complex $Ir(4Fppl)_3$ 4c :

^{1}HNMR (300 MHz, $CDCl_3$) : δ, ppm 7.25 (m, 3H, Ph); 6.56 (m, 3H, Ph); 6.34 (dd, 3H, Ph), 3.80 (m, 3H, CH_2N), 3.39 (m, 3H ,

CH_2N), 3.13 (m, 6H, CCH_2); 2.24 (m,6H, CCH_2C). EIMS : m/z 678, Calc. 678.

4.2.4 Crystallography

Diffraction data for (2-(4-fluorophenyl)-1-pyrroline)$_3$Ir single crystals was collected using a Bruker CCD diffractometer with Mo Kα (λ= 0.71073 Å). Data collection in the 2θ scan mode, cell refinement and data reduction were carried out using program Bruker SHELXTL. The structure was solved by direct methods using the SHELXS-97 package of computer programs. The structure was refined by full-matrix least-squares methods based on F^2 using SHELXL-97. The non-hydrogen atom positions were refined anisotropically whereas the hydrogen positions were not refined.

4.2.5 OLED Fabrication and Testing

Organic layers were fabricated by high-vacuum thermal evaporation onto a glass substrate precoated with an indium-tin-oxide (ITO) layer with a sheet resistance of 20 Ω. Prior to use, the ITO surface was ultrasonicated in a detergent solution followed by rinsing with deionized (DI) water, dipped into acetone, trichloroethylene, and 2-propanol, and then degreased with a vapor of 2-propanol. After degreasing, the substrate was oxidized and cleaned in a UV-ozone chamber before it was loaded into an evaporator. In a vacuum chamber at pressure of 10^{-4} Pa, 50 nm thick 4,4′-bis[(1-naphthyl)(phenyl)amino]-1, 1-biphenyl (NPB) as the hole transporting layer; 20 nm thick complex doped (7%) 4, 4′-bis(9-carbazolyl)-1,1′-biphenyl (CBP) as an emitting layer; 10 nm thick 2,

9-dimethyl-4,7-diphenyl-1, 10-phenanthroline (BCP) as a hole and exciton blocking layer (HBL); 65 nm thick Alq_3 as electron transport layer; and a cathode composed of 1 nm thick lithium fluoride and 200 nm thick aluminum were sequentially deposited onto a substrate to give the device structure. The current-voltage (I-V) profiles and light intensity characteristics for the above-fabricated devices were measured in a vacuum chamber of 10^{-4} Pa at ambient temperature using a Keithley 2400 Source Meter/2000 Multimeter coupled to a PR 650 Optical Meter.

4.3 Results and discussion

4.3.1 Synthesis and Characterization of iridium(III) complexes.

The ligands, 2-phenyl-1-pyrroline, 2-(4-methoxyphenyl)-1-pyrroline and 2-(4-fluorophenyl)-1-pyrroline, have been prepared by following the method described in the literature.[2] These Ir(III)-complexes can be prepared by using phenylpyrroline (ppl) as the cyclometalating ligand precursors (Scheme 1). The tris-cyclometalated complexes can also be prepared from the dichloro-bridged dinuclear $[(C\hat{}N)_2Ir(\acute{\imath}\text{-}Cl)_2Ir(C\hat{}N)_2]$ by heating the Ir complex with a two to three fold excess of cyclometalating ligand in glycerol. The syntheses work equally well for other pyridine-type ligands (e.g., tpyH, 46dfppyH), as well as for phenylpyrazoles (e.g., 46dfppzH, tfmppzH). The dichloro-bridged dinuclear compounds are easily prepared in high yield starting from $IrCl_3 \cdot 3H_2O$. The reaction temperature and nature of the cyclometalated ligand strongly affect the product yield of the reactions. The impurity can be readily removed by recrystallization or column chromatography. All of the complexes examined possess three cyclometalated ligands in a pseudooctahedral coordination geometry around

the metal center.[8,9] All the mononuclear complex dopants with different substitutions are thermally stable up to 220-250℃. The mononuclear complexes can be sublimed easily at reduced pressure. Excited-state lifetimes were measured by exciting the samples at 355 nm with an Opotek optical parametric by a frequency-tripled He-Cd laser.

Scheme 4.1.

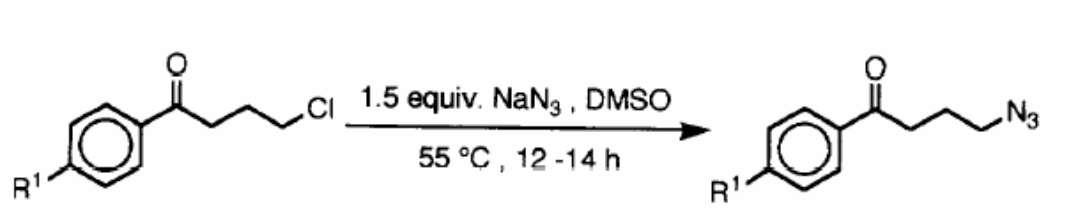

1a R_1= H

1b R_1= Me

1c R_1= F

2a R_1= H

2b R_1= M

2c R_1= F

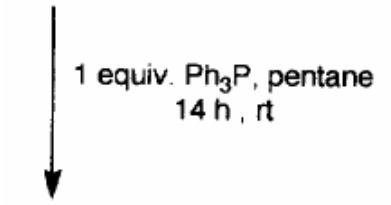

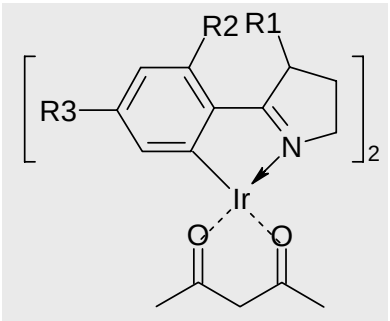

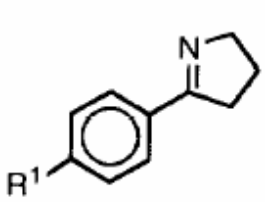

3a R_1= H

3b R_1= OMe

3c R1=F

4a R_1= H，R_2= H，R_3= H

4b R_1= H，R_2= H，R_3= OMe

4c R_1= H，R_2= H，R_3= F

4.3.2 Photoluminescence (PL) spectra

Figure 4.1 shows the PL emission spectra for $(L'^X)_2Ir(acac)$ complexes in CH_2Cl_2 solution at room temperature. It has been observed that three complexes show very strong luminescence from the triplet states in CH_2Cl_2 solution. The strong absorption and emission characteristics derived from the π-π^* and MLCT energy levels make them suitable for use as the luminescent phosphors.[10]

It is observed that the maximum emission peak of $(L'^X)_2Ir(acac)$ has been found in the range of 530-550 nm. Our spectral analysis indicates that all of these complexes emit in the range of 500-600 nm, corresponding to yellow to orange light. It is possible to tune the emission wavelength (λ_{em}) by controlling the band gap of ligand. It has been known that the emission bands from MLCT states are generally broad and featureless, while $^3(\pi$-$\pi^*)$ states typically give highly structured emission. The PL spectra indicate that major emission from mixed states for all Ir(III)-complexes is of MLCT transition type. We can see the $(4OMeppl)_2Ir(acac)$ complex have a extra peak at 441 nm, that is due to nonreaction 4-OMe-2-phenyl-1-pyrroline ligand. We have also observed that changing the substituents on the cyclometalated ligand in $(L'^X)_2Ir(acac)$ typically shows a great influence on the observed maximal emission wavelength in the spectra. The blue-shifting of λ_{em} has been observed in both of the complexes with both –F and –OMe-substituted 2-phenyl-1-pyrroline ligand as compared that that observed in the parent $(2\text{-phenyl-1-pyrroline})_2Ir(acac)$complex. This observation can be attributed to the electron-donating property of –F and –OMe.[11]

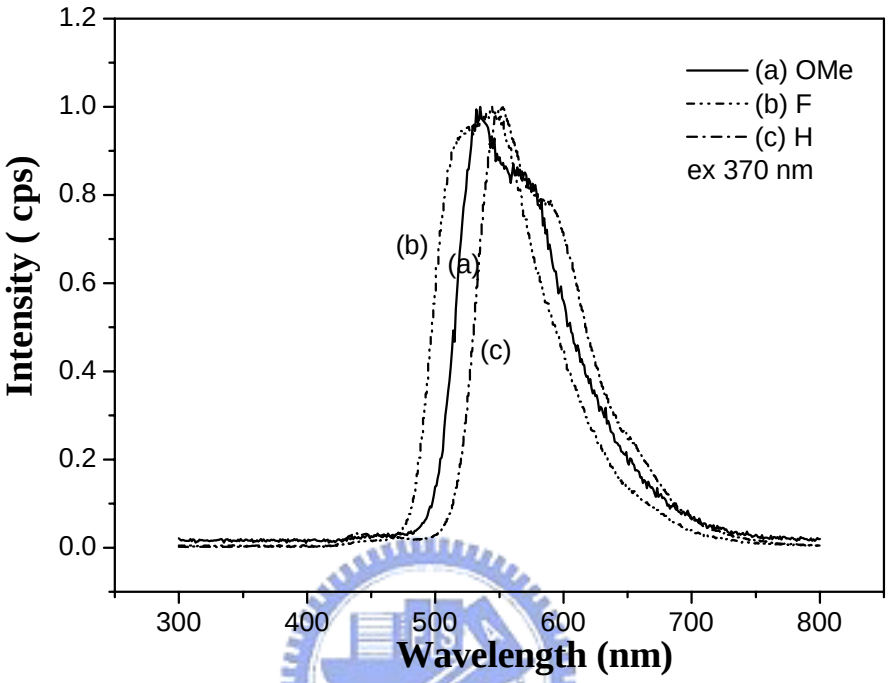

Figure 4.1 Comparison of solution PL spectra for (L'^X)$_2$Ir(acac) complexes at room temperature in CH_2Cl_2.

4.3.3 Structure of (2-(4-fluorophenyl)-1-pyrroline)$_3$Ir Complex :

The crystal structures of these complexes have been determined and an octahedral coordination has been found for the Ir metal center summarized in Table 4.1. The average Ir-C bond length of *fac*-Ir(ppz)$_3$ complexes (Ir-C_{av} = 2.019Å) was found to be shorter than that of the Ir-N bonds (Ir-N_{av} = 2.102 Å), suggesting a similar influence for pyridyl and pyrazolyl groups.[12] However, the Ir-C bond length is similar to that of the analoguous complexes reported.[13] The Ir-C and Ir-N bond lengths for the Ir[2-(4-fluorophenyl)-1-pyrroline]$_3$ complex are given in Table 4.2.

Table 4.1. Crystal data and structure refinement for Ir(III) 2-(4-fluorophenyl)-1-pyrroline complex.

Identification code	my34m	
Empirical formula	C30 H27 F3 Ir N3	
Formula weight	678.75	
Temperature	296(2) K	
Wavelength	0.71073 Å	
Crystal system	Monoclinic	
Space group	P2(1)/n	
Unit cell dimensions	a = 10.9941(6) Å	= 90°.
	b = 17.4820(10) Å	= 94.871(1)°.
	c = 13.2174(7) Å	= 90°.
Volume	2531.2(2) $Å^3$	
Z	4	
Density (calculated)	1.781 Mg/m^3	
Absorption coefficient	5.322 mm^{-1}	
F(000)	1328	
Crystal size	0.40 x 0.20 x 0.05 mm^3	
Theta range for data collection	1.94 to 28.31°.	
Index ranges	$-14 \le h \le 14$, $-23 \le k \le 20$, $-14 \le l \le 17$	
Reflections collected	18439	
Independent reflections	6287 [R(int) = 0.0618]	
Completeness to theta = 28.31°	99.8 %	
Absorption correction	Empirical	
Max. and min. transmission	0.97852 and 0.47949	
Refinement method	Full-matrix least-squares on F^2	
Data / restraints / parameters	6287 / 0 / 334	
Goodness-of-fit on F^2	0.865	
Final R indices [I>2sigma(I)]	R1 = 0.0299, wR2 = 0.0773	
R indices (all data)	R1 = 0.0529, wR2 = 0.0859	
Largest diff. peak and hole	1.244 and -1.046 $e.Å^{-3}$	

Table 4.2. Comparison of selected bond distances (Å) and bond angles(deg) for Ir(III) 2-(4-fluorophenyl)-1-pyrroline complex.

Bond type	Bond distances(Å)
Ir – N1	2.096(3)
Ir – N2	2.113(3)
Ir – N3	2.097(4)
Ir – C6	2.029(3)
Ir – C16	2.010(3)
Ir – C26	2.019(4)
	Bond Angles(deg)
C(16)-Ir(1)-C(26)	93.35(15)
C(16)-Ir(1)-C(6)	95.25(17)
C(26)-Ir(1)-C(6)	95.68(15)
N(1)-Ir(1)-N(3)	92.53(14)
N(1)-Ir(1)-N(2)	97.98(15)
N(3)-Ir(1)-N(2)	95.40(13)

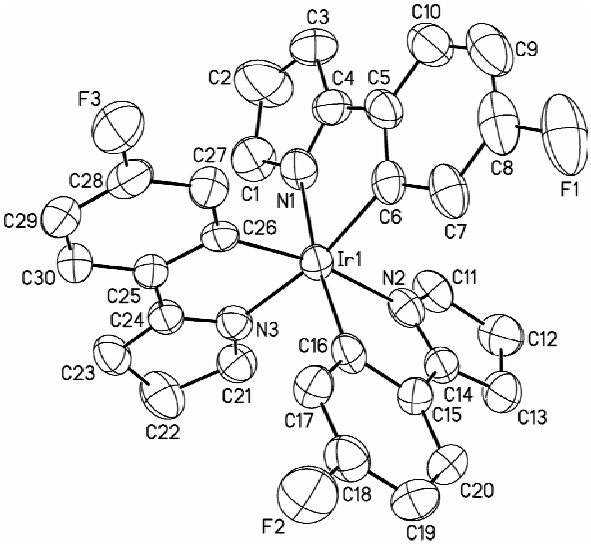

4.3.4 Cyclicvoltametric study

Furthermore, analytical results from cyclic voltammetry indicate that all of the Ir complexes undergo a reversible one-electron oxidation; however, no reduction processes in all Ir(III)-complexes were observed in dichloromethane. A summary of the measured redox potentials relative to an internal ferrocene reference (Cp_2Fe/Cp_2Fe^+=0.45V vs SCE in dichloromethane solvent) is given in Table 3, which indicates that all of the complexes show a reversible oxidation with potentials of 0.70-0.90 V.

4.3.5 Decay lifetime

To understand the temperature-dependent decay behaviors of the phosphorescent dopant, the emission decay lifetime of the $(ppl)_2Ir(acac)$ complex was measured in the temperature range of 8-300 K and the temperature dependent decay lifetime is shown in Figure 4.2. While the integrated phosphorescence intensity showed no temperature dependence, the lifetime increased significantly at temperatures of less than T~ 50K. [14,15] We also measured the quantum efficiency (η_{PL}) for 7%Ir doped-CBP neat film sample of $(ppl)_2Ir(acac)$ by using an integrating sphere equipped with a He-Cd laser (λ = 355 nm) as an excitation source and a multi-channel spectrometer as an optical detector. Based on equation (1) where $N_{emission}$ is the emission photon number from the sample, $N_{absorption}$ is the absorbed photon number by the sample, α is the calibration factor for the measurement setup, λ is the wavelength, h is plank's constant, c is the speed of light, $I_{em}(\lambda)$ is the PL intensity from the sample, $I_{ex,}(\lambda)$ is the intensity of the excitation laser without the sample, and $I'_{ex}(\lambda)$ is the intensity of the excitation laser with the sample. We obtained the η_{PL} = 19.2±3 from this eq.

(1) for 7%$(ppl)_2Ir(acac)$: CBP neat film.[19]

$$\eta_{PL} = \frac{N_{emission}}{N_{Absorption}} = \frac{\alpha \int \frac{\lambda}{hc} I_{em}(\lambda) d\lambda}{\alpha \int \frac{\lambda}{hc} [I_{ex}(\lambda) - I'_{ex}(\lambda)] d\lambda}, \quad (1)$$

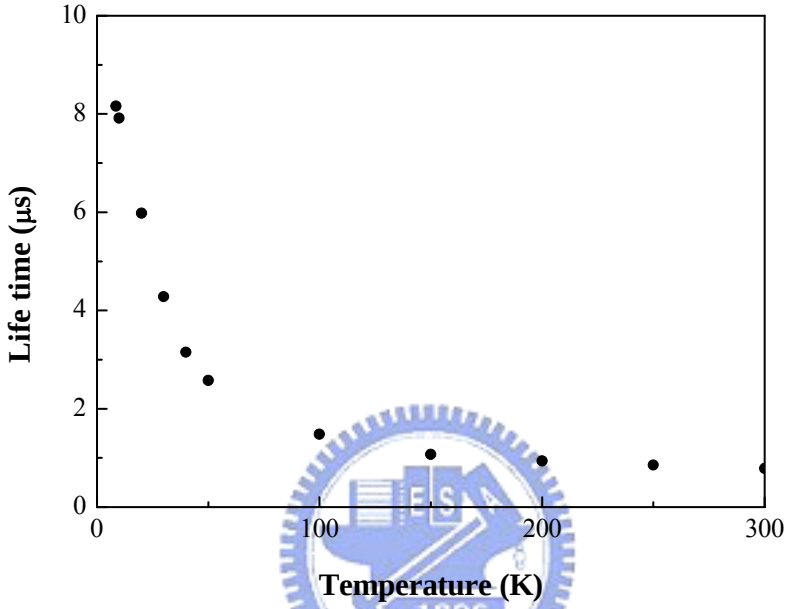

Figure 4.2 Temperature dependences of PL lifetimes for $(ppl)_2Ir(acac)$

4.3.6 Electroluminescence

We have also fabricated three electroluminescent (EL) devices by doping 7 mol % of the three iridium(III) complexes, $(ppl)_2Ir(acac)$ (**D-a**), $(4OMeppl)_2Ir(acac)$ (**D-b**), and $Ir(4Fppl)_3$ (**D-c**) as dopants in the emitting layers, respectively. The device structure with thickness of the layers kept constant (i.e., ITO/NPB (50 nm)/ CBP + 7 % dopant (20 nm) / BCP (10 nm)/Alq_3(65 nm)/LiF(1 nm)/Al (200 nm)) have been represented as shown in Fig. 4.3. The maximum EL efficiency were found to be 4.10, 8.49, and 6.49 cd/A at 9.20, 8.59 and 8.09 (V), respectively. The turn-on voltage was

found to be 7.03, 7.41, and 7.03 V for the devices, **a, b** and **c,** respectively. The luminance efficiency was found to decrease with increasing current density for all the devices which may be attributed to the triplet-triplet annihilation[18] observed in most of the electrophosphorescent OLEDs. The power efficiencies were also found to be 1.40, 3.10 and 2.52 lm/W for the devices, **a, b** and **c**, respectively. At a current density 450 cd/m^2, the brightness of the EL devices **D-a** is 16270 cd/m^2, whereas those for the **D-b** and **c** are 17,086 cd/m^2 and 20,304 cd/m^2, respectively. The C. I. E. chromaticity coordinates were also measured to be (0.48, 0.47), (0.43, 0.52) and (0.36, 0.52) for the EL devices, **a, b** and **c** respectively. The external quantum efficiency (E.Q.E) of the EL device **D-a** was determined to be 1.63%, whereas those for the device **b** and **c** are 3.04% and 6.05%, respectively. All data are shown in Table 4.3. The lower efficiency of the (2-phenyl-1-pyrroline)$_2$Ir(acac)-based OLED relative to that of the (4OMeppl)$_2$Ir(acac)-based EL device may be attributed to a lower phosphorescence efficiency of the former as compared to the latter. Furthermore, no emission from CBP or Alq_3 was observed, indicating a complete energy transfer from the host exciton to the Ir-dopant. Meanwhile, there is no exciton decay in the Alq_3 layer due to the hole blocking action of the BCP layer. As shown in the insets of Fig. 4.4, the device having methoxyl-substituted dopant shows the expected blue-shift and stronger intensity in the EL spectra as compared to that observed in the device with unsubstituted dopant. The EL spectra of **4-F, 4-OMe** and **4-H** devices are similar to the PL spectra of same phosphors in a different current density. Thus, the EL emission is confirmed to be originated from the triplet excited states of the phosphors. It is expected that the devices with the rest of the dopants synthesized and investigated in our work will exhibit more or less

similar EL properties to those of devices **D-a, D-b** and **D-c**.

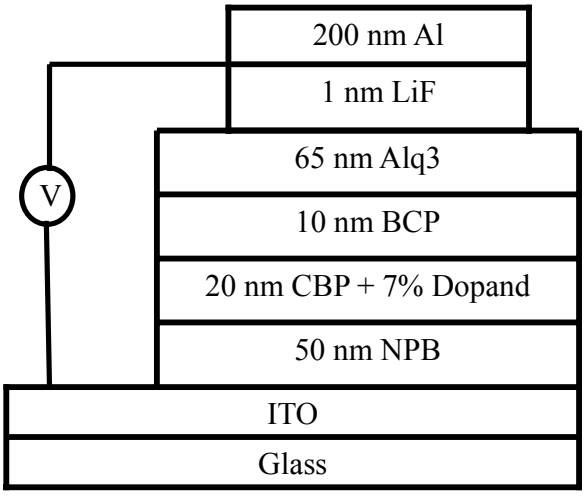

Figure 4.3 EL device structures with $(ppl)_2Ir(acac)$, $(4OMeppl)_2Ir(acac)$, and $Ir(4Fppl)_3$ complexes as dopants.

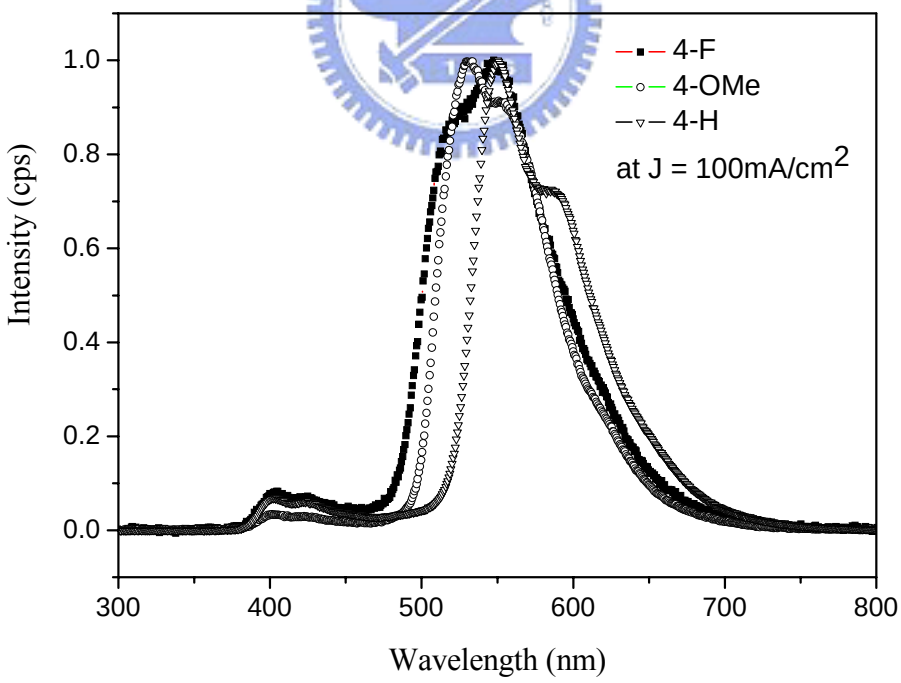

Figure 4.4 Comparison of EL spectra for devices

Table 4.3. EL performance of devices D-a, D-b, and D-c fabricated with $(4\text{-x-ppl})_2\text{Ir(acac)}$ complexes (x = H, OMe, F)

Devices	Voltage (V)	Yield (cd/A)	Efficiency (lm/W)	CIE (x,y)	FWHM (nm)	E.Q.E	$E_{1/2}$ (V)
a (-H)	9.20	4.10	1.40	0.48, 0.47	104	1.63	0.883
b (-OMe)	8.59	8.49	3.10	0.43, 0.52	112	3.04	0.795
c (-F)	8.09	6.49	2.52	0.36, 0.52	116	2.25	0.735

4.4 Conclusion

Cyclometallated iridium complexes have been shown to exhibit high phosphorescence efficiency which made them ideal candidate for OLED applications. We have synthesized a new series of Ir(III)-complex dopants containing various types of substituted phenylpyrroline ligands. These complexes show different quantum efficiencies in solution depending upon the nature of the substituents. The λ_{em} has been tuned by *ca.* 43 nm depending upon the electronic properties of the substituents of the ligands.

Acknowledgements

This research is supported by Program for Promoting University Academic Excellence from Ministry of Education, Taiwan, Republic of China under the Contract 91-E-FA04-2-4-(B).

4.5 References

1. Bignozzi,C. A.; Schoonover, J. R.; Scandola, F.; *Prog. Inorg. Chem*. **44** (1997) 11

2. (a) Lamansky, S.; Djurovich, P.; Murphy, D.; Abdel-Razzaq, F.; Lee, H. F.;

Adachi, C.; Burrows, P. E.; Forrest, S. R.; Thompson, M. E.; *J. Am. Chem. Soc.* **123** (2001) 4304. (b) Thompson, M. E.; Lamansky, S.; Djurovich, P.; Murphy, D.; Abdel-Razzaq, F.; Kwong, R.; Forrest, S. R.; Baldo, M. A.; Burrows, P. E.; patent US 20020034656A1.

3. Brooks, J.; Babayan, Y.; Lamansky, S.; Djurovich, P. I.; Tsyba, I.; Bau, R.; Thompson, M. E.; *Inorg. Chem.*, **41** (2002) 3055.

4.(a) Chin, K.-F.; Cheung, K.-K.; Yip, H.-K.; Mak, T. C.; Che, C. M.; *J. Chem. Soc., Dalton Trans.* **4** (1995) 657 (b) Kalyanasundaram, K.; Gratzel, M.; *Coord. Chem. Rev*. **177** (1998) 347

5. Anderson, P. A.; Anderson, R. F.; Furue, M.; Junk, P. C.; Keene, F. R.; Patterson, B. T.; Yeomans, B. D.; *Inorg. Chem*. **39** (2000) 2721

6. Zhang, Y.; Baer, C. D.; Neto, C. C.; P. O'Brien and Sweigart, D. A.**;** *Inorg. Chem*. **30** (1991) 1685

7. (a) Lamansky, S.; Djurovich, P.; Murphy, D.; Abdel-Razzaq, F.; Lee, H-F.; Adachi, C.; Burrows, P. E.; Forrest, S. R.; Thompson, M. E.; *J. Am. Chem. Soc.* **123** (2001) 4304.

8. Tamayo, A. B.; Alleyne, B. D.; Djurovich, P. I.; Lamansky, S.; Tsyba, I.; Ho, N. N.; Bau, R.; and Thompson, M. E.; *J. Am. Chem. Soc.* **125** (2003) 7377

9. Tang, C. W.; VanSlyke, S. A.; Chen, C. H.; *J. Appl. Phys.* **65** (1989) 3610.

10. (a) Baldo, M. A.; Lamansky, S.; Burrows, P. E.; Thompson, M. E.; Forrest, S. R.; *Appl. Phys. Lett*. **75** (1999) 4. (b) Adachi, C.; Kwong, R. C.; Djurovich, P.; Adamovich, V.; Baldo, M. A.; Thompson, M. E.; Forrest, S. R.; *Appl. Phys. Lett*. **79** (2001) 2082. (c) Jiang, X.; Jen, A. K.; Carlson, B.; Dalton, L. R.; *Appl. Phys. Lett*. **80** (2002) 713

11. Hung, H. W.; Chen, T. M.; *Materials Chemistry & Physics*. (2006) in press

12. Arnold, B. T.; Bert, D. A .; Peter, I. D.; Sergey, L.; Irina, T.; Nam, N. H.; Robert, B.; Thompson, Mark E.; *J. Am. Chem. Soc.* **125** (2003) 7377.
13. Vicente, J.; Arcas, A.; Bautista, D.; Arellano, M. C.; *J. Organomet. Chem*. **663** (2002) 164.
14. Yoshihiko Kanemitsu, Katsunori Suzuki, Michio Kondo, Soichiro Kyushin, Hideyuki Matsumoto; *Physical Review B.* **51** (1995) 10666
15. Kenichi Goushi, Yuichiro Kawamura, Hiroyuki Sasabe, Chihaya Adachi, *Japn. J. Appl. Phys.*, **43** (2004) 937
16. Mundy, P. B.; Larsen, R. B.; Lee, F.; Braden, G.; *J.Org.Chem*. **37** (1972) 1635
17. Tobin, J.; Dickerson, Kim D. Janda; *J.Am.Chem.Soc*. **124** (2002) 3220
18. Iao Tanaka, Shizuo Tokito; *Journal of Applied Physics* **97** (2005) 113532
19. Yuichiro Kawamura, Hiroyuki Sasabe, Chihaya Adachi; *Japn. J. Appl. Phys.*, **43** (2004) 7729

Chapter 5

High Phosphorescence Quantum Efficiency of Red-orange Emitting Ir(III) Complexes

Abstract

Solid-state self-quenching processes of highly efficient Ir(III) phosphorescent emitters are investigated by the measuring thin film photoluminescence (PL) quantum efficiency as a function of doping concentration in a host matrix. We demonstrate that the Ir complexes used as dopants in organic electrophosphorescent diodes exhibit very high PL quantum efficiency (η_{PL}) in the solid-state. The red-orange emitting complex, bis[(4-trifluoromethyl)2-phenylbenzthiazole-N, C](acetylacetonato) iridium(III) [Ir(4-CF_3bt)$_2$(acac)] were prepared as codeposited films of different concentration with 4,4'-bis(*N*-carbazolyl)-2,2'-biphenyl, a commonly used host material. The maximum the photoluminescence (PL) quantum efficiency (η_{PL}) values for [Ir(4-CF_3bt)$_2$(acac)] and Bis(2-phenylquinoline) (acetylacetonato) iridium(III) [Ir(2-phq) $_2$acac] have been determined to be 64% at 1.13 mol% (corresponding to 2.0wt%) and 80% at 1.38 mol% (corresponding to 2.0wt%), respectively.

5.1 Introduction

Organic light-emitting devices (OLEDs) based on small organic molecules have been attracting much attention ever since Tang first demonstrated a highly efficient OLEDs.[1] To achieve higher quantum efficiency, phosphorescent OLEDs that harvest both singlet and triplet excitions have been demonstrated. [2-4] The photophysical properties of organic phosphors in a molecularly doped thin film, the photoluminescence (PL) quantum efficiency (η_{PL}) can provide important information on how to optimize the external electroluminescence (EL) efficiency (η_{EL}) of OLEDs. In previous work, cyclometalated Ir(III) complexes were reported to be promising candidates for phosphorescent dopants because they can emit with high efficiency at room temperature from the triplet metal-to-ligand charge-transfer (^{3}MLCT) state.[5,6] It is well known that many fluorescent materials are severely quenched as neat films due to significant overlap of absorption and emission. While phosphorescent Ir (III) complexes emitting from mixed ^{3}MLCT/π-π* transitions tend to be less absorptive in the region of emission, they are also known to suffer from significant PL quenching at increased dopant concentrations. Since the emission decay processes in fluid solution markedly differ from those in a rigid solid state, the phosphorescent decay processes of Ir(III) complexes in a practical OLED device configuration should be investigated by measuring the absolute η_{PL} in a solid-state film. In this study, we have determined and reported the absolute η_{PL} of phosphorescent Ir(III) complexes and their dependencies for doping concentrations by using an integrating sphere. [7]

5.2 Experimental Section

5.2.1 Materials

All of the preparative work involving iridium(III) trichloride hydrate ($IrCl_3 \cdot 3H_2O$, Alfa Aesar Company Ltd.), 2-ethoxyethanol ($H_5C_2OC_2H_4OH$, Fluka) and all other reagents (Tokyo Chemical Industry, Japan) were carried out in an inert atmosphere and used without further purification.[8,9] The ligands, 4-trifluoromethyl)2-phenylbenzthiazole and complexes have been prepared by following the method described in the literature.[10]

5.2.2 Instruments

UV-visible spectra were measured on an Agilent 8453 spectrophotometer. Photoluminescent spectra were carried out with Fluorolog ISA JOBIN YOON-Spex spectrophotometer. Comparative quantum efficiencies have been measured using spectra ARC sense analysis, v 1.08 software and $(bt)_2Ir(acac)$ as a reference. NMR spectra were recorded on Varian 300 MHz. MS spectra (EI and FAB) were taken by micromass TRIO-2000. Elemental analyses have been carried out by Heraeus CHN-O-RAPID. Cyclic voltammo gram analyses were performed by TG-DTA analysis was carried out by SEIKO 1TG/DTA 200.

5.2.3 Crystal structure determination

Diffraction data for $(CF_3bt)_2Ir(acac)$ were collected at 25°C on a Bruker CCD diffractometer with Mo Kα radiation (λ= 0.71073). Data collection in the 2θ scan mode, cell refinement and data reduction were carried out with the using program Bruker SHELXTL. The structure was solved by direct

methods using the SHELXS-97 package of computer programs. The structure was refined by full-matrix least-squares methods based on F^2 using SHELXL-97. The non-hydrogen atom positions were refined anisotropically whereas the hydrogen positions were not refined.

5.2.4 Film for measurement of absolute PL quantum efficiency

Organic layer were deposited by high-vaccum (10^{-6} Torr) thermal evaporation onto a precleaned glass substrate precoated with an indium-tin-oxide (ITO) anode. Organic films were fabricated at a thickness of 100 nm by conventional thermal vacuum deposition 10^{-3} Pa on precleaned quartz substrates for measurement of absolute PL quantum efficiency and on silicon substrates for measurement of transient photoluminescence. The doping concentration and film thickness were controlled by two quartz crystal microbalances calibrated for thickness and two thermal evaporating sources. The η_{PL} of the films was measured under N_2 flow using an integrating sphere (Labsphere Co., 10 cm diameter) with a 325-nm cw HeCd laser (Kinmon TK5651) as the excitation source and multichannel spectrometer (Hamamatsu PMA-11) as the optical detector. The system for η_{PL} measurements was calibrated by using a standard light source and it was confirmed that a neat film of tris(8-quinolinolato)aluminum(III) complex, as a standard fluorescent emitter, showed an η_{PL} of 20±1% in our system.[7] Furthermore, the transient photoluminescence was measured using a streak camera (Hamamatsu C4334) with a N_2 gas laser (MNL 200, Laser Technik Berlin, λ= 337 nm, pulse width ~500 ps, and repetition rate =20 Hz) as the excitation source. The measurements were done under a low pressure (~10^{-1} Pa) in a cryostat.

5.2.5 OLED Fabrication

Organic layers were fabricated by high-vacuum thermal evaporation onto a glass substrate precoated with an indium-tin-oxide (ITO) layer with a sheet resistance of 20 Ω. Prior to use, the ITO surface was ultrasonicated in a detergent solution followed by a deionised water rinse, dipped into acetone, trichloroethylene, and 2-propanol, and then degreased in 2-propanol vapor. After degreasing, the substrate was oxidized and cleaned in a UV-ozone chamber before it was loaded into an evaporator. In a vacuum chamber at pressure Torr, 500 Å of NPB as the hole transporting layer; 200 Å the complex doped (7%) CBP as the emitting layer; 100 Å of 2, 9-dimethyl-4,7-diphenyl-1, 10-phenanthroline (BCP) as a hole and exciton blocking layer (HBL); 650 Å of Alq_3 as electron transport layer; and a cathode composed of 10 Å lithium fluoride and 2000 Å aluminium were sequentially deposited onto the substrate to give the device structure shown in Figuer 5.1. Device current-voltage and light intensity characteristics were measured using KEITHLEY 2400 and PR 650, respectively.

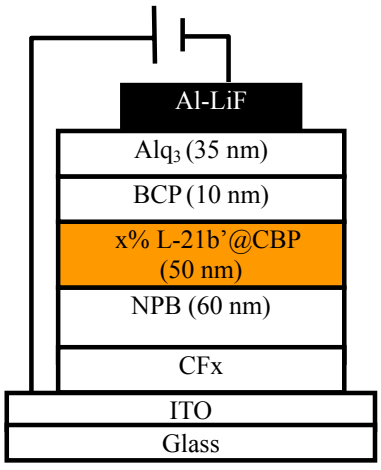

Figure 5.1 EL device structures with Ir(4-CF_3bt)$_2$(acac):CBP and Ir(2-phq)$_2$acac :CBP complexes as dopants.

5.2.6 Syntheses.

(a)Synthesis of xbt (x = 4CF_3 and bt = (2-phenyl)benzthiazole)

These were prepared in a general method [8,9] where 10 mmol o-aminothiophenol was dissolved into 20 ml of 1-methyl-pyrrolidinone under inert atmosphere; then the stoichiometric amount of the corresponding acid chloride was added slowly at room temperature. The mixture was heated at 100°C for one hour. After cooling the solution was poured into cold water and the mixture was adjusted to pH 8-9 with 7N aqueous ammonia. A white coloured solid compound was separated out. The crude material was filtered, washed with water for several times and purified by column chromatography.

(4-CF_3)bt (1). (4-trifluoromethyl)2-phenylbenzthiazole (yield 84 %). ^{1}HNMR (300 MHz, $CDCl_3$) : δ, ppm 8.21 (d, 2H, J 7.8 Hz), 8.11 (d, 1H, J 7.8 Hz), 7.94 (d, 1H, J 7.2, Hz), 7.76 (d, 2H, J 8.1 Hz), 7.53 (td, 1H, J 1.2, 8.1 Hz), 7.43 (d, 2H, J 0.9, 8.1 Hz). EIMS: m/z: 279, Calc. 279.

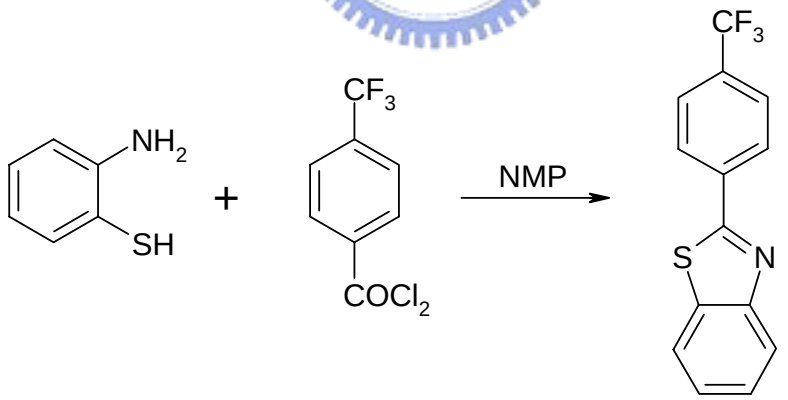

(1)

(b) Syntheses of the dichoro-bridged iridium(III) complexes

These were prepared [8-9] by refluxing the mixture of $IrCl_3$ (1 mmol) and the ligands (4-CF_3bt) (2.4 mmol) in 2-ethoxyethanol for 24~25h. The orange-yellow mixtures was cooled to room temperature and 20 ml 1 M HCl

was added to precipitate the product. The mixture was filtered and washed with 100 ml 1M HCl followed by 50 ml methanol solution for several times then dried.

$[Ir(4\text{-}CF_3bt)_2Cl_2]_2$ (2). Yield 67 %. (Found : C, 42.5; H, 1.8; N 3.3. Calc. for $C_{56}H_{40}N_4O_4S_4Cl_2Ir_2$: C, 42.9; H, 1.8; N, 3.6 %). ^{1}HNMR (300 MHz, $CDCl_3$) : ^{1}HNMR (300 MHz, $CDCl_3$) : δ, ppm 8.59 (dd, 4H, J 0.75, 7.5 Hz), 7.64 (d, 4H, J 8.1 Hz), 7.49 (dd, 4H, J 1.2, 7.8 Hz), 7.13 (m, 12H), 6.19 (s, 4H). FABMS: m/z 1567, Calc. 1567.

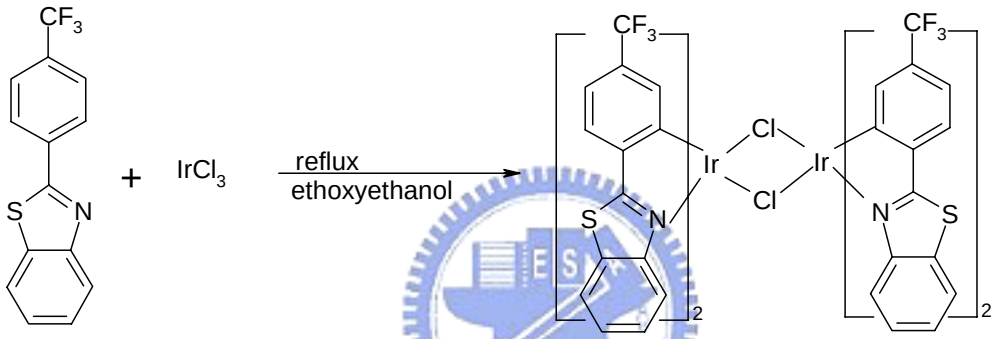

(2)

(c) Syntheses of $(4\text{-}CF_3bt)_2Ir(acac)$

The chloride bridged dimer, $[Ir(4\text{-}CF_3bt)_2Cl_2]_2$ (0.1 mmol), acetylacetone (0.3 mmol) and sodium carbonate (1 mmol) were mixed in 10 ml of 2-ethoxyethanol (30 ml) [9]. The mixture was refluxed under nitrogen for 11 hrs. The reaction was then cooled and the precipitate filtered. The product was purified by recrystallisation from a solution of the mixture of dichloromethane and methanol (2 : 1).

$Ir(4\text{-}CF_3bt)_2(acac)$ (3). Yield 81 %. (Found : C, 46.5; H, 2.5; N 3.1. Calc. for $C_{33}H_{21}N_2O_4F_6S_2Ir$: C, 46.7; H, 2.5; N, 3.3 %). ^{1}HNMR (300 MHz, $CDCl_3$) : δ, ppm 8.06 (d, 2H, J 8.1 Hz), 7.96 (d, 2H, J 8.7 Hz), 7.74 (d, 2H, J 8.1 Hz), 7.49 (m, 4H), 7.12 (d, 2H, J 7.8 Hz), 659 (s, 2H), 5.13 (s, 1H), 1.78 (s, 6H). FABMS : m/z 847, Calc. 847

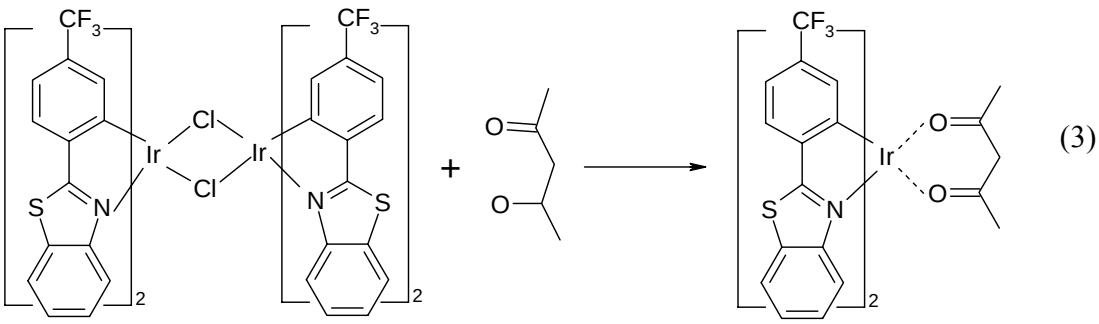

(3)

5.3 Results and discussion

5.3.1 UV-Vis absorption spectra.

Figure 5.2 shows the absorption bands of [Ir(4-CF_3bt)$_2$(acac)] complex. It suggests that the bands can be classified in two types – intense bands are observed in the ultra-violet part of the spectrum (250-350 nm) can be assigned to the allowed ligand-centered (π-π^*) transitions, somewhat weaker bands are observed in the lower part of energy (λ_{max} >385 nm). The band position, size and the extinction coefficients suggest that these were recognized as MLCT transition,[13,14] ^{1}MLCT and ^{3}MLCT transitions have been resolved in the range, 385-450 nm. The long tail toward lower energy is assigned to ^{3}MLCT transitions, gains intensity by mixing with the higher lying ^{1}MLCT transition through the spin-orbit coupling of iridium(III).[13] This mixing is strong enough in these complexes that the formally spin forbidden ^{3}MLCT has an extinction coefficient that is almost equal to the spin-allowed ^{1}MLCT transition. The presence of another transition around 360 nm of the complexes is also well pronounced which corresponds to an admixture of MLCT and ligand π-π^* states.

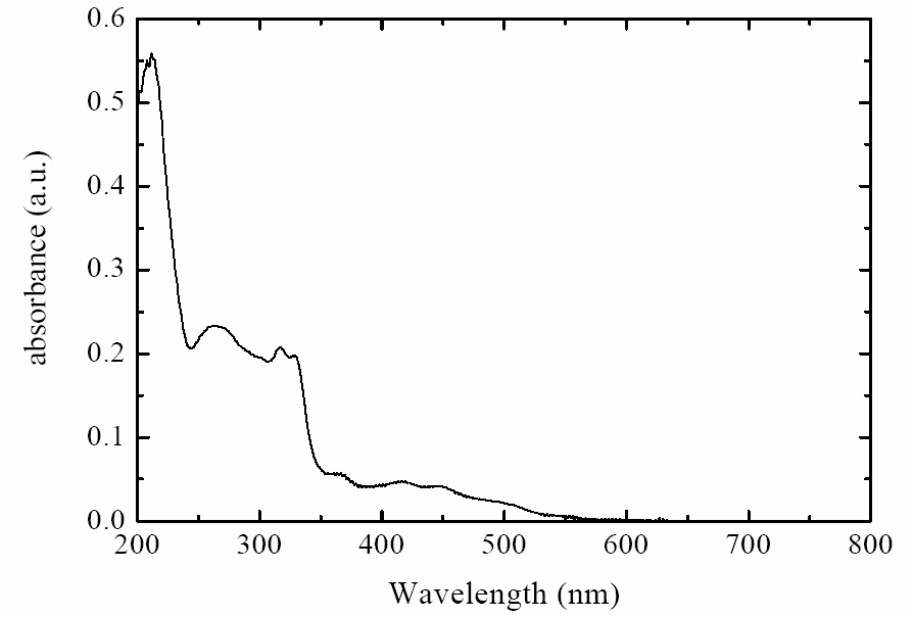

Figure 5.2 shows the absorption bands of [Ir(4-CF_3bt)$_2$(acac)] complex.

5.3.2 Description of crystal structure of (CF_3bt)$_2$Ir(acac)

Molecular diagram of the complex is shown in Figure 5.3. Crystallographic data are given in Table 5.1, and selected bond lengths and bond angles are presented in Table 5.2. The complex has an octahedral coordination geometry around Ir and prefers *cis*-C,C *trans*-N,N chelate disposition instead of *trans*-C,C *trans*-N,N chelate. Electron-rich sigma-phenyl ligands normally exhibit very strong *trans*-influence and *trans*-effect. Therefore, the *trans* C-C arrangement is expected to be higher in energy (thermodynamics) and more labile (kinetics). This well-known phenomenon has been recently referred to as "transphobia".[15] The Ir-C bonds of these complexes (Ir-C_{av}= 1.992(6) Å) are shorter than the Ir-N bonds (Ir-N_{av} = 2.053(5) Å). The Ir-C bond length is similar to the analogues complexes reported.[16-18] The Ir-N bond lengths also fall within the range of values for the similar type of reported complexes.[16-18] The Ir-O bond lengths

of 2.131(4) and 2.138(4) Å are longer than the mean Ir-O value of 2.088 Å reported and reflect the large *trans* influence of the phenyl groups. All other bond lengths and bond angles within the chelate ligands are analogues to the similar type of complexes.[16-18] Thermal ellipsoid values for the atoms C19, C33, F1-F6 are exceptionally high which suggests that the severe steric interaction between the substituents, trifluoromethyl between two separate ligands.

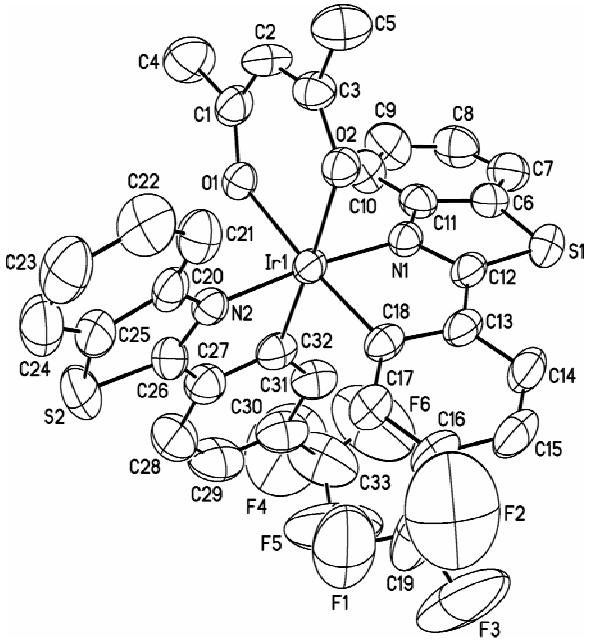

Figure 5.3 ORTEP drawing of $(CF_3\text{-bt})_2Ir(acac)$

Table 5.1. Crystal Data and Structure Refinement for $(CF_3bt)_2Ir(acac)$

Empirical formula	$C_{33}\ H_{21}\ F_6\ Ir\ N_2\ O_2\ S_2$
Formula weight	847.84
Temperature	295(2) K
Wavelength	0.71073 Å
Crystal system	Orthorhombic
Space group	Pbca
Unit cell dimensions	a = 12.5646(6) Å
	b = 17.9936(9) Å
	c = 27.8150(14) Å
Volume	6288.5(5) $Å^3$
Z	8
Density (calculated)	1.791 mg/m^3
Absorption coefficient	4.449 mm^{-1}
F(000)	3296
Crystal size	0.40 x 0.30 x 0.10 mm^3
Theta range for data collection	1.46 to 28.29°.
Index ranges	$-16 \le h \le 16$, $-18 \le k \le 23$, $-36 \le l \le 37$
Reflections collected	37577
Independent reflections	7633 [R(int) = 0.0523]
Absorption correction	Empirical
Max. and min. transmission	0.95767 and 0.50780
Refinement method	Full-matrix least-squares on F^2
Data / restraints / parameters	7633 / 0 / 415
Goodness-of-fit on F^2	1.082
Final R indices [I>2sigma(I)]	R1 = 0.0488, wR2 = 0.0856
R indices (all data)	R1 = 0.0876, wR2 = 0.0969
Largest diff. peak and hole	1.089 and -1.707 $e.Å^{-3}$

Table 5.2. Selected Bond Distancess [Å] and Angles [°] for $(CF_3bt)_2Ir(acac)$

Atom(1)- Atom(2)	Distance (Å)
Ir(1)-C(32)	1.989(6)
Ir(1)-C(18)	1.994(6)
Ir(1)-N(1)	2.049(5)
Ir(1)-N(2)	2.056(5)
Ir(1)-O(2)	2.131(4)
Ir(1)-O(1)	2.138(4)

5.3.3 Property of Solid-state

Concentration quenching in neat films of both monomeric[11] and dendrimeric [12] phosphorescent materials has been reported. In the previous paper[11], we have observed that the famous red-emitting $Btp_2Ir(acac)$:CBP in film exhibited a maximum η_{PL} of 51% at 1.4 mol% (corresponding to 2.0 wt%). We also measured the quantum efficiency (η_{PL}) for thin film sample of $Ir(4\text{-}CF_3bt)_2(acac)$ and Ir(2-phq) $_2$acac complexes by using an integrating sphere equipped with a He-Cd laser (λ = 355 nm) as an excitation source and a multi-channel spectrometer as an optical detector to compare the η_{PL}. Based on equation (1) [7] where $N_{emission}$ is the emission photon number from the sample, $N_{absorption}$ is the absorbed photon number by the sample, γ is the calibration factor for the measurement setup, λ is the wavelength, h is plank's constant, c is the speed of light, $I_{em}(\lambda)$ is the PL intensity from the sample, $I_{ex}(\lambda)$ is the intensity of the excitation laser without the sample, and $I'_{ex}(\lambda)$ is the intensity of the excitation laser with the sample. From eq. (1) we obtained the η_{PL} = 64% and 80%, respectively, for $Ir(4\text{-}CF_3bt)_2(acac)$ and Ir(2-phq) $_2$acac at 2 wt%.[7]

$$\eta_{PL} = \frac{N_{emission}}{N_{absorption}} = \frac{\alpha \int \frac{\lambda}{hc} I_{em}(\lambda) d\lambda}{\alpha \int \frac{\lambda}{hc} [I_{ex}(\lambda) - I'_{ex}(\lambda)] d\lambda} \qquad (1)$$

The η_{PL} as a function of doping content of Ir(4-CF_3bt)$_2$(acac) and Ir(2-phq)$_2$acac film samples doped into a conventional host material 4,4'-bis (*N*-carbazolyl)-2,2'-biphenyl (CBP) of are compared and shown in Figure 5.4. Both Ir(III) complex films emit red-orange light and exhibit high η_{PL} of 64% and 80% at 2 wt% as compared to that of than $Btp_2Ir(acac)$:CBP film (η_{PL} of 51% at 2 wt%). The experimental doping concentrations of the Ir(III) complexes ranged from 2 wt% to 33 wt%. Data analysis indicates that with increasing dopant concentration that the EQE of the devices increases monotonically as shown in Figure 5.5. We have found that η_{PL} decreased with increasing dopant concentration of Ir(4-CF_3bt)$_2$(acac) and Ir(2-phq)$_2$(acac) complexes.

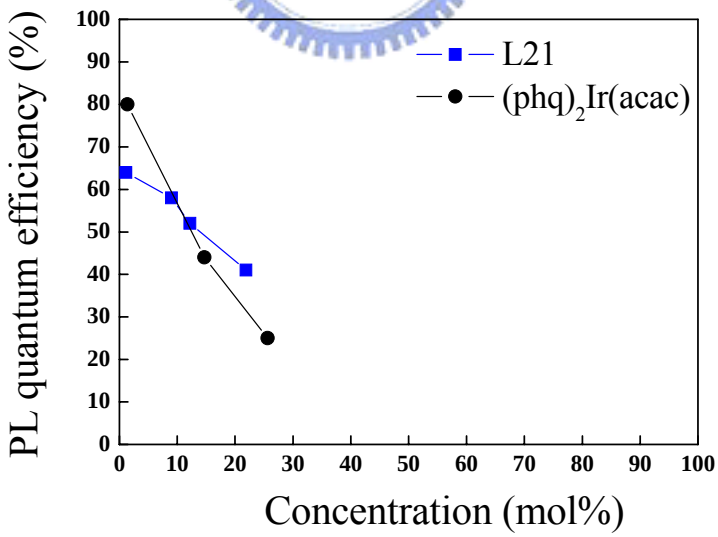

Figure 5.4 PL quantum efficiency η_{PL} vs dopant concentration in thin film samples of Ir(4-CF_3bt)$_2$(acac):CBP and Ir(2-phq)$_2$acac :CBP

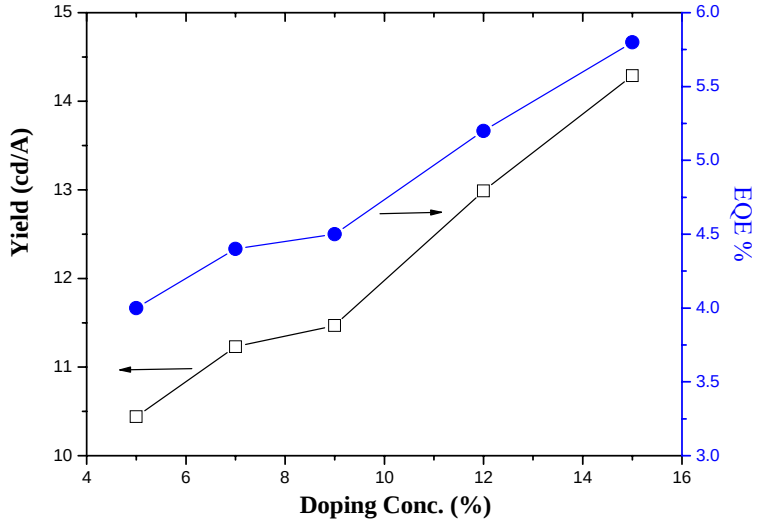

Figure 5.5 Dopant concentration dependence of vs yield and EQE of Ir(4-CF_3bt)$_2$(acac): CBP film

However, at a dopant concentration as high as 33 wt% , PL intensity of the two complexes show very different values. Our Ir(4-CF_3bt)$_2$(acac) complex exhibits still 70% of its maximum value, but that of Ir(2-phq) $_2$acac complex only reaches 30% of that though Ir(2-phq) $_2$acac complex show higher η_{PL} at 2 wt%. This suggests that concentration quenching in the Ir(4-CF_3bt)$_2$(acac):CBP film is less effective than observed for the Ir(2-phq) $_2$acac :CBP film. These observations can be rationalized by the steric factor of the molecular structure of Ir(4-CF_3bt)$_2$(acac) that hinders possible stacking between molecules and weakens the quenching in the film of Ir(4-CF_3bt)$_2$(acac) as compared to that in Ir(2-phq) $_2$acac : CBP film. We also measured the solution $\eta_{PL,}$ and it was found to be 56% and 73% for Ir(4-CF_3bt)$_2$(acac) and Ir(2-phq) $_2$acac in the dichloroethane at 300K, respectively.

Emission lifetime (τ_e) was also measured in tempature range of 8-300 K, and the temperature dependence of τ_e and PL intensity is shown in Figure

5.6. The PL intensity of the Ir(4-CF_3bt)$_2$(acac) :CBP film showed no significant temperature dependence between 8 and 300 K. These result s suggest that the Ir(4-CF_3bt)$_2$(acac) has an intrinsic nonradiative decay processes that appears to function independently of temperature.

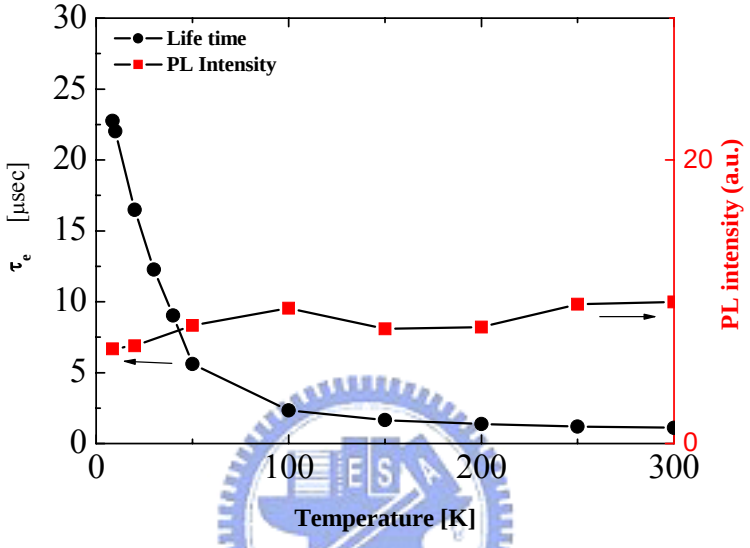

Figure 5.6 Temperature dependence of decay lifetime and PL intensity for Ir(4-CF_3bt)$_2$(acac).

5.3.4 Description of OLEDs prepared with (CF_3bt)$_2$Ir(acac) dopants in emissive layer with varying concentration.

Based on the experimental $\eta_{PL,}$ we have fabricated the Ir(4-CF_3bt)$_2$(acac)-based EL device in varying dopant concentration at 5% (device **a**), 7% (device **b**), 9% (device **c**), 12% (device **d**) and 15% (device **e**) and the device structure is ITO/ N,N'-diphenyl-N,N'-bis(1-naphthyl)-(1,1'-biphenyl)-4,40-diamine (NPB) (60 nm)/ CBP: x% Ir(4-CF_3bt)$_2$(acac) (50 nm)/ bathocuproine (BCP)(10 nm)/ tris-(8-hydroxyquinoline) aluminum (Alq) (35 nm)/ LiF/ Al. The EL performances are shown in the table 5.3 and

corresponding EL spectra are shown in Figure 5.7. We have found that the external quantum efficiency (EQE) of the EL devices **a-e** is 4.0, 4.4, 4.5, 5.2 and 5.8. The maximum yields were found to be 10.4, 11.2, 11.5, 13.0 and 14.3 cd/A at 13.2, 13.1, 12.7, 12.4 and 12.3 (V), respectively. The power efficiencies were also found to be 2.49, 2.69, 2.83, 3.29 and 3.64 lm/W for the devices, **a, b, c, d** and **e**, respectively. The observed EQE of thin film sample of $Ir(4\text{-}CF_3bt)_2(acac)$: CBP was found to be 5.8% with dopant content at 15 wt% indicates weak quenching effect in the film.

Table 5.3 EL Performance of devices **a**, **b**, **c**, **d** and **e** fabricated with different content of $Ir(4\text{-}CF_3bt)_2(acac)$ complex

Device	Voltage (V)	Yield (cd/A)	$CIE_{x,y}$	Peak Wavelength (nm)	Power efficiency (lm/W)	E.Q.E. (%)
a	13.2	10.4	(0.51, 0.47)	568	2.49	4.0
b	13.1	11.2	(0.51, 0.47)	568	2.69	4.4
c	12.7	11.5	(0.52, 0.47)	572	2.83	4.5
d	12.4	13.0	(0.52, 0.46)	572	3.29	5.2
e	12.3	14.3	(0.52, 0.46)	572	3.64	5.8

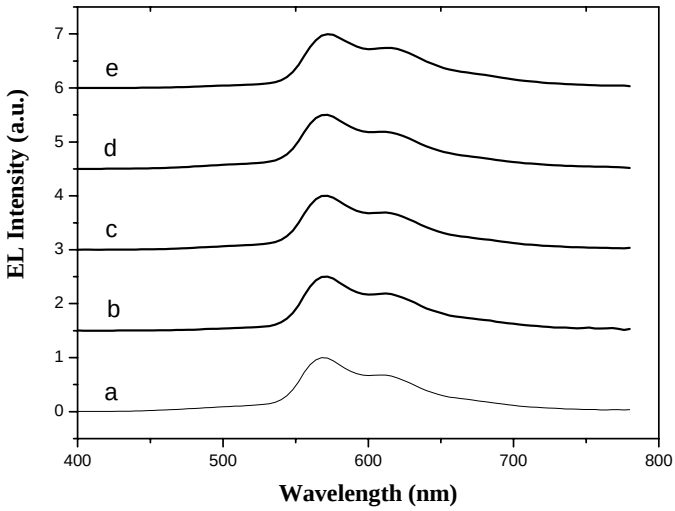

Figure 5.7 EL spectra of devices **a**, **b**, **c**, **d** and **e** fabricated with different dopant contents of Ir(4-CF_3bt)$_2$(acac) complex

5.4 Conclusion

In conclusion, the η_{PL} of Ir(4-CF_3bt)$_2$(acac) and Ir(2-phq)$_2$(acac) complexes were measured in the solid-state by using an integration sphere and was found to reach 64% and 80% (at 2 wt%), respectively. In particular, Ir(4-CF_3bt)$_2$(acac) still exhibitsη_{PL} of 41% at dopant concentration as high as 33 wt%. The observed η_{PL} of 70% can be attributed to weak quenching effect and it is predominant for red-orange emitting materials. We have also reported and rationalized a series of high EQE with varied dopant concentrations in a device.

5.5 References

1. Tang, C. W. and Vanslyke, S. A.: *Appl. Phys. Lett.* 51 (1987) 913.
2. Baldo, M. A.; O'Brien, D. F.; You, Y.; Shoustikov, A.; Sibley, S.; Thompson, M . E. and Forrest, S. R.: *Nature* 395 (1998) 151.
3. Baldo, M. A.; Lamansky, S.; Burrows, P. E.; Thompson, M. and Forrest, S.

R.: *Appl. Phys. Lett*. 75 (1999) 4.

4. Adachi, C.; Baldo, M. A.; Forrest, S. R.; Lamamsky, S.; Thompson, M. E. and Kwong, R. C.: *Appl. Phys. Lett*. 78 (2001) 1622.
5. King, K. A.; Spellane, P. J. and Watts, R. J.; *J. Am. Chem. Soc*. 107 (1985) 1431
6. Lamansky, S.; Djurovich, P.; Murphy, D.; Abdel-Razzaq, F.; Adachi, C.; Burrows, P. E.; Forrest, S. R. and Thompson, M. E.; *J. Am. Chem. Soc*. 123 (2001) 4303
7. Kawamura, Y.; Sasabe, H. and Adachi,C.; *Jpn. J. Appl. Phys., Part 1* 43 (2004) 7729
8. Zhang, Y.; Baer, C. D.; Neto, C. C.; O'Brien, P. and Sweigart**,** D. A.; *Inorg. Chem*. 30 (1991) 1685
9. (a) Lamansky, S; Djurovich, P.; Murphy, D.; Abdel-Razzaq, F.; Lee, H-F.; Adachi, C.; Burrows, P. E.; Forrest, S. R.; Thompson, M. E. *J. Am. Chem. Soc.* 123 (2001) 4304. (b) Thompson, M. E.; Lamansky, S; Djurovich, P.; Murphy, D.; Abdel-Razzaq, F.; Kwong, R.; Forrest, S. R.; Baldo, M. A.; Burrows, P. E. patent US 20020034656A1.
10. Laskar I. R., Chen. T. M., *Chem. Mater.* 16 (2004) 111.
11. Kawamura, Y.; Goushi, K.; Brooks, J.; Brown, J. J.; Sasabe, H. and Adachi, C.; *Appl. Phys. Lett.* 86 (2005) 071104
12. Namdas, E. B.; Ruseckas, A.; Sammuel, I. D.W.; Lo, S.-C. and Burn, P. L.; *J. Phys. Chem. B* 108 (2004) 1570
13. Maestri, M. D.; Sandrini, V.; Blazani, U.; Maeder and VonZelewsky, A.; *Inorg. Chem.*, 26 (1987) 1323.
14. Colombo, M. G.; Hauser, A. and H. U. Gu¨ del, *Inorg. Chem.*, 32 (1993) 3088.
15. Vicente J.; Arcas, A.; Bautista, D.; Arellano, M. C. R. de *J. Organomet.*

Chem. 663 (2002) 164.

16 Garces, F. O.; Dedian, K.; Keder, N. L.; Watts, R. J.; *Acta Crystallogr.* C49 (1993) 1117.

17 Urban, R; Krämer, R.; Mihan, S.; Polborn, K.; Wagner, B.; Beck, W. *J. Organomet. Chem*. 2000, 1039.

18 Neve, F.; Crispini, A. *Eur. J. Inorg. Chem.* 2000, 1039.

Chapter 6

The Characterization and Fabrication of White-Emitting Electrophosphorescent OLEDs

Abstract

OLED white light of two wave bands with systematic phosphorescent designs which need high-efficiency, high-brightness and long lifetime orange light. We have developed and fabricated highly efficient white organic light-emitting devices (WOLEDs) with very broad emission based on an orange emitter, bis (4-triflurophenyl)benzothiozolato-N,$C^{2'}$) iridium(acetylacetonate) [Ir(4-CF_3bt)$_2$acac] and tri(2-phenylquinoline) iridium complexes. A white-light device with one of the highest EL efficiencies of 8.6 % with Commission Internationale d'Eclairage (CIE) coordinates of (x＝0.350, y＝0.396) has been demonstrated.

6.1 Introduction

White organic light-emitting devices (WOLEDs) have been attracting increasing attention due to their various promising applications. White organic light-emitting devices (WOLEDs) can be used in flat-panel displays and as an alternative lighting source and full color displays through color filters backlights for liquid displays. WOLEDs coupled with color filter (CF) have become popular as one of the major methodologies to fabricate full color devices. This is primarily due to the cost and mass production consideration in manufacturing as discreet red, green and blue (RGB) pixilation process can be accomplished without using the precision shadow mask. However, introducing CF on WOLEDs significantly reduces light intensity and results in low efficiency for full-color displays.

In recent years, organic electrophosphorescent materials provide one of the major breakthroughs in the device efficiency. 100% excitons were converted into the triplet excited state through inter-system crossing via the presence of a heavy metal atom, which is corresponding to an external quantum efficiency of 20% theoretically[1]. These phosphorescent emitters are most promising for achieving high-efficiency WOLEDs. Compared to the fluorescence emission, the triplet emitters show much high inner quantum efficiency of 100% in theory.[2] Efficiently phosphorescent small molecular-based white light-emitting diodes (WOLEDs) have been demonstrated by many groups.[3–5] For example, by using small molecule host, there were several high-efficiency WOLEDs based on phosphorescent materials reported in literature. D'Andrade demonstrated a white light device with iridium(III)bis(4,6-di-fluorophenyl)-pyridinato-N,C^2) picolinate (FIrpic), bis(2-phenyl-benzothiozolato-N,$C^{2'}$) iridium(acetylacetonate) (bt_2Iracac) and bis(2-(2'-benzo-[4,5-a]thienyl)pyridinato-N,C^3)

iridium(acetylacetonate) ($btp_2Iracac$) as blue, yellow and red emitters, respectively [6]. The maximum luminance yield of 11 cd/A and an external quantum efficiency (EQE) of 5.2% with a Commission Internationale d'Eclairage (CIE) coordinates of (0.37, 0.40) were reported[6]. However, the thicknesses of three emissive layers are very critical in achieving saturated white light emission. To prevent energy transfer between multiple dopants, fine controlling of exciton diffusion in multilayer devices is necessary. To circumvent the problem, D'Andrade employed a single platinum phosphor, platinum (II) (2-(4',6'-difluorophenyl) pyridinato-N,$C^{2'}$) (6-methyl-2,4-heptanedionato-O, O) (FPt2), for blue emission, as well as green to red emission that is generated from excimers [7]. The WOLED has a maximum EQE of 4.4 % which corresponds to 10.1 cd/A. Since the excimer formation is affected under different current densities, the white light device shows a large change in CIE coordinates from (0.40, 0.44) to (0.35, 0.43) under a luminance range of 40 cd/m^2 to 5000 cd/m^2. A very high-efficiency WOLEDs of 18 cd/A with CIE coordinates of (0.35, 0.36) was reported by Tokito et al [8]. Bis{2-[3,5-Bis(trifluoromethyl) phenyl]-pyridinato -N,$C^{2'}$} iridium(III) picolinate [$(CF_3ppy)_2Ir(pic)$] and $btp_2Iracac$ were used as greenish-blue and red-emitting phosphorescent materials. A high triplet energy host, 4,4'-bis(9-carbazolyl)-2,2'-dimethyl-biphenyl (CDBP)[9] was also introduced, instead of 4,4'*N,N'*-dicarbazole-biphenyl (CBP), to confine excitons and avoid back energy transfer from a blue emitter to the host. Although this simple two-element white light device can provide better color balance near (0.33, 0.33), the lack of green emission shows poor color gamut in full-color displays and low color rendering for general lighting application. To generate white light emission, an exciton blocking layer must be inserted between two emissive layers to tune ratio of two colors and also avoid

energy transfer. However we have synthesized the different orange phosphorescent emitter with central metal of Ir which shows intense and broad emission from 540 nm to 700 nm [10]. In this work, we combined a known blue phosphorescent emitter, iridium(III) bis[4',6'-difluoro-phenylpyridinato)tetrakis(1-pyrazolyl)borate] (FIr6) and demonstrated a white light device with a full width at half maximum (FWHM) over 260 nm by using *two* phosphor dopants. The WOLED shown in this paper has also delivered one of the best $CIE_{x,y}$ color coordinate of [0.350, 0.396] and a maximum external quantum efficiency (EQE) of 8.6%. In our experiments, ten devices have been fabricated and investigated.

6.2 Experiment Section

6.2.1 Materials Synthesis

(a) synthesis of 4-CF_3bt (bt = (2-phenyl)benzothiazole):

This complex was prepared via a general method[11] where 10 mmol of *o*-aminothiophenol was dissolved into 20 mL of 1-methyl-pyrrolidinone under an inert atmosphere; then the stoichiometric amount of the corresponding acid chloride was added slowly at room temperature. The mixture was heated at 100 °C for 1 h. After cooling, the solution was poured into cold water and the mixture was adjusted to pH 8-9 with 7 N aqueous ammonia. A white-colored solid compound was separated out and the crude material was filtered, washed with water several times, and further purified by column chromatography.

(4-CF_3)bt (4-trifluoromethyl)2-phenylbenzothiazole (yield 84%). ^{1}H NMR (300 MHz, $CDCl_3$): δ8.21 (d, 2H, J = 7.8 Hz), 8.11 (d, 1H, J = 7.8 Hz), 7.94

(d, 1H, J = 7.2, Hz), 7.76 (d, 2H, J = 8.1 Hz), 7.53 (td, 1H, J = 1.2, 8.1 Hz), 7.43 (d, 1H, J = 0.9, 8.1 Hz). EIMS: m/z 279, calcd 279.

(b) synthesis of Dichloro-Bridged Iridium(III) Complexes

These were prepared[12] by refluxing the mixture of $IrCl_3 \cdot 3H_2O$ (1 mmol) and the ligands ($4CF_3bt$) (2.4 mmol) in 2-ethoxyethanol for 24-25 h. The orange-yellow mixtures were cooled to room temperature and 20 mL of 1 M HCl was added to precipitate the product. The mixture was filtered and washed with 100 mL of 1 M HCl followed by 50 mL of methanol solution several times and then dried.

$[Ir(4\text{-}CF_3bt)_2Cl]_2$ Yield 67%. (Found: C, 42.5; H, 1.8; N, 3.3. Calcd for $C_{56}H_{28}Cl_2F_{12}N_4S_4Ir_2$: C, 42.9; H, 1.8; N, 3.6%). ^{1}H NMR (300 MHz, $CDCl_3$): δ8.59 (dd, 4H, J = 0.75, 7.5 Hz), 7.64 (d, 4H, J = 8.1 Hz), 7.49 (dd, 4H, J = 1.2, 7.8 Hz), 7.13 (m, 12H), 6.19 (s, 4H). FABMS: m/z 1567; calcd 1567.

(c)Syntheses of Monomer $(4\text{-}CF_3bt)_2Ir(acac)$

The chloride-bridged dimer, $(4\text{-}CF_3)bt_2Ir(\mu\text{-}Cl)_2x/ybt_2$ (0.1 mmol), acetylacetone (0.3 mmol), and sodium carbonate (1 mmol) were mixed in 10 mL of 2-ethoxyethanol (30 mL). The mixture was refluxed under nitrogen for 11-12 h. Then the reaction was cooled and the precipitate filtered. The product was purified by recrystallization from a solution of the mixture of dichloromethane and methanol (2:1).

$Ir(4\text{-}CF_3bt)_2(acac)$ Yield 81%. (Found: C, 46.5; H, 2.5; N, 3.1. Calcd for $C_{33}H_{21}F_6N_2O_2S_2Ir$: C, 46.7; H, 2.5; N, 3.3%). ^{1}H NMR (300 MHz, $CDCl_3$): δ 8.06 (d, 2H, J = 8.1 Hz), 7.96 (d, 2H, J = 8.7 Hz), 7.74 (d, 2H, J = 8.1 Hz),

7.49 (m, 4H), 7.12 (d, 2H, J = 7.8 Hz), 659 (s, 2H), 5.13 (s, 1H), 1.78 (s, 6H). FABMS: m/z 847, calcd 847.

6.2.2 OLED Device Fabrication

The organic layers were deposited by high vacuum ($<10^{-3}$ Pa) thermal evaporation onto an indium-tin-oxide (ITO) coated glass substrate, which had previously been degreased with solvents and cleaned in a UV-ozone chamber. First, a hole transport layer (HTL) consisting of 4,4'-bis[N-(1-naphthyl)-N-phenyl-amino]biphenyl (NPD) was deposited. Second, a different thick emitter layer was formed by codepositing different wt % (4-trifluoromethyl)2-phenylbenzothiazole)iridium Ir(4-CF_3bt)$_2$(acac) and host, and a 10-nm-thick BCP was deposited as an ETL and a hole blocking layer (HBL). Finally, a ETL consisting of tris(8-quinolinolato)aluminum (Alq3) was deposited. A cathode, consisting of a 100-nm-thick Mg-Ag (10:1) layer followed by a 10-nm-thick Ag cap, was deposited through a 1-mm-diameter opening in a shadow mask placed on the sample surface. We obtained current density (J)-voltage (V)-luminance (L) characteristics using a semiconductor parameter analyzer (Agilent, E5273A) with an optical power meter (Newport, model 1930-C). The EL spectra were obtained by using a multichannel spectrometer (Ocean Optics, SD2000).

6.3 Results and Discussions

The white-light device incorporating the blue triplet phosphor and orange-emitting device with different dopant concentrations and thickness. The detailed molecular structure and device architecture are shown in the Figure 5.1. The 4,4'-bis[N-(1-naphthyl)-N-phenyl-amino]biphenyl (NPD) is the hole transport layer, Ir(4-CF_3bt)$_2$(acac) doped mCP is the orange-emissive layer**,** bathocuproine(BCP) is the hole blocking layer, *tris*(8-quinolinato) aluminum (Alq_3) is the electron transport layer**,** and MgAg/Ag is the bilayer cathode. A multi-layered structure of NPD/EML/BCP/Alq_3/MgAg/Ag was deposited on the substrate by resistive heating with a thickness of 30, 10, 40, 100, and 10 nm for NPD, BCP, Alq_3, MgAg, and Ag, respectively. In the devices, a thin layer of mCP is inserted between the NPD layer and the EML. Here in, mCP efficiently prevents the leakage of both excitions and electrons from the EML into NPD , increasing color purity and carrier balance in the emissive layer. With the blue phosphorescent FIr6 introduced into white light devices, the architecture of devices is ITO/ NPD / mCP: FIr6/mCP: Ir(4-CF_3bt)$_2$(acac) (10 nm)/ BCP (10 nm)/Alq_3 (40 nm)/ MgAg (100 nm)/Ag(10 nm). Here, we fixed the dopant concentration of FIr6 at 10% and 15%, and varied the Ir(4-CF_3bt)$_2$(acac) doping level at 2%, 10%, and 15% , respectively. It is also noted that mCP with higher triplet energy than CBP were employed in the fabrication of white-light device to achieve higher efficiency[13]. All devices were hermetically sealed prior to testing**. We** show all devices structure in Table 6.1. Electroluminescent (EL) spectra, luminance yield and Commission Internationale l'Eclairage -$CIE_{x,y}$ color coordinates were measured by a spectrometer (Ocean Optics, SD2000).

Table 6.1 All devices structure of WOLEDs

	Device Structure
1	ITO/a-NPD(20nm)/mCP(10nm)/mCP:10wt%FIr6(45nm)/mCP: 10wt%L-21b(5nm) BCP(10nm)/Alq3(40nm)/MgAg(100nm)/Ag(10nm)
2	ITO/a-NPD(20nm)/mCP(10nm)/mCP:10wt%FIr6(40nm)/mCP:2wt%L-21b (10nm)/BCP(10nm)/Alq3(40nm)/MgAg(100nm)/Ag(10nm)
3	ITO/a-NPD(30nm)/mCP:10wt%L-21b(30nm)/mCP:10wt%FIr6(20nm) BCP(10nm)/Alq3(40nm)/MgAg(100nm)/Ag(10nm)
4	ITO/a-NPD(30nm)/mCP:10wt%L-21b(10nm)/mCP:10wt%FIr6(40nm) BCP(10nm)/Alq3(40nm)/MgAg(100nm)/Ag(10nm)
5	ITO/a-NPD(30nm)/mCP:15wt%L-21b(30nm)/mCP: 15wt%FIr6(20nm)/ BCP(10nm)/Alq3(40nm)/MgAg(100nm)/Ag(10nm)
6	ITO/a-NPD(30nm)/mCP:10wt%L-21b(40nm)/mCP:10wt%FIr6(10nm) /BCP(10nm)/Alq3(40nm)/ MgAg(100nm)/Ag(10nm)
7	ITO/a-NPD(20nm)/mCP(10nm)/mCP:10wt%FIr6(40nm)/mCP:10wt%L-21 b(10nm)/BCP(10nm)/Alq3(40nm)/LiF(0.5nm)/Al(70nm)
8	ITO/a-NPD(20nm)/mCP(10nm)/mCP:10wt%FIr6(39nm)/mCP(2nm)/ mCP: 10wt%L-21(9nm)/BCP(10nm)/Alq3(40nm)/LiF(0.5nm)/Al(70nm)
9	ITO/a-NPD(20nm)/mCP(10nm)/mCP:10wt%FIr6(39nm)/mCP(2nm)/ mCP:10WT%L-21b(9nm)/BCP(10nm)/Alq3(40nm)/LiF(0.5nm)/Al(70nm)
10	ITO/a-NPD(30nm)/mCP:10wt%Ir(Phq)3(30nm)/mCP:10wt%FIr6(20nm) /BCP(10nm)/Alq3(40nm)/MgAg(100nm)/Ag(10nm)
11	ITO/a-NPD(30nm)/CBP:15wt%-L-21b(10nm)/mCP:15wt%-FIr6(40nm) /Bphen(50nm)/MgAg(100nm)/Ag(10nm)

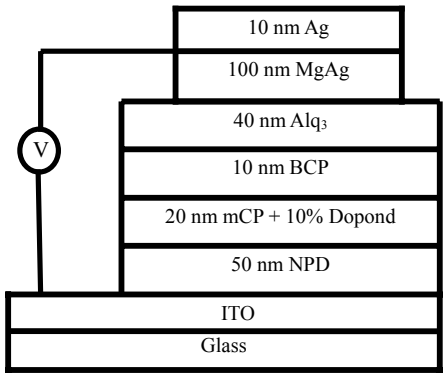

Figure 6.1 The device structure for Device-1

Show in Figure 6.1 is the device structure for Device-1, the multi-layered structure consists of ITO/ α-NPD (20nm)/ mCP (10nm)/ mCP : 10wt% FIr6 (45nm)/ mCP : 10wt% Ir(4-CF_3bt)$_2$(acac) (5nm)/ BCP (10nm)/ Alq_3 (40nm)/ MgAg (100nm)/Ag (10nm). The turn-on voltage and external quantum efficiency (EQE) of the device were found to reach 3.4V and 2.8% (at 15.1mA/cm^2), respectively. The device with comparable CIE (x,y) coordinates of (0.442, 0.468) was observed at 100 mA/cm^2. The device did not exhibit good external quantum efficiency (EQE). These results can be rationalized by considering the thickness of the blue emitter that causes the exaction trapped in the blue layer, therefore, the layer thickness needs to be increased. Thus, we have designed the second with the device structure of device 2, in which have reduced the layer thickness of FIr6 and increased red-orange layer simultaneously. The turn-on voltage and EQE of the device were then found to reach 4.1V and 5.9% (at 1.9mA/cm^2), respectively. But the device shows comparable CIE (x,y) coordinates of (0.466, 0.474) that is similar to that at 100 mA/cm^2. Although we have improved the EQE, but we still failed to obtain white emission. We can see both devives 1 and 2 show the same problem. The blue emission was observed to be weaker than red

emission, which may be related to energy transfer between blue emitter and red emitter. Therefore, we added one layer of mcp to avoid energy transfer among emitting layer. The structure of device 3 can be described as ITO/ α -NPD (20nm)/ mCP (10nm)/ mCP:10wt% FIr6 (39nm)/ mCP (2nm)/ mCP:10wt% L-21b (10nm)/ BCP (10nm)/ Alq3 (40nm)/ MgAg (100nm)/ Ag (10nm), from which no improvement of was obserred. For this problem, we chose the other way that decrease the orange dopant content to increase blue emission. So device 4 was fabricated. We have found that the turn-on voltage and EQE of the device can reach 3.9V and 6.7% (at 0.16mA/cm^2), respectively. The white emission with CIE (x,y) coordinates of (0.429, 0.475) at 100 mA/cm^2 has also been obserred to be improved. However, to investigate the effect of cathode we fabricated devices 5 and 6. The all EL spectra and the results are summarized in Figure 6.2.

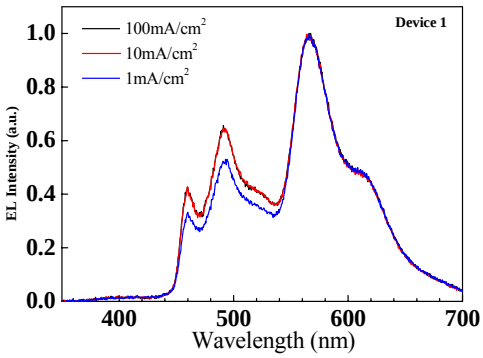
Device 1
100mA/cm2
10mA/cm2
1mA/cm2
EL Intensity (a.u.)
Wavelength (nm)

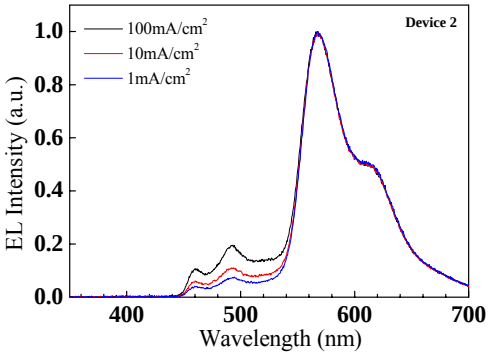
Device 2
100mA/cm2
10mA/cm2
1mA/cm2
EL Intensity (a.u.)
Wavelength (nm)

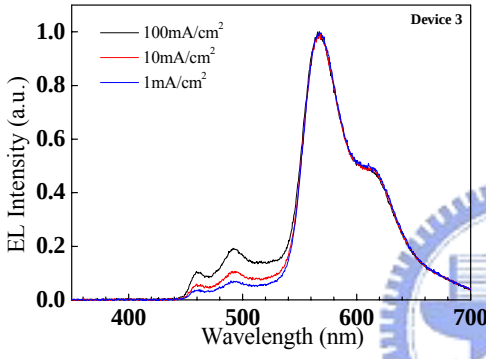
Device 3
100mA/cm2
10mA/cm2
1mA/cm2
EL Intensity (a.u.)
Wavelength (nm)

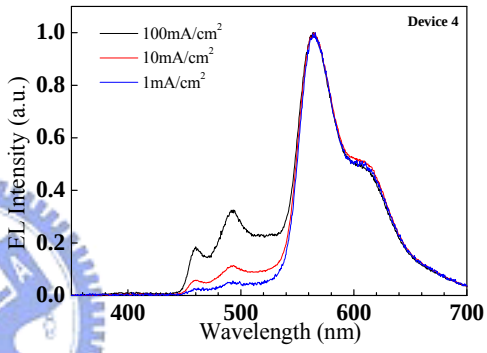
Device 4
100mA/cm2
10mA/cm2
1mA/cm2
EL Intensity (a.u.)
Wavelength (nm)

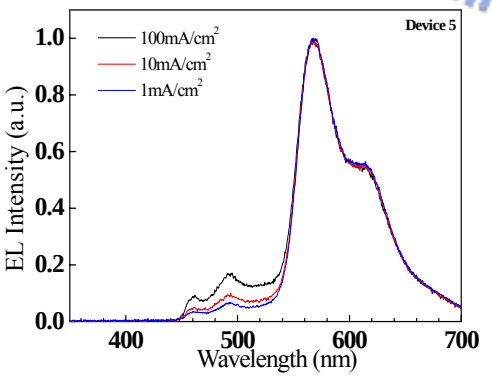
Device 5
100mA/cm2
10mA/cm2
1mA/cm2
EL Intensity (a.u.)
Wavelength (nm)

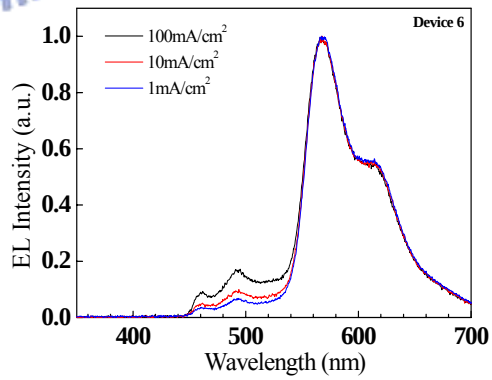
Device 6
100mA/cm2
10mA/cm2
1mA/cm2
EL Intensity (a.u.)
Wavelength (nm)

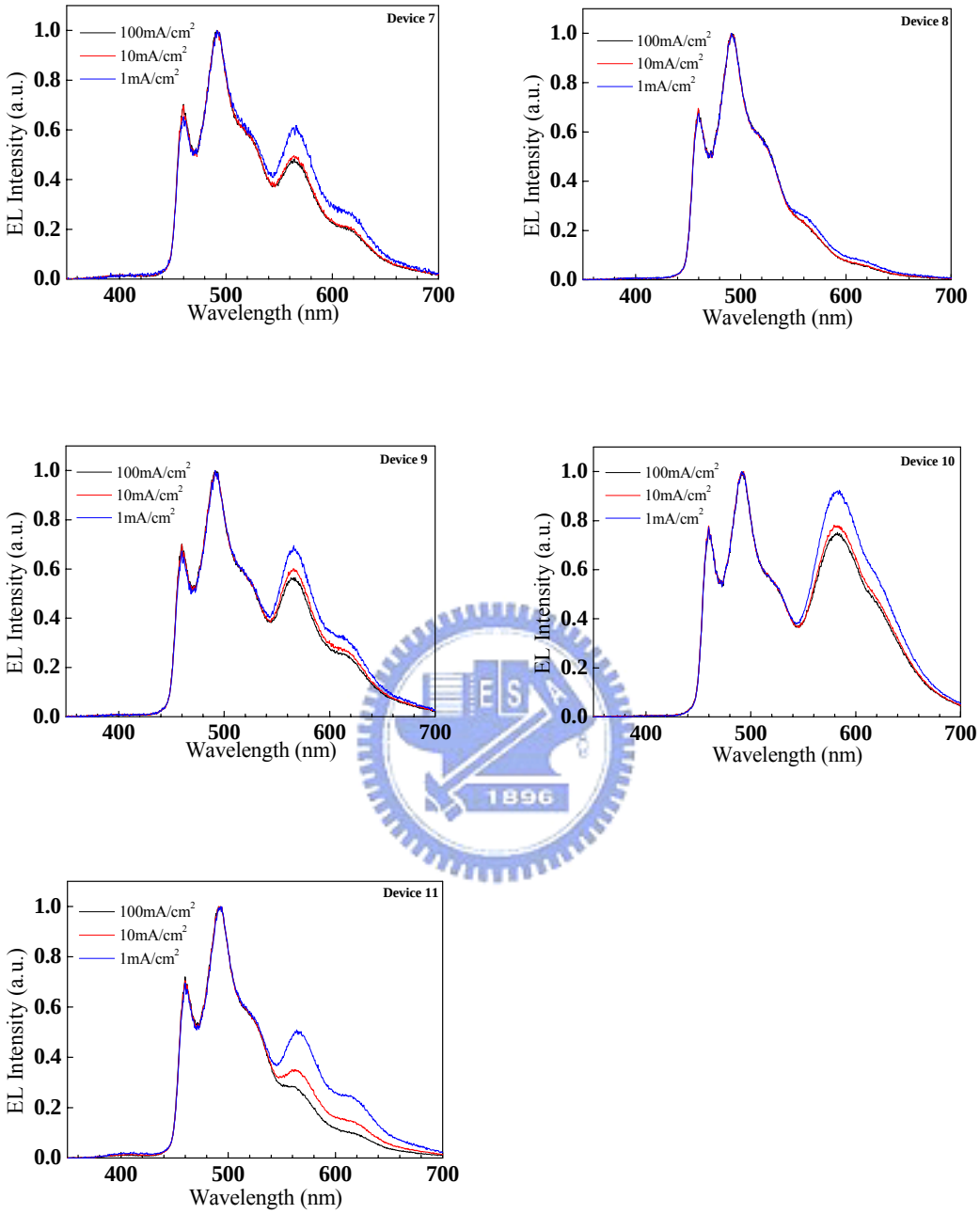

Figure 6.2 EL spectra and performance of devices 1-11

Although we have changed the fabrication conditions that obviously improved the blue emission, we also varied the sequence of the blue and red emitters that we meant to avoid the energy transfer to form four different devices whose performance was summarized in Table 6.2. We show the cie data in different current density and get the best EQE in Table 6.2.

Table 6.2. Comparison of EL performance for white light devices 1-11.

Device	1 mA/cm^2 CIE (x, y)	10 mA/cm^2 CIE (x, y)	100 mA/cm^2 CIE (x, y)	Turn-on voltage (V)	EQE
1	(0.494,0.480)	(0.473,0.473)	(0.442,0.468)	3.4	2.8% (at 15.1mA/cm^2)
2	(0.496,0.478)	(0.487,0.477)	(0.466,0.474)	4.1	5.9% (at 1.90mA/cm^2)
3	(0.495,0.481)	(0.484,0.480)	(0.463,0.477)	4.2	5.3% (at 0.73mA/cm^2)
4	(0.492,0.489)	(0.476,0.486)	(0.429,0.475)	3.9	6.7% (at 0.16mA/cm^2)
5	(0.503,0.474)	(0.495,0.474)	(0.476,0.473)	3.9	6.0% (at 0.15mA/cm^2)
6	(0.503,0.474)	(0.495,0.474)	(0.476,0.473)	4.1	5.0% (at 0.34mA/cm^2)
7	(0.291,0.416)	(0.269,0.404)	(0.266,0.403)	3.7	3.3% (at 95.2mA/cm^2)
8	(0.202,0.384)	(0.190,0.379)	(0.189,0.380)	3.5	3.0% (at 42.9mA/cm^2)
9	(0.308,0.419)	(0.293,0.411)	(0.286,0.408)	3.7	3.9% (at 77.8mA/cm^2)
10	(0.372,0.401)	(0.354,0.396)	(0.350,0.396)	3.5	8.6% (at 2.70mA/cm^2)
11	(0.279,0.405)	(0.238,0.392)	(0.214,0.383)	3.2	3.7% (at 14.6mA/cm^2)

White-light OLED of dichromatic bands with systematic phosphorescent designs requires high-efficiency, high-brightness and long lifetime orange light. Since the Ir(4-CF_3bt)$_2$(acac) exhibit the color

deficiency, we used Ir(2-phq)$_3$ to replace. The PL spectra of Ir(2-phq)$_3$ to compare the Ir(4-CF$_3$bt)$_2$(acac) is shown in the Figure 6.3. From the literature[14] the company to use the orange dopant of Iridium complex Ir(2-phq)$_3$ and host LT-N420[13] (Tg =174°C), HTL is LT-N120 (Tg =164°C), ETL is LT-N820, this component structure, brightness is 820cd/m^2 for 4.5V driving voltage, efficiency is 22.3 cd/A, CIE =(0.57, 0.42). The lifetime exceeds 10,000 hours (initial stage 2000cd/m^2 at 25 °C / DC ON). We also can see the two complexes emission peak is 569 nm and 589 nm. So the Ir(2-phq)$_3$ more red shift than Ir(4-CF$_3$bt)$_2$(acac). Thus, we chose the Ir(2-phq)$_3$ to be the orange dopant to fabricate a new device. The EL spectra of D-10 indicated that the intensity of red emission was enhanced with increasing dopant content Ir(2-Phq)$_3$. Since the red emission increases, more intense white-light can be obtained.

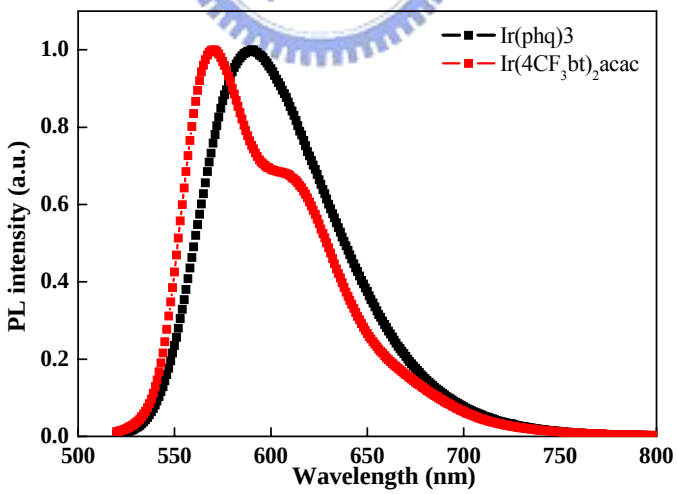

Figure 6.3 The PL solution for complexes Ir(2-phq)$_3$ and Ir(4-CF$_3$bt)$_2$(acac)

The correlation of EQE and current density for Devices was plotted in Figures 6.4. Both of the EL efficiencies of the device were found to reach a maximum in a much reasonable current density range of 0.01-1000 mA/cm^2. The corresponding EQE of the four WOLEDs were found to reach 2.8% (at 0.34mA/cm^2), 5.9% (at 1.90mA/cm^2), 5.3% (at 0.73mA/cm^2), 6.7% (at 0.16mA/cm^2), 6.0% (at 0.15mA/cm^2), 5.0% (at 0.34mA/cm^2), 3.3% (at 95.2mA/cm^2), 3.0% (at 42.9mA/cm^2), 3.9% (at 77.8mA/cm^2) and 8.6% (at 2.7mA/cm^2), respectively.

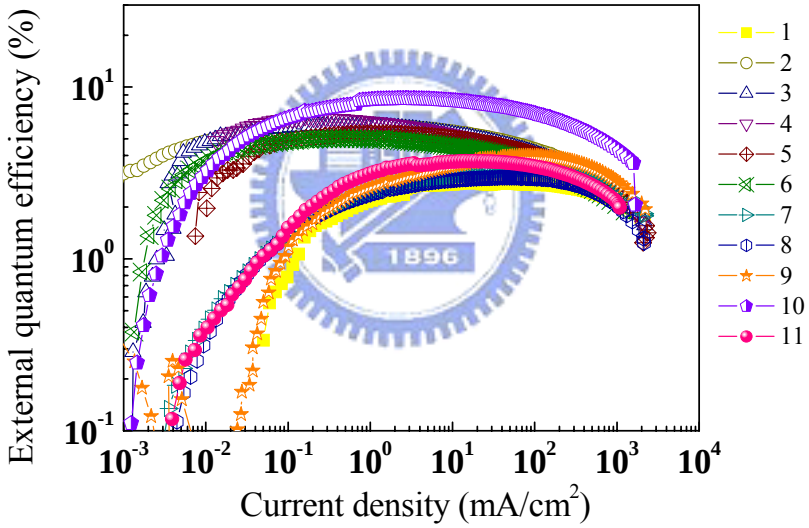

Figure 6.4 External quantum efficiency versus current density for WOLEDs.

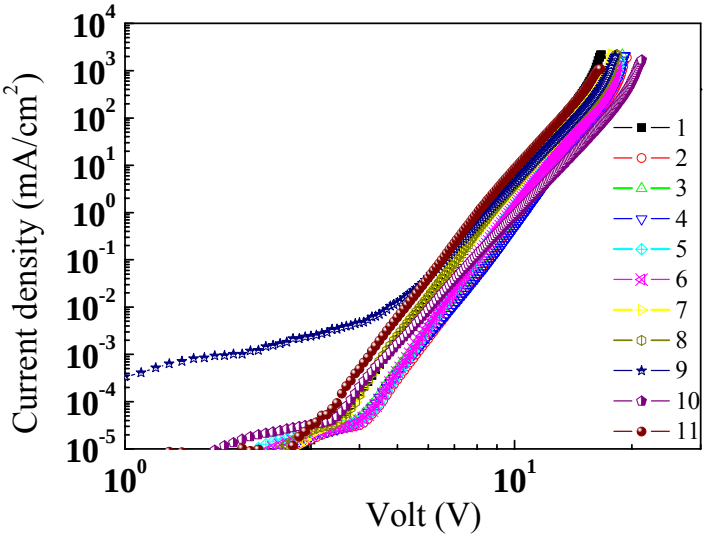

Figure 6.5 External quantum efficiency versus current density for WOLEDs.

The device 10 also demonstrates a good CIE coordinates of (0.35, 0.396). These WOLEDs described in this paper have also been discovered to deliver one of the best luminance efficiencies ever reported in the literature. A WOLED with constant chromaticity is significantly important for display application. A $CIE_{x,y}$ color shift of 0.05 is the maximum tolerance for human eyes. The WOLEDs with multi-emissive phosphors doped layers tend to cause CIE color shift which requires finely control of exciton diffusion in the multi-layer devices to overcome the problem.

6.4 Conclusion

In conclusion, we have demonstrated high-efficiency WOLEDs with complexes of $Ir(4\text{-}CF_3bt)_2(acac)$, $Ir(2\text{-}phq)_3$ and FIr6. The efficiency was illustrated by the remarkably high EQE of 8.6%. Our WOLEDs also shows a stable chromaticity with a CIE coordinates of (0.350, 0.396) under different

luminances. According the work by Holmes et al [15], with the Frpic compound the device with structure of ITO/CuPC/ α -NPD/mCP:6% Frpic/BAlq3/LiF/Al exhibited η_{ext}=7.5% The FIr6:Mcp device get the η_{ext} <3.0% from the literature[16](device structure ITO/NPD(400 Å) / FIr6:mCP (10%, 250 Å)/Alq3 (250 Å)/LiF/Al). The device with two emitting layers fabricated in our work not only reached the external quantum efficiency of 8.6%, but also avoided the expected energy transfer. We believe that if more suitable host can be used, the EQE of WOLED's can be further increased.

6.5 References

1. Adachi, C.; Baldo, M. A.; Thompson, M. E. and Forrest, S. R.; *J. Appl. Phys.* 30 (2001) 5048
2. Baldo, M. A.; O'Brien, D. F.; You, Y.; Shoustikov, A.; Sibley, S.; Thompson, M. E. and Forrest, S. R.; *Nature*. 395 (1998**)** 151
3. D'Andrade, B. W.; Holmes, R. J. and Forrest, S. R.; *Adv. Mater. Weinheim,Ger.* 16 (2004**)** 624.
4. Tokito, S.; Lijima, T.; Tsuzuki, T. and Sato, F.; *Appl. Phys. Lett*. 83 (2003) 2459
5. Adamovich,V.; Broods, J.; Tamayo, A.; Alexander, A. M.; Djurovich, P. I.; D'Andrade, B. W.; Adachi, C.; Forrest, S. R. and Thompson, M. E. *New J. Chem*. 26 (2002) 1171
6. D'Andrade, B. W.; Thompson, M. E. and Forrest, S. R. *Adv. Mater.* 14 (2002**)** 147.
7. (a) D'Andrade, B. W.; Brooks, J.; Adamovich, V.; Thompson, M. E. and Forrest, S. R.; *Adv. Mater.* 14 (2002) 1032. (b) Hung, L. S.; Zheng, L. R. and Mason, M. G.; *Appl. Phys. Lett.* 78 (2001) 673.
8. (a) Tokito, S.; Iijima, T.; Tsuzuki, T. and Sato, F.; *Appl. Phys. Lett.* 83

(2003) 2459. (b) Holmes, R. J.; Forrest, S. R.; Tung, Y.-J.; Kwong, R. C.; Brown, J. J.; Garon, S. and Thompson, M. E.; *Appl. Phys. Lett.* 82 (2003) 2422.

9. (a) Tokito, S.; Iijima, N.; Tsuzuki, T. and Sato, F.; *Appl. Phys. Lett.* 83 (2003) 569. (b) O'Brien, D. F.; Baldo, M. A.; Thompson, M. E. and Forrest, S. R.; *Appl. Phys. Lett.* 74 (1999) 442.
10. Laskar, I. R.; Hsu, S.-F.; Chen, T.-M. *Polyhedron* 24 (2005) 881.
11. Lamansky, S.; Thompson, M.E.; Adamovich, V.; Djurovich, P.I.; Adachi, C.; Baldo, M.A.; Forrest, S.R.; Kwong, R.; US patent, 0182441 A1, 2002.

12. (a) Lamansky, S.; Djurovich, P.; Murphy, D.; Abdel-Razzaq, F.; Kwong, R.; Tsyba, I.; Bortz, M.; Mui, B.; Bau, R.; Thompson, M. E. *Inorg. Chem.* 40 (2001) 1704. (b) Lamansky, S.; Djurovich, P.; Murphy, D.; Abdel-Razzaq, F.; Lee, H.-F.; Adachi, C.; Burrows, P. E.; Forrest, S. R.; Thompson, M. E.; *J. Am. Chem. Soc.* 123 (2001) 4304. (c) Thompson, M. E.; Lamansky, S.; Djurovich, P.; Murphy, D.; Abdel-Razzaq, F.; Kwong, R.; Forrest, S. R.; Baldo, M. A.; Burrows, P. E. U.S. Patent 20020034656A1.

13. Adamovich, V.; Brooks, J.; Tamayo, A.; Alex, M.; Djurovich, I.; D'Andrade, W.; Adachi, C.; Forrest, R. and Thompson, M. E.; *New J. Chem*. 26 (2002) 1171-1178

14. http://www.lumtec.com.tw/News.html

15. Holmes, R. J.; D'Andrade, B. W.; Forrest, S. R.; Ren, X.; Li, J. and Thompson, M. E.; *Appl. Phys. Lett.*, 82 (2003) 2422

16. Ren, X.; Li, J.; Holmes, R. J.; Djurovich, P. I.; Forrest, S. R. and Thompson, M. E.; *Chem. Mater*. 16 (2004) 4743

Chapter 7

The Synthesis new dendrimer and properties of solution processable phosphorescent

Abstract

We have pursued the development of highly luminescent solution-processible electrophosphorescent dendrimers. We synthesized first–generation dendrimers consisting of a *fac*-tri-(2-phenylbenzthiazole) iridium core, hole-transporting 2-ethylhexyloxy surface groups, ethynylbenzene group and biphenyl based dendrons. Morphologically smooth amorphous films of these dendrimers were formed by spin-coating them from solutions. We observed that the photoluminescence quantum yield (PLQY) of the (G1-bt_3Ir) compound dendrimer was approximately 1.5 times higher than that of the pristine complex $Ir(bt)_3$ in solution. The external quantum efficiency of OLEDs using the film containing a mixture of the first-generation dendrimer and an electron-transporting material was found to be as high as 4.14%.

7.1 Introduction

Organic light-emitting diodes (OLEDs) are currently under intense investigation for application in the next generation of flat-planel-display technologies. Over the past few years, significant progress has been made in electroluminescence, because of the continuing discovery of novel and improved materials. In the OLED, display application, in particular, small molecular materials are the most advanced and there are already a number of displays on the markets. Light-emitting materials for these devices can be divided into three classes: organic small molecules,[1] conjugated polymers,[2-3] and dendrimers. Although, molecular materials are mainly processed by evaporation which requires a long time for fabrication, solution processing which can be applicable to the polymers and dendrimers offer very quick and a low cost approach to large area full color displays. Therefore, solution processing for the formation of OLEDs is important for the success of the technology. In the previous study, solution-processed light-emitting layers containing fluorescent conjugated polymers and dendrimers have been reported. [4-8]

In this study, we have pursued the development of highly luminescent solution-processible electrophosphorescent dendrimers.[9] Dendrimers are macromoles that are comprised of three components: a central core, dendrons (branches), and surface groups that are located at the the distal ends of the dendrons. Dendritic structures allow the control of intermolecular interactions between phosphorescent emitters; thus, they make it possible to tune the charge-transporting properties independently from light emission. Conjugated dendrimers have a number of potential advantages over conjugated polymers for use in OLEDs. First, they can be produced via the synthesis giving a greater flexibility over the properties.[11]

Second, the processing and electronic properties such as light emission, and the surface groups can be selected to give the desired solubility. Third, the generation of the dendrimer gives molecular control over the intermolecular interactions that are vital to enhance OLED characteristics.[12] Finally, both fluorescent and phosphorescent[13] dendrimers are easily accessible. The advantage of phosphorescent light-emitting materials is that they can harvest emission from both singlet and triplet excited states so that it is theoretically possible to achieve OLEDs with 100% internal quantum efficiency. In this chapter, we compare photoluminescence (PL) dynamics of *cis*-$Ru(bpy)_2Cl_2$ with the simple molecule in solution, and neat films. In solution and blends, these dendrimers are characterized by high PL quantum yield (QY) vales. We also report the electrochemical, photophysical, properties and device performance of the dendrimer.

7.2 Experimental Section

7.2.1 Materials Synthesis

The structures of and synthetic pathways to the dendrimers are shown in Schemes 1. The dendrimer contains 2-ethylhexyloxy surface groups and biphenyl based dendrons attached to the iridium(III) complex cores. These are the same dendrons and surface groups as used for the green-light emitting phosphorescent dendrimers. Symmetric iridium(III) complexes are often prepared in a two step process from iridium(III) chloride trihydrate.[14] The first step forms a chloro-bridged iridium dimer which was then reacted with excess ligand to give the complex. The strategy for the preparation of asymmetric complex G1 dendrimer complexes was to isolate the chloro bridged iridium dimer, which was an intermediate in the formation of the symmetric green-emitting dendrimer and, subsequently, reacted with the

ligand.

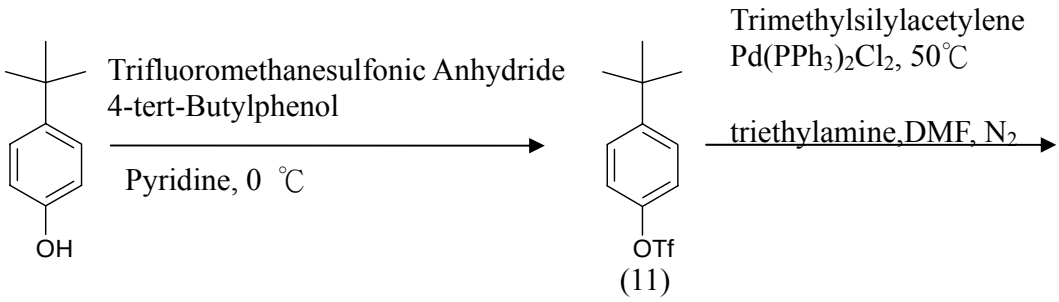

(11)

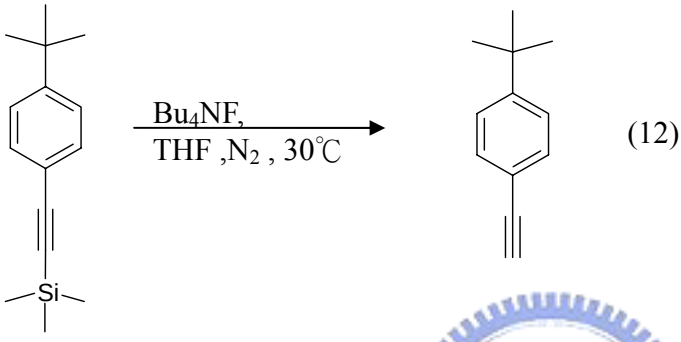

(12)

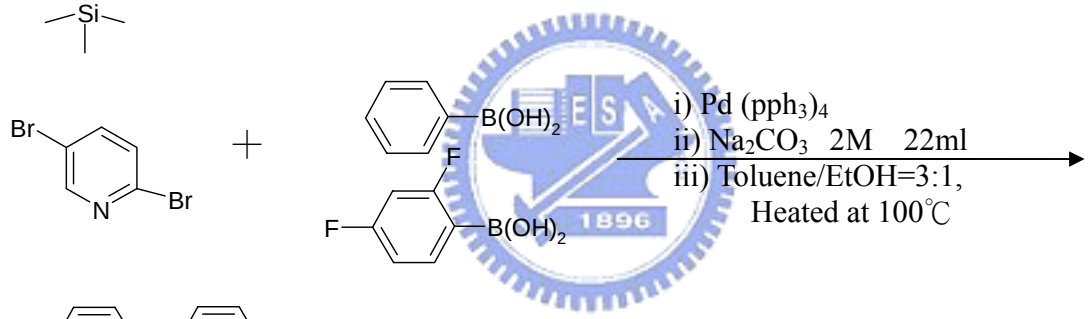

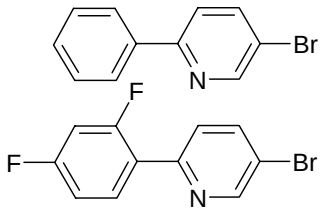

(13)

(14)

(13) + (12) → (14)

Triphenylphosphine, Copper Iodide
Triethylamine, Pd(dba)2, 65℃, 26hours

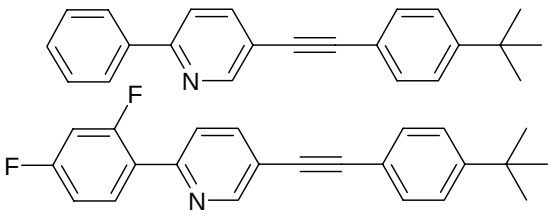

(15)

(16)

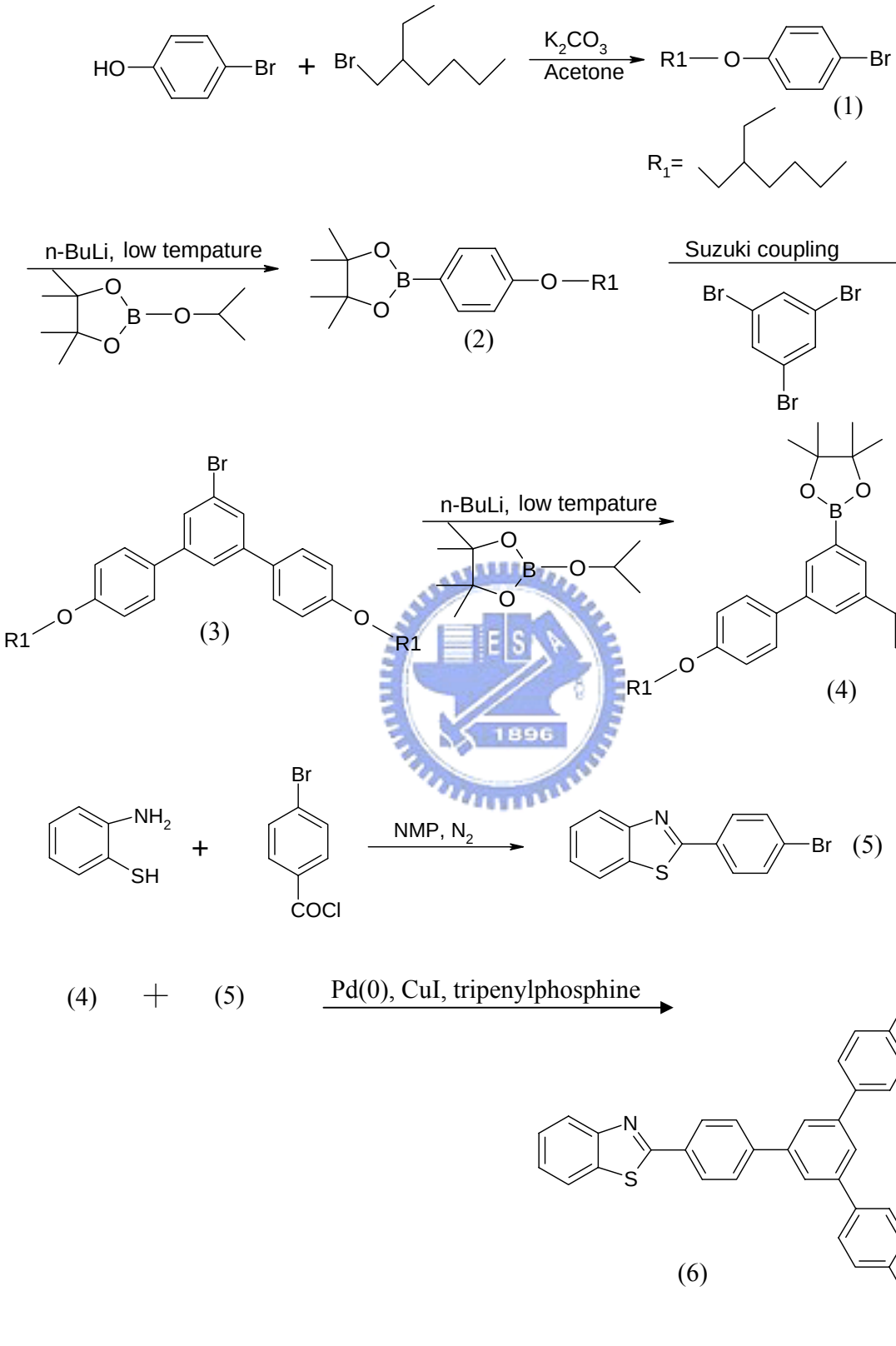
HO
Br
Br
K2CO3
Acetone
R1
O
Br
(1)
R1=
n-BuLi, low tempature
B
O
O
O
O
B
O
R1
(2)
Suzuki coupling
Br
Br
Br
Br
O
R1
(3)
n-BuLi, low tempature
B
O
O
O
O
R1
O
O
R1
(4)
NH2
SH
+
Br
COCl
NMP, N2
N
S
Br
(5)
(4) + (5)
Pd(0), CuI, tripenylphosphine
R1
O
N
S
(6)
O
R1

(6)
(15)
(16)

$\xrightarrow[N_2(g),\ 24\ hours]{IrCl_3 \cdot 3H_2O,\ 2\text{-}EtOCH_2CH_2OH,\ H_2O,}$ Ir dimer complexes

(6)
(15)
(16)

＋

$\xrightarrow{AgOSO_2CF_3,\ 110℃,\ 16\ hours}$

(8)
(17)
(18)

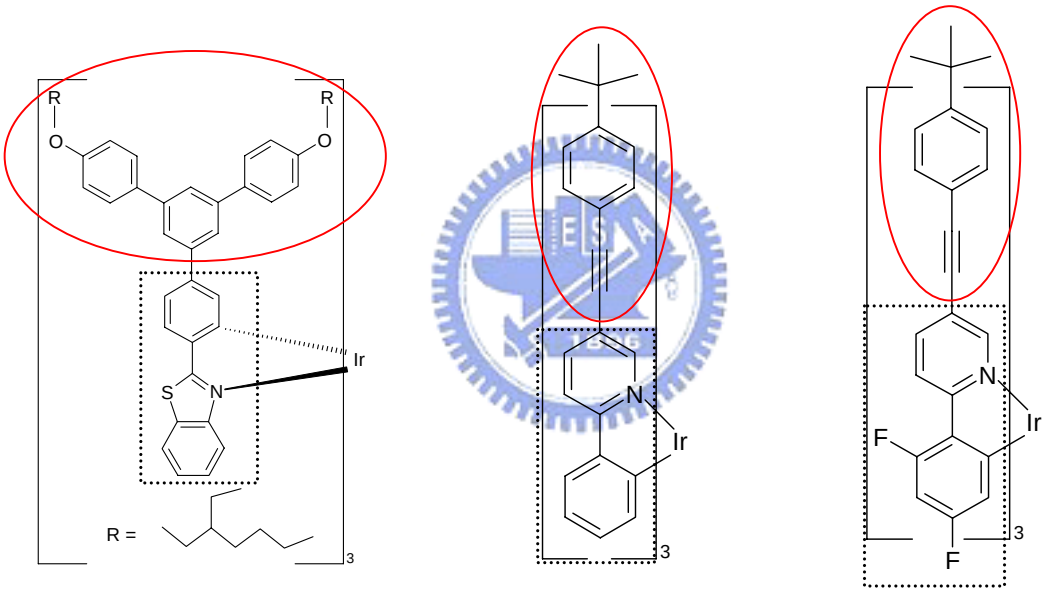

(8) (17) (18)

▯ = core, ⬭ = dendrons

Scheme 1 The structures of and synthetic pathways

The dimer was prepared by reacting four equivalents of G1dendrimer with iridium (III) chloride trihydrate in a 2-ethoxyethanol/water mixture heated at 140℃. Crude dimmer complexes precipitated from the reaction mixture were easily collected by filtration before further purification by chromatography. Under these conditions, we obtained the dimmer complexes with the yield of 70%.[15]

On the synthesis of tri-iridium complex which was prepared in a general method[15] where 10 mmol aminithiophenol was dissolved into 20 ml of 1-methyl-pyrrolidinone under inert atmosphere; then, the stoichiometric amount of the corresponding acid chloride was added slowly at room temperature. The mixture was then heated at 100°C for one hour. After cooling, the solution was poured into a cold water and the mixture was adjusted to pH 8-9 with 7N aqueous ammonia. A white-coloured solid compound was separated out. The crude material was filtered, washed with water for several times and dried under vacuum.

Bromo-4-(2′-ethylhexyloxy)benzene (1) (Scheme 1, p139). It was synthesized by Williamson reaction. p-Bromophenol (17.3 g, 0.1 mol), 1-bromo-2-ethylhexane (44.4 g, 0.23 mol.) and potassium carbonate (27.6 g, 0.2 mol) were mixed in acetone (100 ml) and heated with refluxing. After 24 hours, the reaction mixture was allowed to cool to room temperature and water was added. The organic layer was separated and the aqueous solution was extracted with diethylether three times. The combined organic layers were washed with aqueous sodium hydroxide solution (10 %) and saturated sodium chloride solution, dried over magnesium sulfate and filtered. After removing the solvent, the residue was distilled under reduced pressure to afford a colorless oil (75 %). 1H NMR ($CDCl_3$): δ_H (300 MHz; $CDCl_3$) :

0.90 (m, 6H), 1.22 – 1.58 (m, 8H), 1.72 (m, 1H), 3.80 (d, 2H), 6.78 (d, 2H), 7.36 (d, 2H); m/z (EI): 286, fragmented masses: 174 [−$CH_2CH_2(CH_2CH_3)CH_2CH_2CH_2CH_3$], Calc. 285.

G0-B(OCMe$_2$)$_2$ (2) (Scheme 1). *tert*-Butyllithium (1.5 M, 3.8 mL, 5.66 mmol) was added to a solution of 1-bromo-4-(2'-ethylhexyloxy)benzene (**1**) (1.01 g, 3.54 mmol) in anhydrous tetrahydrofuran (7 mL) that had been cooled in an dry ice/acetone bath under argon. The mixture was stirred at -78 °C for 1 h. 2-Isopropoxy-4,4,5,5-tetramethyl-1,3,2-dioxaborolane (0.87 mL, 4.26 mmol) was added rapidly to the cold mixture, and the mixture was stirred at -78 °C for 2 h. The mixture was allowed to warm room temperature and then stirred at room temperature for 65 h. The reaction was quenched with water (3 mL), and the two layers were separated. The aqueous layer was extracted with ether (3 × 7 mL), and then the organic layer and the ether extracts were combined, dried over anhydrous magnesium sulfate, and filtered. The solvent was completely removed and the residue purified by column chromatography over silica gel using ethyl acetate-light petroleum (0:1 to 1:10) as eluent to give **2** (806 mg, 69%). δ_H (300 MHz; $CDCl_3$): 0.87-0.97 (6 H, m, Me), 1.30-1.58 (20 H, m, CH_2 and Me), 1.70-1.78 (1 H, m, CH), 3.88 (2 H, m, $ArOCH_2$), 6.91 and 7.76 (4 H, AA'BB', ArH). *m/z* [EI] 331, calc. 332.

G1-Br (3) (Scheme 1). A mixture of **2** (380 mg, 1.14 mmol), 1,3,5-tribromobenzene (163 mg, 0.520 mmol), *tetrakis* (triphenylphosphine)palladium(0) (33 mg, 0.029 mmol), aqueous sodium carbonate (2 M, 0.5 mL), ethanol (0.5 mL), and toluene (1.5 mL) was deoxygenated and then heated with refluxing under argon for 24 h. The mixture was allowed to cool, and water (3 mL) and ether (4 mL) were added.

The organic layer was removed, and the aqueous layer was extracted with ether (3 × 5 mL). The organic layer and the ether extracts were combined, dried over anhydrous magnesium sulfate, and filtered, and then the solvent was completely removed. The residue was purified by column chromatography over silica gel using dichloromethane-light petroleum (0:1 to 1:10) as eluent to give **3** (202 mg, 60%). δ_H (400.1 MHz; $CDCl_3$): 0.87-1.03 (12 H, m, Me), 1.32-1.63 (16 H, m, CH_2), 1.76-1.86 (2 H, m, CH), 3.93 (4 H, m, $ArOCH_2$), 7.03 and 7.56 (8 H, AA'BB', sp H), and 7.66 (3 H, m, G1-bp H). *m*/*z*: 564 and 566 (M^+); Fragmented masses 486, 452, 340, Calc. 565.

G1-B(OCMe$_2$)$_2$ (Scheme 1) (4). *tert*-Butyllithium (1.5 M, 4.8 mL, 7.2 mmol) was added to a solution of **3** (2.02 g, 3.57 mmol) in anhydrous ether (12 mL) that had been cooled in a dry ice/acetone bath under argon. The mixture was stirred at -78 °C for 1.5 h, and then 2-isopropoxy-4,4,5,5-tetramethyl -1,3,2-dioxaborolane (0.9 mL, 4.4 mmol) was added rapidly to the mixture. The mixture was allowed to warm to room temperature over 3 h and then stirred at room temperature for additional 62 h before being quenched with water (5 mL). The organic layer was removed, and the aqueous layer was extracted with ether (3 × 5 mL). The organic layer and the ether extracts were combined, dried over anhydrous magnesium sulfate, and filtered, and then the solvent was completely removed. The residue was purified by column chromatography over silica gel using ethyl acetate-light petroleum (1:10) and then ethyl acetate-light petroleum (0:1 to 1:30) as eluent to give **4** (1.63 g, 75%). δ_H (500.0 MHz; $CDCl_3$): 0.91-1.00 (12 H, m, Me), 1.31-1.64 (28 H, m, CH_2 and Me), 1.73-1.82 (2 H, m, CH), 3.91 (4 H, m, $ArOCH_2$), 7.00 and 7.63 (8 H, AA'BB', sp H), 7.85 (1 H, m, G1-bp H), and 7.97 (2 H,

m, G1-bp H). *m*/*z* [EI] 486 (fragmented mass was obtained; compound is unstable under irradiation); Calc. mass 612.

3-G1-Lig (6) (Scheme 1). A mixture of **4** (100 mg, 0.163 mmol), 2-(3'-bromophenyl)benzothiazolato (**5**) (32 mg, 0.137 mmol), tetrakis(triphenylphosphine)palladium(0) (11 mg, 0.010 mmol), aqueous sodium carbonate (2 M, 0.1 mL), ethanol (0.1 mL), and toluene (0.3 mL) was deoxygenated and then heated at reflux under argon for 20 h. The mixture was allowed to cool to room temperature, and water (4 mL) and ether (4 mL) were added. The organic layer was removed, and the aqueous layer was extracted with ether (3 × 5 mL). The organic layer and the ether extracts were combined, washed with brine (8 mL), dried over anhydrous magnesium sulfate, and filtered, and then the solvent was completely removed. The residue was purified by chromatography over silica gel using dichloromethane-light petroleum (1:50 to 1:10) as eluent to give **6** (87 mg, 99%). δ_H (400.1 MHz; $CDCl_3$): 0.92-1.03 (12 H, m, Me), 1.32-1.67 (16 H, m, CH_2), 1.76-1.86 (2H, m, CH), 3.95 (4H, m, $ArOCH_2$), 7.01 (5H, m), 7.40 (1H, td, J = 9.0; 1.2 Hz), 7.52 (1H, td, *J* = 7.2; 1.2 Hz), 7.64 (5H, m), 7.75 (3H, d, J, 3 Hz), 7.81 (1H, m), 7.93 (1H, m), 8.10 (1H, m), 8.20 (1H, m). *m*/*z* [EIMs] 697; Calc. 695.

3-G1-(Irbt$_2$D-μ-Cl)$_2$ (7) (Scheme 1). A mixture of **6** (294 mg, 0.459 mmol), iridium chloride trihydrate (41 mg, 0.12 mmol), water (1.0 mL), and 2-ethoxyethanol (3.0 mL) was heated (bath temperature: 125-135 °C) under argon for 24 h. After cooling, the resultant mixture was passed through a column of silica gel using ethyl acetate-light petroleum (0:1 to 1:10), dichloromethane, and then methanol as eluents. The filtrate was collected (≈

600 mL) and concentrated to about 50 mL. An orange solid precipitated and was collected by filtration. The residue was washed with methanol (≈10 mL). The bright yellow solid was dried (177 mg) and then reprecipitated from a dichloromethane-methanol mixture to give impure iridium dimer (125 mg). Excess **5** amount of was collected from the filtrate. *m*/*z* [MALDI: OTf]: fragmented mass obtained 1582 ($Irbt_2D$), Calc. 3231.

(G1-bt_3Ir) (8) (Scheme 1) The two products were used without further purification for the next step. A mixture of the above-obtained iridium complex, recycled **6**, and silver trifluoromethanesulfonate (34 mg, 0.133 mmol) was heated (bath temperature: 120 °C) for 16 hr under argon. The reaction was then allowed to cool to room temperature, and the mixture was purified by column chromatography over silica gel using dichloromethane-hexane (0:1 to 1:3) as eluent to give **8** (95 mg, 39%). δ_H (300 MHz; $CDCl_3$): 0.92-1.03 (36H, m, Me), 1.31-1.66 (48H, m, CH_2), 1.73-1.86 (6H, m, CH), 3.95 (12H, m, $ArOCH_2$), 6.57 (5H, m), 6.93 (15H, m), 7.22 (15H, m), 7.51 (15H, m), 7.73 (2H, m) and 7.82 (2H, d, J 8.1 Hz); *m*/*z* [MALDI: OTf]: 2277, Calc. 2274.

(2-phenylbenzthiazole)$_2$Ir(μ-Cl)$_2$Ir(2-phenylbenzthiazole)$_2$ (**9**). It has been prepared by following the method described in Chapter 5.

Ir(2-phenylbenzthiazole)$_3$ (**10**). The complex **9**, bt and $Ag(CF_3SO_3)$ were dissolved in dichloromethane and stirred for few minutes. Solvent was sucked off under vacuum and heated at ~120-125 °C for 16 h. Dichloromethane was added into the residue, stirred for few minutes and filtered. δ_H (300 MHz; $CDCl_3$): 6.61 (3H, d, 7.8 Hz), 6.68 (3H, d, 8.4 Hz),

6.81 (3H, t, 7.8 Hz), 6.91 (6H, dd, 7.5, 13.5 Hz), 7.19 (3H, t, 8.1 Hz), 7.66 (3H, d, 7.5 Hz), 7.80 (3H, d, 8.1 Hz); m/z (FABMS): 823, Calc. 822.

1-(*tert*-butylphenyl)-4-trifluoromethanesulfonate (11). Triethylamine and DMF were added into a mixture containing 4-(*tert*-butyl-phenol), $Pd(PPh_3)_2Cl_2$ and copper(I) iodide. The resulting mixture was stirred at room temperature for 1.5 h and then poured into 50 ml of 3 M hydrochloric acid. After extraction with methylene chloride, the combined organic extracts were washed with water and brine, dried over anhydrous sodium sulfate and evaporated in vacuo to give a red brown oil, which was then purified by column chromatography eluting with hexane, and then hexane/ethyl acetate (12:1) to give 20.1 g of the title compound as white crystals (97% yield). ^1H NMR (300 MHz, $CDCl_3$): 7.44655 (d, 2H), 7.18603 (d, 2H), 1.33846 (s, 9H), EIMS : m/z 282, Calcd. 282.

1-(*tert*-butylphenyl)-4-ethynylbenzene (12). A mixture of 4-(tert-butylphenyl)-trifluoromethanesulfonate (1.00 g, 2.96 mmol), trimethylsilylacetylene (0.50 mL, 3.54 mmol), $Pd(PPh_3)_2Cl_2$ (0.119 g, 0.169 mmol), triethylamine (2.0 mL) and DMF (5.0 mL) was stirred under nitrogen at 50 °C overnight. The reaction mixture was slowly poured into cold hydrochloric acid (3 M) and was then extracted with methylene chloride. The organic extracts were washed with water and brine, dried over anhydrous sodium sulfate and the solvent was then evaporated. The resulting black solid was then purified by passing through a silica gel column eluting with hexane. It was disilylated by adding a sample of Bu_4NF (0.27 g, 0.857 mmol) to a THF solution of [[4-(tert-butylphenyl)]-ethynyltrimethylsilane (0.221 g, 0.772 mmol in 2.0 mL of THF). The solution was stirred at room temperature for 30 min and poured into water. It was extracted with

methylene chloride. The organic extracts were washed with water, dried over anhydrous sodium sulfate and evaporated in vacuo to give a yellow solid. It was then purified by passing through a short silica gel column, eluting with hexane to afford 0.150 g as a white solid (90%, mp 86–87°C). 1H NMR (300 MHz,$CDCl_3$) : 7.45 (t, 2H,), 7.35 (t, 2H,), 3.05 (s, 1H), 1.31 (s, 9H). EIMS : m/z 158, Calcd. 158.

2-phenylpyridine-5-bromomide (13). It has been prepared by following the method described in the literature.[16] ^{1}H NMR (300 MHz,$CDCl_3$) : 8.88 (s, 1H,), 8.09 (d, 2H), 7.89 (d, 1H), 7.55 (m, 2H), 7.39 (m, 2H). EIMS : m/z 233, Calcd. 233.

(2, 5-difluoride-2-phenylpyridine)-5-bromomide (14). It has been prepared by following the method described in the literature.[16] ^{1}H NMR (300 MHz,$CDCl_3$) : 8.75 (s, 1H,), 7.96 (m, 1H), 7.86 (d, 1H), 7.65 (d, 1H), 6.88 (m, 2H). EIMS : m/z 269, Calcd. 269.

2-phenylpyridine -5-[(*tert*-butylphenyl)-4-ethynylbenzene] G1-(PPy) (15). The mixture containing 3,5-triiodobenzene (0.0528 g, 0.116 mmol) and (12), $Pd(PPh_3)_2Cl_2$ (0.0124 g, 0.0184 mmol), copper(I) iodide (0.0011 g, 0.00578 mmol) and triethylamine (10 mL) were stirred at room temperature for 8.5 h and was then poured into hydrochloric acid (3 M). After extraction with methylene chloride, the organic extracts were washed with water and dried over anhydrous sodium sulfate and the solvent was then evaporated. The resulting crude product was purified by flash chromatography using hexane as the eluent to give 0.161 g as a yellow powder. ^{1}H NMR (300 MHz,$CDCl_3$) : 8.82 (m, 1H,), 7.85 (dd, 2H), 7.73 (m, 1H), 7.45 (m, 5H), 1.39 (m, 9H). EIMS : m/z 311, Calcd. 311.

2, 5-difluoride-2-phenylpyridine-5-[(*tert*-butylphenyl)-4-ethynylbenzene] G1-(FPPy) (16). The mixture containing 3,5-triiodobenzene (0.0528 g,

0.116 mmol) and (12), $Pd(PPh_3)_2Cl_2$ (0.0124 g, 0.0184 mmol), copper(I) iodide (0.0011 g, 0.00578 mmol) and triethylamine (10 mL) were stirred at room temperature for 8.5 h and was then poured into hydrochloric acid (3 M). After extraction with methylene chloride, the organic extracts were washed with water and dried over anhydrous sodium sulfate and the solvent was then evaporated. The resulting crude product was purified by flash chromatography using hexane as the eluent to give 0.161 g as a yellow powder. ^{1}H NMR (300 MHz,$CDCl_3$) : 8.83 (s, 1H,), 8.05 (m, 1H), 7.75 (dd, 1H), 7.42 (dd, 4H), 6.89 (m, 2H), 1.35 (m, 9H). EIMS : m/z 347, Calcd. 347.

G1-(2-phenylpyridine-5-[(*tert*-butylphenyl)-4-ethynylbenzene])$_3$Ir G1-(PPy)$_3$ Ir (17). ^{1}H NMR (300 MHz, $CDCl_3$): 7.81 (d, 3H), 7.66 (d, 3H), 7.21 (m, 3H), 6.92 (m, 9H), 6.68 (d, 3H), 6.62 (d, 3H), EIMS : m/z 211, Calcd. 211.

G1-(2,5-difluoride-2-phenylpyridine-5-[(*tert*-butylphenyl)-4-ethynylbenzene])$_3$Ir G1-(FPPy)$_3$Ir (18). ^{1}H NMR (300 MHz, $CDCl_3$): 8.82 (d, 1H), 7.86 (m, 1H), 7.76 (m, 5H), 7.41 (m, 13H), 6.92 (m, 7H), 4.10 (m, 6H), 1.31 (s, 9H), EIMS : m/z 1231, Calcd. 1231

7.2.2 Fabrications and Characterizations of OLEDs based on Ir complex

The bilayer films were fabricated as a sandwiched structure between cathode (Ca) and indium-tin oxide (ITO) coated glass anode electrodes. ITO-coated glass substrates were cleaned sequentially in ultrasonic baths of detergent, 2-propanol/deionized water (1:1 volume) mixture, toluene, de-ionized water, and acetone. All spin coating processes were done in the air. Approximately 50 nm-thick hole injection layer of poly(ethylenedioxythiophene) doped with poly(styrenesulfonate)

(PEDOT:PSS) was spin-coated on top of ITO from a 0.7% dispersion in water and dried at 150°C for 1 hr under vacuum.

Thin films of dendrimers of Ir complexes doped to host in toluene solutions were spin-coated upon the PEDOT layer and dried at 70°C under vacuum for 1h. The film thickness obtained was ca. 50 nm, which was measured by an Alpha-Step 500 surface profiler (KLA Tencor, Mountain View, CA). The total coating thicknesses of PEDOT and polymers were about 100 nm.[17] Finally, 30 nm thick of TPBi [1,3,5-tris(2-N-phenylbenzimidazolyl)benzene] and 35 nm thick of Ca and 100 nm thick of Al electrodes were thermally evaporated through a shadow mask onto the polymer films using an AUTO 306 vacuum coater (BOC Edwards), typical evaporations being carried out at base pressures lower than 2×10^{-6} Torr. The active area of each EL device was characterized following a published protocol.[17]

7.2.3 Solution Quantum Yield Measurement

The most reliable method for measuring solution quantum yield (Φ_F) is the comparative method reported by Williams *et al*.,[18] which involves the use of well characterised standard samples with known Φ_F values. Essentially, solutions of the standard and test samples with identical absorbance at the same excitation wavelength can be assumed to be absorbing the same number of photons. Hence, a simple ratio of the integrated fluorescence intensities of the two solutions the quantum yield. Since Φ_F for the standard sample we used, *cis*-$Ru(bpy)_2Cl_2$, is 80%, it is trivial to calculate the Φ_F for the test sample. Absolute values are calculated using the standard samples which have a fixed and known fluorescence

quantum yield value, according to the following equation[18]:

$$\Phi_X = \Phi_{ST}\left(\frac{Grad_X}{Grad_{ST}}\right)\left(\frac{\eta_X^2}{\eta_{ST}^2}\right)$$

Where the subscripts ST and X denote standard and test respectively, Φ is the fluorescence quantum yield, *Grad* is the gradient from the plot of integrated fluorescence intensity *vs* absorbance, and η is the refractive index of the solvent.

7.3 Results and Discussions

7.3.1 Photophysical Properties

The optical properties of the 2-phenylbenzthiazole iridium(III) complexes- $Ir(bt)_3$ can be systematically changed by attaching substituents to the ligand. We have compared the solution UV-Vis absorption spectra of bt_3Ir and the first-generation (G1-bt_3Ir) (Fig. 7.1). First, we present UV-Vis absorption spectra of bt_3Ir, which can be divided into two regions. The absorption band extending from 350 nm to 500 nm, corresponds to the singlet-singlet metal-to-ligand charge transfer transitions. The transition bands observed can be assigned as intraligand (IL) (π-π*) transitions (bt^-) and metal-to-ligand charge-transfer (^{1}MLCT) (dπ(Ir) → π* (bt^-)) transitions, respectively. The absorption at around 390 nm has been assigned to the metal to ligand singlet charge transfer state (MLCT^1).[10] Additionally, the spectra of all these complexes exhibit weaker absorption tails towards more low energy regions (440-480 nm), which may be attributed to triplet metal-to-ligand charge-transfer transitions (^{3}MLCT). Secondly, we mention the UV-Vis absorption spectra of (G1-bt_3Ir) indicate that the fact of slight red shift in the the absorptions wavelength of the metal complex core for either

generation illustrates that the meta arrangement around the branching phenyls to a first approximation breaks the conjugation between the dendron and the 2-phenylbenzthiazole ligand. The first phenyl ring of the dendron is in conjugation with the 2-phenylbenzthiazole moiety in the ligand. The increased conjugation length gives rise to a small red shift for the metal complex absorptions when compared to bt_3Ir and (G1-bt_3Ir), as indicated in Fig 7.1. The UV-Vis absorption spectra of the dendrimers were found to shift slightly in the solvent.

The solution PL spectra of bt_3Ir and (G1-bt_3Ir) are shown and compared in Fig. 7.2. The comparison of the PL spectra between bt_3Ir and (G1-bt_3Ir), shows the same spectral structure, although a slight red-shift of PL a peaks from 547 nm to 569 nm and a shoulder from 588 nm to 615 nm was observed. This red shift can be attributed to an increase in conjugation length caused by the first phenyl ring of the dendron being in conjugation with the 2-phenylbenzthiazole moiety. This again illustrates the importance of the connection point of the dendron to the ligand. The PL spectra of bt_3Ir and the dendrimers are shown in Fig. 7.2, respectively. The peaks at 554 and 572 nm and shoulders at 591 and 617 nm are observed, respectively. The two spectra were found to exhibit similar spectral features. This figure shows that all of these complexes emit in the range of 550-620 nm, corresponding to orange light.

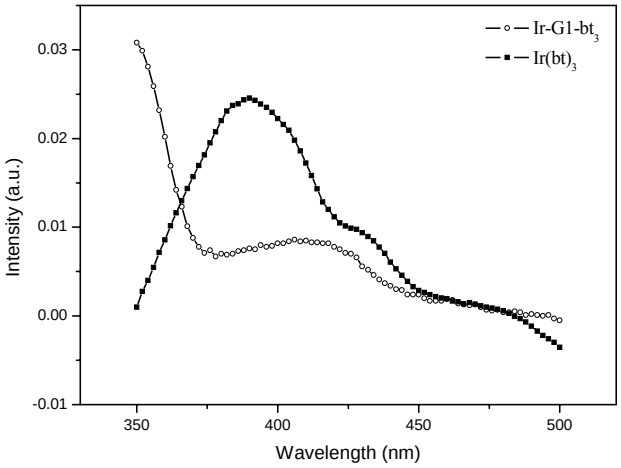

Figure 7.1. Comparison of the UV-Vis absorption spectra of (G1-Ir-bt_3) and $Ir(bt)_3$ complexes in CH_2Cl_2.

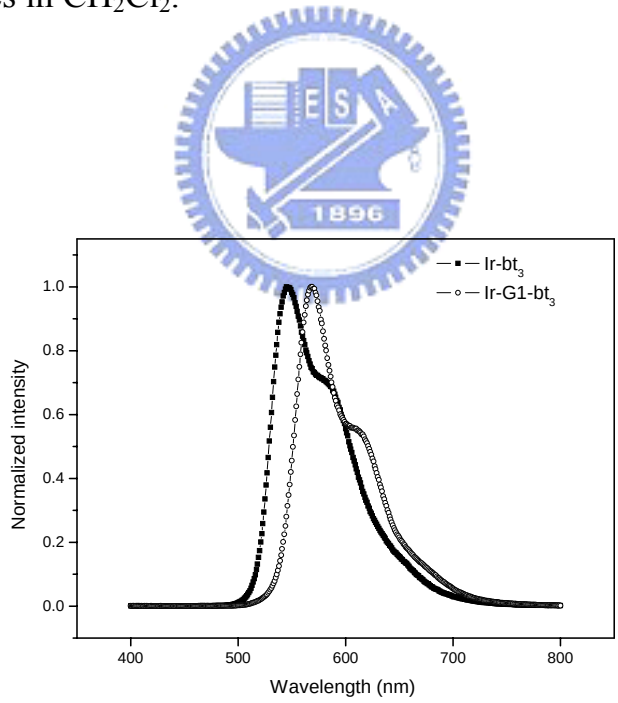

Figure 7.2 Comparison of solution PL spectra for (G1-Ir- bt_3) and $Ir(bt)_3$ complexes in CH_2Cl_2.

It is known that the emission bands from MLCT states are generally

broad and featureless, while $^3(\pi\text{-}\pi^*)$ states typically give highly structured emission. A finial aspect of the PL study was used to determine whether energy could be transferred efficiently from the dendrons to the core. The photoluminescence excitation (PLE) spectra shown in Fig. 7.3 inform us the energy transfer. Since the PLE spectrum will overlap with the UV-visible absorption spectrum of (G1-bt_3Ir) compound, not only direct excitation of the core metal complex but also efficient energy transfer from the dendron to the ligands should occur.[15] The photophysical properties of the dendrimer were estimated further by measuring the photoluminescence quantum yield (PLQY) in solution. We observed that the PLQY of the (G1-bt_3Ir) compound dendrimer was approximately 1.5 times higher than that of the pristine complex $Ir(bt)_3$ in solution (Chloroform). In solution the (G1-bt_3Ir) compound dendrimer had a high PLQY of 90% and the pristine complex bt_3Ir had a PLQY of 62% by integrating sphere respectively. This observation is consistent with reduced intermolecular core-core interactions for the dendrimer. The PLQY in solution of $Ir(ppy)_3$ has been reported to be between 40% and 50% which is similar to that of IrppyD.[19] When the dendrimer was blended with 4,4'-bis(N-carbazolyl)biphenyl (CBP), a commonly used host material, in a ratio of 15%, the emission was only observed from the dendrimer.

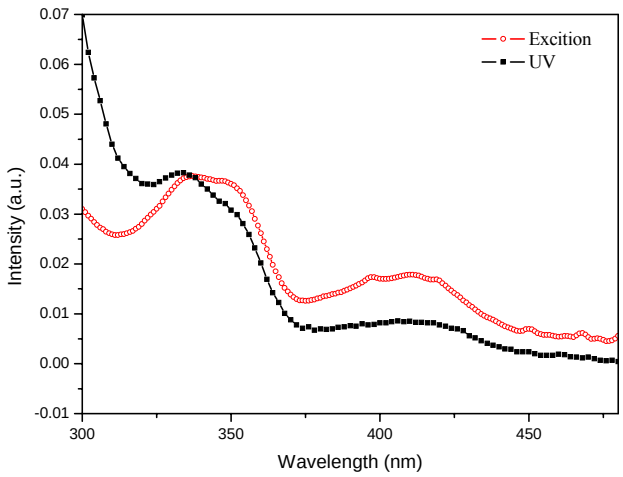

Figure 7.3 The PLE spectra of Ir-G1-bt_3 dendrimer in CH_2Cl_2 at room tempature

7.3.2 Electrochemical Properties

The finial part of the study on the materials was electrochemical analysis of their electronic properties. Although the PLE spectra indicated that energy transfer from the dendrons to the core was efficient, the wide band gap suggests that charge should be injectioned directly into the organometallic core. The devices fabricated used ITO as the anode and Mg/Ag as the cathode and the electroluminescent properties of the complexes were investigated. The choice of host and electron-transporting/ hole-blocking layer can have a strong effect on the device performance, and we therefore investigated each of the components. We used [4,4',4''-tris(N-carbazolyl)triphenylamine (TCTA) instead of CBP as the host. But we not get the good data. So we change TCTA to CBP. The EL device performance was investigated using (G1-bt_3Ir) and $(bt)_3$Ir as a dopant, respectively, and CBP [4, 4′-bis(9-carbazolyl)-1,1′-biphenyl] as the host in

the emitting zone. As shown in Figure 7.4 the device structure used in this work is typically multi-layered, employing indium tin oxide (ITO) as the anode, PEDOT:POSS as the hole transporting material, (G1-bt_3Ir) and $(bt)_3Ir$ as the dopant, TPBI as the electron-transport/hole blocking material, MgAg as the electron- injection layer and aluminum as the cathode. As shown in Figure 7.4. TPBI has been used as an electron-transporting layer for OLEDs based on fluorescent emitters and as host for phosphorescent emitters.[20] The HOMO and LUMO of TPBI were found to be 6.7 eV and 2.7 eV and the thicknesses of the PEDOT:POSS and TPBI layers were 35 and 30 nm, respectively.

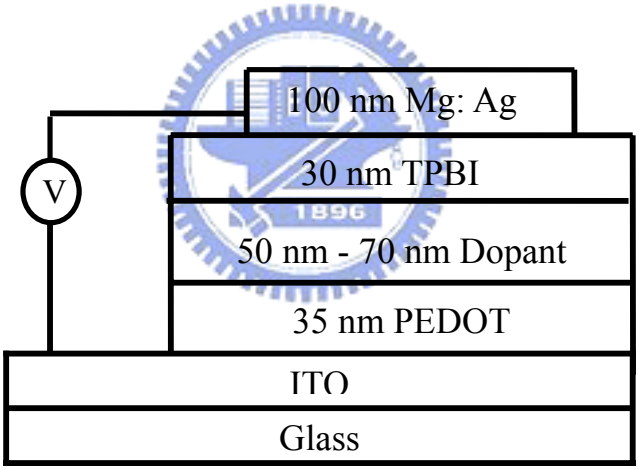

Figure 7.4 EL device structure with the (G1-bt_3Ir) and $(bt)_3Ir$ as a dopant.

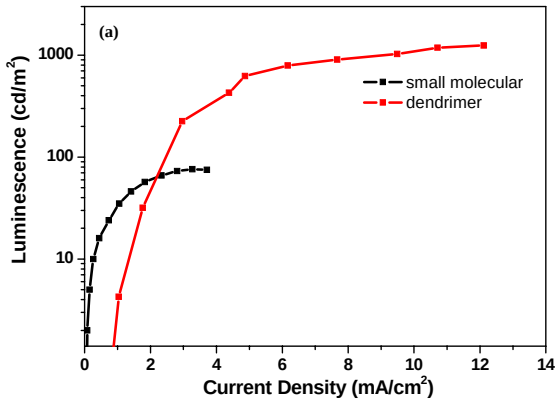

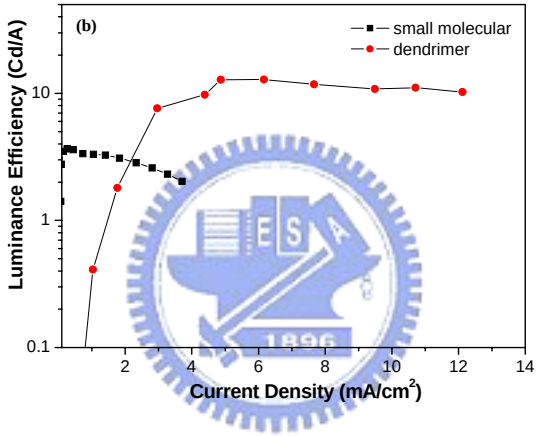

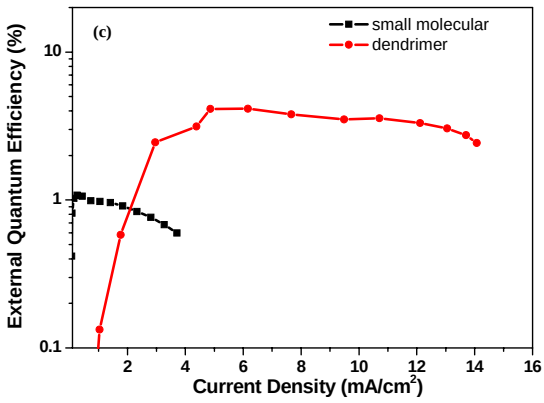

Figure 7.5 Currentdensity dependance of luminance (a), luminance efficiency (b), and EQE (c) for (Ir-G1-bt_3) and $Ir(bt)_3$

It has been observed that the quantum efficiency of the devices based on (G1-bt_3Ir) and $(bt)_3Ir$ was found to increase with increasing current density and it reaches a maximum at 12.83 cd/A and 3.65 cd/A, respectively, and the characteristics shown in Figure 7.5. The turn-on voltage was found to be 7.0 and 5.0 for the devices based on (G1- bt_3Ir) and $(bt)_3Ir$, respectively.

Futhermore the luminance efficiency was found to decrease with increasing current density for both devices, which may be attributed to the triplet-triplet annihilation. The Commission Internationale de L'Eclairage (C.I.E) co-ordinates of the (G1-bt_3Ir) and bt_3Ir devices was determined from the EL spectra to be (0.539, 0.455) and (0.486, 0.501), respectively. On comparison of the efficiency of devices based on (G1-bt_3Ir) and $(bt)_3Ir$ efficiency was found to be higher throughout the applied current densities, as indicated in Table 7.1.

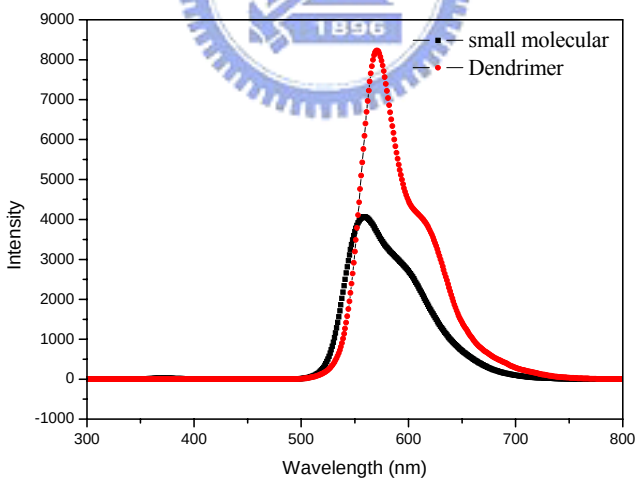

Figure 7.6 Comparison of EL spectra for devices based on (G1-bt_3Ir) and $(bt)_3Ir$ complexes

Futhermore, the luminance and the quantum yield are also found to be higher at lower current densities. Furthermore, no emission from CBP was observed, indicating a complete energy transfer from the host exciton to the Ir-dopant. The EL spectra of (G1-bt_3Ir) and $(bt)_3Ir$ devices are similar to the corresponding PL spectra of same phosphors in a dilute solution (Figure 7.6). Thus, the EL emission is confirmed to originate from the triplet excited states of the phosphors. The final important observation of these dendritic devices is that the efficiency of the devices stay reasonably constant over a range of brightness (Figure 7.5), which can be attributed to the balanced charged injection and the uniform distribution of the dopant in the host layer.

Table 7.1 Comparative study of the electroluminescent properties of three EL devices based on (G1-bt_3Ir) and $(bt)_3Ir$ as a dopant. Device structure: ITO/PEDOT(35 nm)/ dopant /TPBI (30 nm)/MgAg (100 nm)

	$Ir(bt)_3$	(G1-bt_3Ir)
EL Color	orange	orange
Peak wavelength (nm)	559	571
C.I.E.coordinate (x,y)	（0.486, 0.501）	（0.539, 0.455）
E.Q.E	1.08 (at 0.26 mA/cm^2)	4.14 (at 6.16 mA/cm^2)
Efficiency (Cd/A)	3.65 (at 0.26 mA/cm^2)	12.83 (at 6.16 mA/cm^2)
Bandwidth(nm)	84	76

We also fabricated another device based on dendrimer $(bt)_3Ir$ to compare the EL performance against (G1-bt_3Ir) device. The dendrons was modified with 2-ethylhexyloxy surface groups to ethynylbenzene group for increasing the solubility. The device structure is the same for comparison. We synthesized the $Ir(ppy)_3$ and $Ir(Fppy)_3$ dopants, respectively. The dendrimer G1-$Ir(ppy)_3$ and G1-$Ir(Fppy)_3$ were also synthesized to compare with devices based on small molecule complexes. Since the ethynylbenzene group increases the ring length and vibration , the EL spectra of the dendrimers G1-$Ir(ppy)_3$ and G1-$Ir(Fppy)_3$ were found to show red shifting, as represented in the Fig. 7.7.

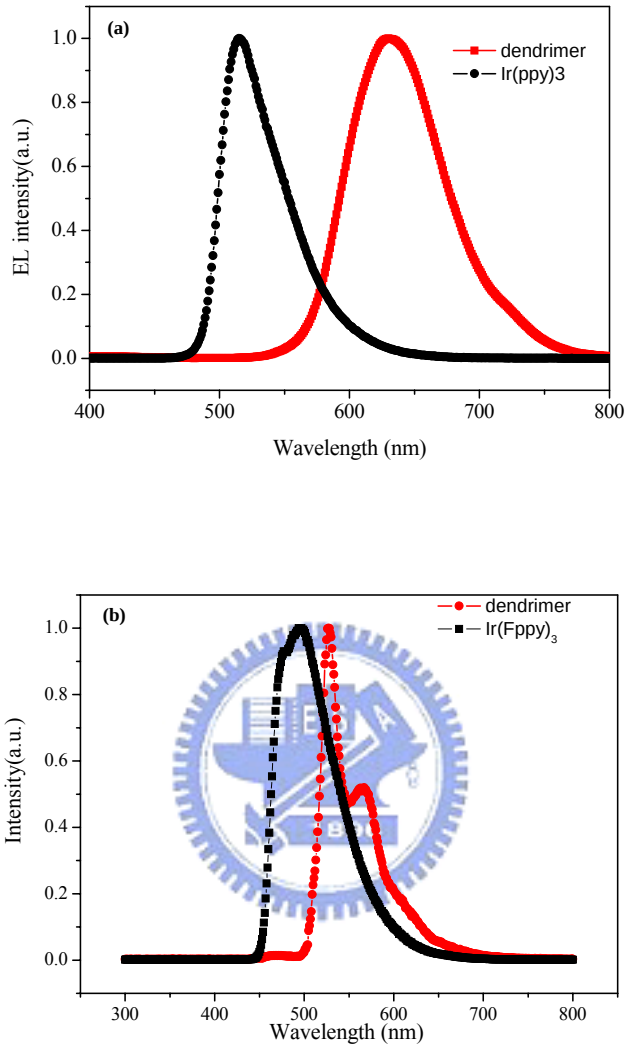

(b)

Figure 7.7 Comparison of EL spectra for (a) G1-$Ir(ppy)_3$ and $Ir(ppy)_3$ complexes and (b) G1-$Ir(Fppy)_3$ and $Ir(Fppy)_3$ complexes

We also fabricated devices with the same structure to compare against the (G1-bt_3Ir) device as a reference. Both EL devices based on $Ir(ppy)_3$ and G1-$Ir(ppy)_3$ show green luminescence and the luminescence

efficiency, current density, voltage and EQE were also invesitgated. We have observed that the quantum efficiency of both devices (G1-$Ir(ppy)_3$) and $Ir(ppy)_3$ was found to increase with increasing current density and it reaches a maximum at 0.28 cd/A and 0.14 cd/A, respectively, as shown in Figure 7.8. The turn-on voltage was found to be 8.0 and 18.0 volts for the devices (G1-$Ir(ppy)_3$) and $Ir(ppy)_3$, respectively. The luminance efficiency was found to decrease with increasing current density for both devices, which may be attributed to the triplet-triplet annihilation. On comparison of two devices with the corresponding devices based on (G1-$Ir(ppy)_3$) and $Ir(ppy)_3$ the efficiency is always higher throughout all the applied current densities range, as indicated in Fig 7.8, whereas the luminance and the quantum yield were also found to be higher at lower current densities. Thus, the EL emission is confirmed to originate from the triplet excited states of the phosphors. The Commission Internationale de L'Eclairage (C.I.E).co-ordinates of the devices based on $Ir(ppy)_3$ and (G1-$Ir(ppy)_3$) was measured to be (0.32, 0.62) and (0.64, 0.35), respectively. The final important observation of deviced based on dendritic complexes is that the efficiency of the devices stay reasonably constant over a range of brightness. Althought the performance and structure of EL devices have not been optimized, we have discovered the one with solution processible dendrimer shows higher efficiency than that with small molecule complex. The EL performance of devices with $Ir(ppy)_3$ and G1-$Ir(ppy)_3$ are summarized in Table 7.2.

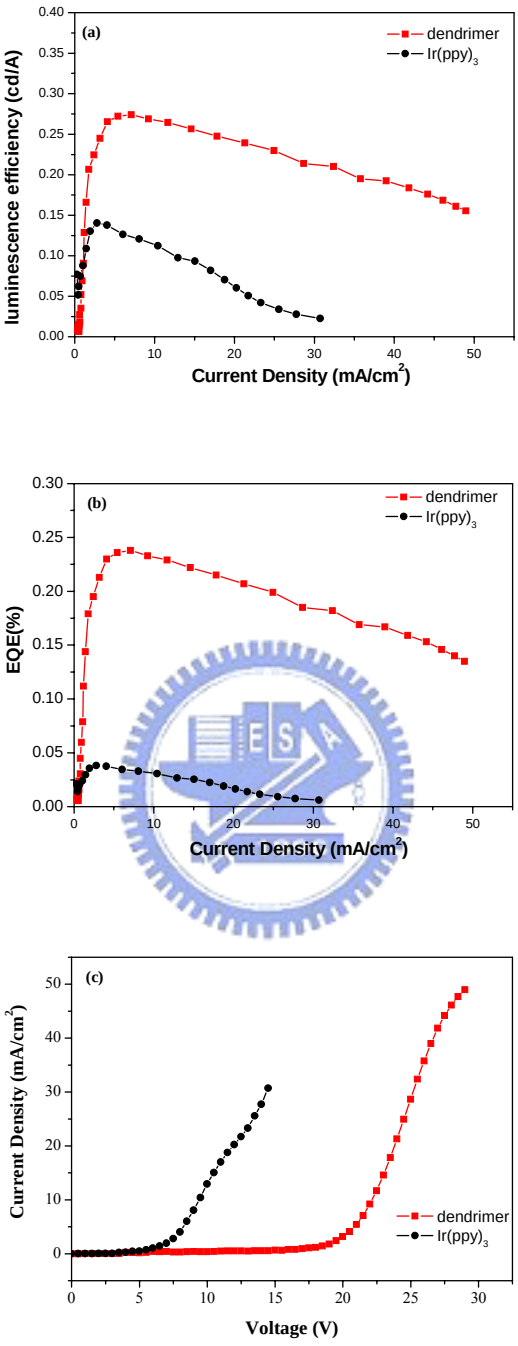

Figure 7.8 Comparison of (a) Efficiency versus luminance, showing the relatively efficiencies, (b) EQE vs current density, and (c) voltage vs current density for $Ir(ppy)_3$ and G1-$Ir(ppy)_3$

Table 7.2 Comparative study of the electroluminescent properties of three EL devices based on $Ir(ppy)_3$ and G1-$Ir(ppy)_3$ as a dopant. Device structure: ITO/PEDOT(35 nm)/ dopant /TPBI (30 nm)/MgAg (100 nm)

	$Ir(ppy)_3$	(G1-$Ir(ppy)_3$)
EL Color	Green	red
Peak wavelength (nm)	523	620
C.I.E.coordinate (x,y)	(0.32, 0.62)	(0.64, 0.35)
E.Q.E	0.04 (at 4.0 mA/cm^2)	0.25 (at 8.0 mA/cm^2)
Efficiency (Cd/A)	0.14 (at 0.26 mA/cm^2)	0.28 (at 6.16 mA/cm^2)
Bandwidth(nm)	95	120

We have also fabricated EL deviced based on blue-emitting dopants, the $Ir(Fppy)_3$ and G1-$Ir(Fppy)_3$, with the device structure maintained similar as previously obsecribed for other dendrimers. However, the surface morphology of the fabricated film device was found not smooth and the devices exhitbited blue-green and yellow-green emission when a positive voltage was applied. For the fabricated $Ir(Fppy)_3$ device, no electroluminescence data were collected since the device was found to quench rapidly. The device based on dendriner G1-$Ir(Fppy)_3$ was also found to show low luminescence. The current-voltage and voltage –luminance characteristics for the device were summarized based on G1-$Ir(Fppy)_3$ in Figure 7.9. The turn-on voltage for emission was found to be 15V, and the

maximum luminescence efficiency was 0.2 Cd/A. The external quantum efficiency (EQE) were showN in Figure 7.9 (b). We also noted when the current density exceeds 20 mA/cm^2, the EQE, luminance, and brightness were found to decreased. The EL performance and relevant data are summarized in Table 7.3.

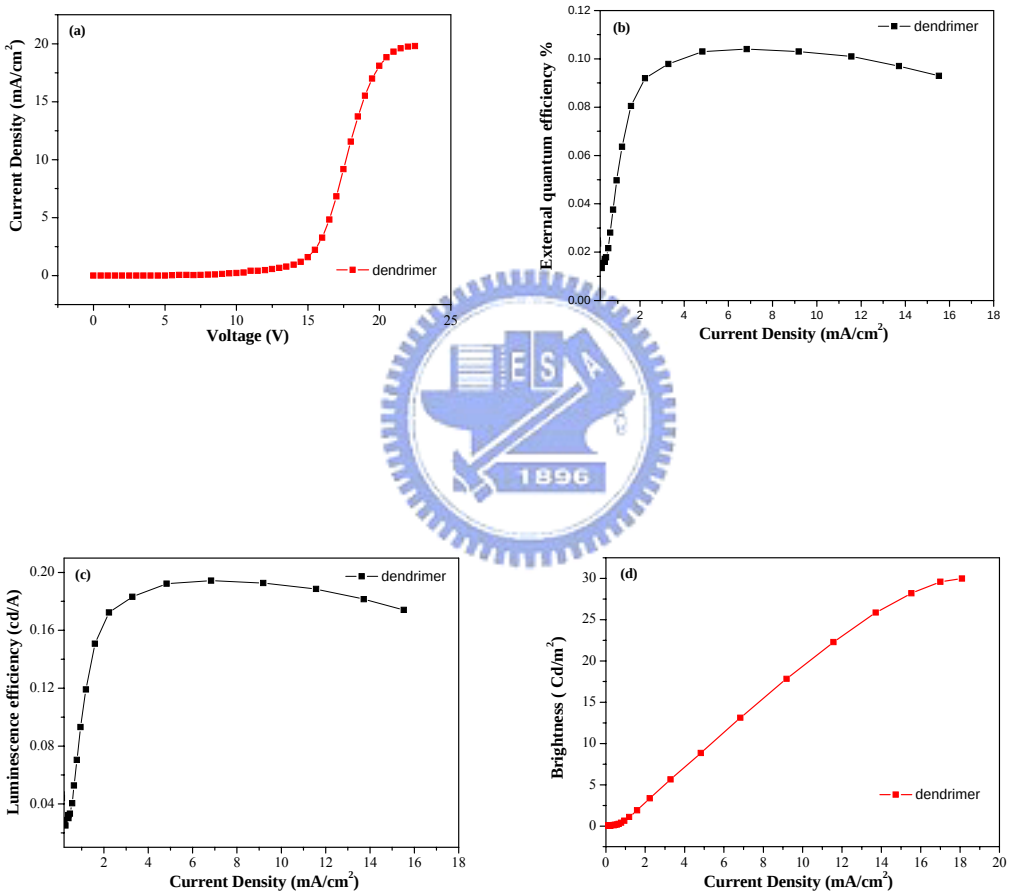

Figure 7.9 (a) voltage vs current density (b) EQE vs current density (c) luminance vs current density (d) luminance vs current density about G1-Ir(Fppy)$_3$

Table 7.3 Comparative study of the EL properties of two devices based on $Ir(Fppy)_3$ and G1-$Ir(Fppy)_3$ as a dopant. Device structure: ITO/PEDOT(35 nm)/ dopant /TPBI (30 nm)/MgAg (100 nm)

	$Ir(Fppy)_3$	(G1-$Ir(Fppy)_3$)
EL Color	Blue-green	Green-yellow
Peak wavelength (nm)	490	540
C.I.E.coordinate (x,y)	(0.18, 0.36)	(0.28, 0.50)
E.Q.E (%)	–	0.11 (at 8.0 mA/cm^2)
Efficiency (Cd/A)	–	0.20 (at 8.0mA/cm^2)
Bandwidth (nm)	120	100

7.5 Conclusion

We have developed a simple synthetic route prepare to solution -processible iridium complex-cored dendrimer. The dendrimer was solution processible and formed good-quality blended film. However, the dendrons can be used to control the important intermolecular interactions for phosphorescent dendrimer. Our work demonstrated that energy can be transferred efficiently from the dendrons to the emissive core. Comparison of the PLQY of the dendrimer and pristine complex shows that the device with dendrons as the emitting chromophore exhibits higher quantum yield. The simple device structures with a solution-processed dendrimer containing a light-emitting chromophore are amongst the most efficient

solution-processed devices ever reported. We believe that solution processing opens up the possibility of patterning of phosphorescent materials.

7.5 References

1. Tang, C. W.; Van Slyke, S. A. *Appl. Phys. Lett.* 51 (1987) 913

2. Friend , R. H.; Gymer, R. W.; Holmes, A. B.; Burroughes, J. H.; Marks, R. N.; Tallani, C.; Bradley, D. D. C.; Dos Santos, D. A.; Bredas, J. L.; Logdlund, M.; Salaneck, W. R. *Nature* 397 (1999) 121

3. Cao, Y.; Parker, I. D.; Yu, G.; Zhang, C.; Heeger, A. *Nature* 397 (1999) 414

4. Markham, J. P. J.; Lo, S.-C.; Magennis, S. W.; Burn, P. L.; Samuel, I. D. W. *Appl. Phys. Lett*. 80 (2002) 2645

5. Lo, S. -C.; Male, N. A. H.; Markham, J. P. J.; Magennis, S. W.; Burn, P. L.; Salata, O. V.; Samuel, I. D. W. *Adv. Mater*. 14 (2002) 975

6. Pillow, J. N. G.; Halim, M.; Lupton, J. M.; Burn, P. L.; Samuel, I. D. W. *Macromolecules* 32 (1999) 5985

7. Webber, P. W.; Liu, Y. J.; Devadoss, C.; Bharathi, P.; Moore, J. S. *Adv. Mater.* 8 (1996) 237

8. Freeman, A. W.; Shannon, C. K.; Malenfant, P. R. L.; Thompson, M. E.; Frechet, J. M. J. *J. Am.Chem. Soc.* 122 (2000) 12385

9. Ebinazar B.; Namdas, Arvydas Ruseckas; Ifor D. W. Samuel; Shin-Chun Lo; Paul, L. Burn. *J. Phys. Chem. B* 108 (2004) 1570

10. Hay, P. J. , *J. Phys. Chem. A*. 106 (2002) 1634

11. G. Pillow, J. N.; Halim, M.; Lupton, J. M.; Burn, P. L.; Samuel, I. D. W.;*Macromolecules* 32 (1999) 5985

12. (a) Lupton, J. M.; Samuel, I. D. W. R.; Beavington, M. J.; Frampton, P. L.; Burn, H.; *Phys. Rev.* B 63 (2001) 5206. (b) Lupton, J. M.; Samuel, I. D. W.; Beavington, R.; Frampton, M. J.; Bassler, H. P.; Burn, L.; *Adv. Mater.* 13 (2001) 258

13. Lupton, J. M.; Samuel, I. D. W.; Beavington, R.; Frampton, M. J.; Burn, P. L.; *Adv. Funct. Mater.* 11 (2001) 287

14. Lo, S.-C.; Namdas, E. B.; Burn, P. L. and Samuel, I. D. W. ; *Macromolecules,* 36 (2003) 9721

15. Michael J. Frampton, Ebinazar B. Namdas, Shih-Chun Lo, Paul L. Burn and Samuel, I. D. W. ; *J. Mater. Chem*. 14 (2004) 2881

16. Marsais, F.; Pineau, Ph.; Nivolliers, F.; Mallet, M.; Turck, A.; Godard, A. and Queguiner, G.; *J. Org. Chem*. 57 (1992) 565-573

17. Dhami, S.; de Mello, A. J.; Rumbles, G.; Bishop, S. M.; Phillips, D. and Beeby, A.; *Photochem. Photobiol.*, 61 (1995) 341.

18. Williams, A. T. R.; Winfield, S. A. and Miller, J. N.; *Analyst*, 108 (1983) 1067

19. (a) King, K. A.; Spellane, P. J.; Watts, R. J.; *J. Am. Chem. Soc*. 107 (1985) 1431 (b) Wang, Y.; Herron, N.; Grushin, V. V.; LeCloux, D. D.; Petrov, V. A.; *Appl, Phys, Lett*. 79 (2001) 449

20. Adachi, C.; Baldo, M. A.; Forrest, S. R.; Lamansky, S.; Thompson, M. E.; Kwong, R. C.; *Appl. Phys. Lett.* 2001,78,1622

Chapter 8
Conclusion and Future Work

In the present work, We have prepared and characterized a series of substituted 2-phenylbenzthiazole (4-CF_3, 4-Me, 4-OMe, 4-F, 4-CN, and 3-F) ligands. The intermediate di-irrido and the six-coordinated mononuclear iridium(III) dopants of the above ligands have been synthesized and characterized. These complexes are thermally stable between 275 and 300℃ depending upon the types and volatility of substituents. They emit bright green-yellow to orange-red light. We have also successfully synthesized a series of new Ir complexes with modified functional groups to tuning emissive colors. Four new cyclometallated iridium complex dopants using various types of substituted (2-phenyl)benzoxazole ligands have been synthesized and shown to exhibit high phosphorescence efficiency, which made them ideal for OLED applications. All the complexes show one-electron oxidation in solution and bright green emission. We have fabricated and investigated three EL devices and observed that the device dopants with substituted ligands show the higher luminance yield compared to the dopant with unsubstituted ligands. In addition, a new series of Ir(III)-complex dopants containing various types of substituted phenylpyrroline ligands. These complexes show different quantum efficiencies in solution depending upon the nature of the substituents. The peak emission wavelengths of the dopants can be finely tuned depending upon the electronic properties of the substituents as well as their positions in the ring.

We have determined the η_{PL} of Ir(4-CF_3bt)$_2$(acac) and Ir(2-phq) $_2$acac

complexes were measured in the solid-state by using an integration sphere and was found to reach 64% and 80% (at 2 wt%), respectively. In particular Ir(4-CF_3bt)$_2$(acac) still exhibits η_{PL} of 41% at dopant concentration as high as 33 wt%. The observed η_{PL} of 70% can be attributed to weak quenching effect and it is predominant for red-orange emitting materials. We have also reported and rationalized a series of phosphorescent dopants with high EQE at varied dopant concentrations in a device. We demonstrated high-efficiency WOLEDs with complexes of Ir(4-CF_3bt)$_2$(acac), Ir(2-phq)$_3$ and FIr6. The efficiency was illustrated by the remarkably high EQE of 8.6%. Our WOLEDs also shows a stable chromaticity with a CIE coordinates of (0.350, 0.396) under different luminances. The device with two emitting layers fabricated in our work not only reached the external quantum efficiency of 8.6%, but also avoided the energy transfer between. We believe that if more suitable host, can be used the EQE of WOLED's can be further increased.

Last, we have developed a simple synthetic route to solution processible iridium complex cored dendrimer. The dendrimer were solution processible and formed good-quality blended film. However, the dendrons can control the important intermolecular interactions for phosphorescent dendrimer. The dendrimer are also shown that the energy can be transferred efficiently from the dendrons to the emissive core. Comparison of the PLQYs of the dendrimer and pristine complex shows that having dendrons on the emitting chromophore can obtain the high efficiency. The simple device structures with a solution-processed dendrimer containing a light-emitting chromophore are amongst the most efficient solution-processed devices reported. We believe that solution processing opens up the possibility of patterning of phosphorescent materials.

List of Publications and Presentations

A. Journal Papers:

[1] Hsiao-Wen Hong and Teng-Ming Chen, “Effect of substituents on the photoluminescent and electroluminescent properties of substituted cyclometalated iridium(III) complexes”, Materials Chemistry and Physics, Vol. 101, 2007, pp. 170-176

[2] Hsiao-Wen Hong and Teng-Ming Chen, “Synthesis and Electroluminescence Studies of the New Iridium(III) Complexes with 2-Phenyl-1-pyrroline Ligands”, Japanese Journal of Applied Physics,Vol. 45, No. 9A, 2006, pp. 7121-7125

[3] Hsiao-Wen Hong and Teng-Ming Chen, “High phosphorescence quantum efficiency of red-orange emitting Ir(III) complexes”, in submitted, Polyhedron (2006)

[4] Hsiao-Wen Hong and Teng-Ming Chen, “The Synthesis of new dendrimer and properties of solution processable phosphorescent”, in submitted, Tetrahedron Letters

B. International Conference Papers and Posters

[1] Hsiao-Wen Hong and Teng-Ming Chen, ”Design and Synthesis of Advanced Materials and Fabrication of OLED Devices”. 6th Chitose International Forum (CIF6) on Photonics Science & Technology-Organic Semiconductor Device Physics-High efficiency electrophosphorescence and organic transistors. December 9-11, 2005 in Hotel Nikko (JAL) Chitose, Hokkaido, Japan

[2] Hsiao-Wen Hong and Teng-Ming Chen, Poster presentation on *Syntheses, Photoluminescence and Electroluminescence of Some New Phosphorescent Iridium(III)-based Materials.* International Display Manufacturing Conference & Exhibition Taipei Int’L Convention Center, Taiwan, Feb. 21-24, 2005

[3] Hsiao-Wen Hong and Teng-Ming Chen, Poster presentation on *Syntheses, Photoluminescence and Electroluminescence of Some New Blue-Emitting Phosphorescent Iridium(III)-based Materials.*Chinese Chemical Society Conference, Tai-chung, Taiwan, 19-21 November, 2004

[4] Hsiao-Wen Hong and Teng-Ming Chen, *Syntheses, photoluminescence and electroluminescence of some new blue-emitting phosphorescent iridium*(Ⅲ)*-based materials.* The Third International OLED and PLED Workshop on Advanced Functional Materials, Hsin-Chu, Taiwan, 18, November, 2004

[5] Hsiao-Wen Hong and Teng-Ming Chen, Poster presentation on *Effect of Substituents on the Photoluminescent and Electroluminescent Properties of Substituted Cyclometallated Complexes of Iridium(III).* Taiwan Display Conference (TDC), Taipei, Taiwan, 10-11 June, 2004;

[6] Hsiao-Wen Hong and Teng-Ming Chen, Poster presentation on *Syntheses, photoluminescence, and electroluminescence of some new orange-emitting phosphorescent iridium(III)-based materials.* International Display Manufacturing Conference & FPD Expo Taipei Int'L Convention Center, Taiwan, Feb. 18-21, 2004;

[7] Hsiao-Wen Hong and Teng-Ming Chen, Poster presentation on *Syntheses, photoluminescence, and electroluminescence of some new orange-emitting phosphorescent iridium(III)-based materials.* Chinese Chemical Society Conference, Chung-Li, Taiwan, 27-28 November, 2003;

[8] 2003, "The Second International OLED and PLED Workshop" in National Taiwan Normal University, Taipei, The Third Prize for excellent posters .

Awards

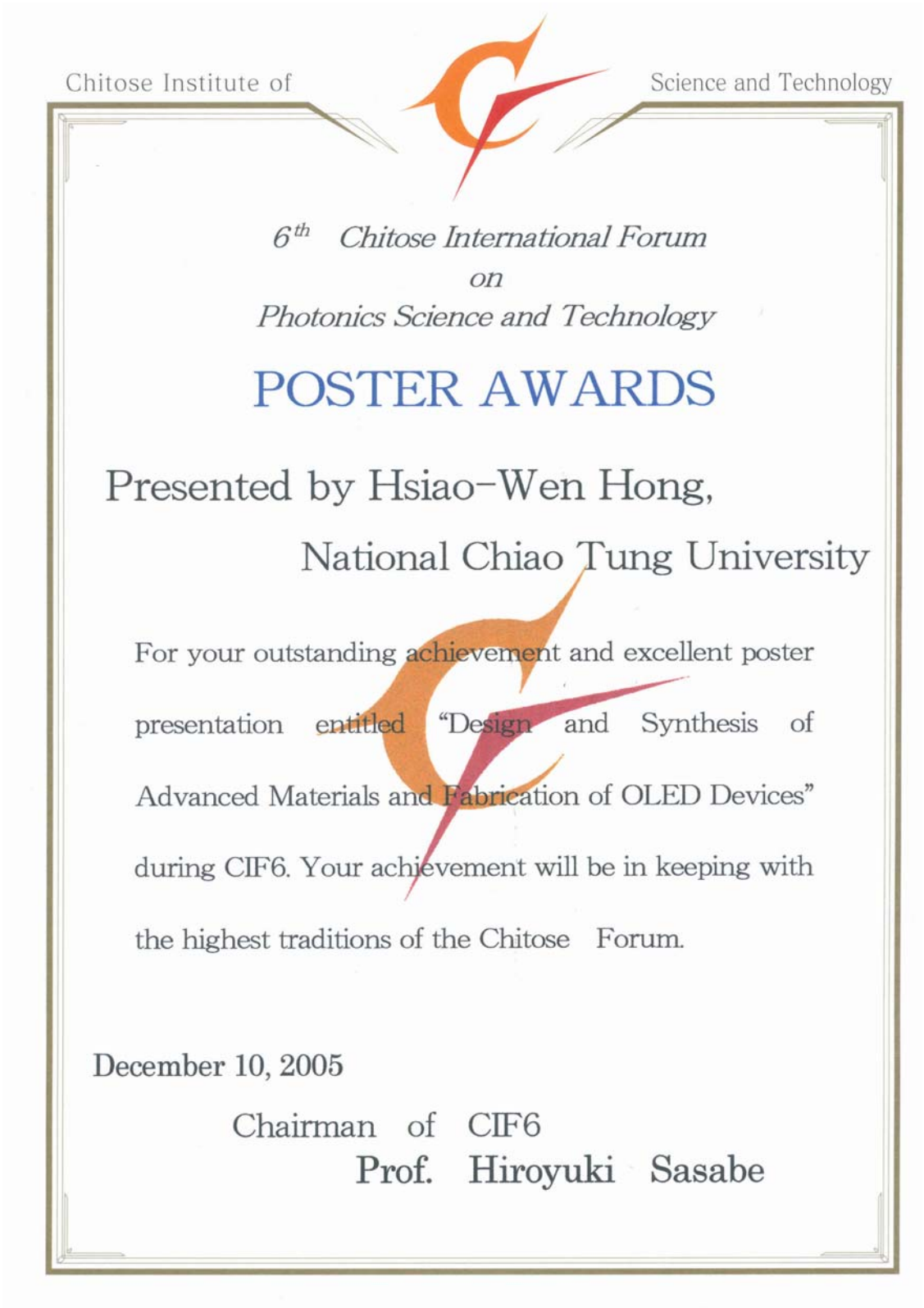

Chitose Institute of Science and Technology

6th Chitose International Forum
on
Photonics Science and Technology

POSTER AWARDS

Presented by Hsiao-Wen Hong,
National Chiao Tung University

For your outstanding achievement and excellent poster presentation entitled "Design and Synthesis of Advanced Materials and Fabrication of OLED Devices" during CIF6. Your achievement will be in keeping with the highest traditions of the Chitose Forum.

December 10, 2005

Chairman of CIF6
Prof. Hiroyuki Sasabe